EXPERIMENTAL STUDIES OF SODIUM - SILICON CLATHRATE COMPOUNDS

A thesis submitted for the degree of Doctor of Philosophy of the

University of London

by

KUNG EK SIM

Physics Department

The Blackett Laboratory

Imperial College of Science and Technology

LONDON SW7 2BZ

April 1983

ABSTRACT

Clathrate semiconductor compounds, Na_xSi_{136}, with the same structure as the gas hydrates have been prepared by the thermal degradation of NaSi for a number of different Na concentrations. The Na atoms occupy partially sites in the centre of slightly distorted silicon tetrahedral cages. The sodium to silicon distances are between 3.16 and 3.97 Å, which are all too large for any appreciable direct bonding by any two nearest-neighbour Na atoms.

The paramagnetic susceptibilities of these Na_xSi_{136} compounds have been investigated in the temperature range between 1.5 and 20 K using a Faraday Balance. The temperature dependent susceptibility shows an amorphous antiferromagnetic behaviour which follows the Curie-Weiss law. For low Na concentration samples, the electrons tend to be localized. On the high concentration side, the 3s electrons of the nearest-neighbour Na atoms tend to be coupled antiparallel.

Electron paramagnetic reasonance studies on Na_xSi_{136} compounds show four hyperfine split lines. The g-values equal 2, however, the hyperfine constants are about 40% of the free Na atom. A model calculation has been made to examine the influence of the Si cage on the Na 3s wavefunction; this calculation shows that it is possible to account for the reduced hyperfine constant.

Optical absorption of one sample has been measured.

An existing AC calorimeter was greatly improved in order to try and measure the specific heat of these Na_xSi_{136} compounds, however, unresolved technical problems prevented any useful measurements.

CONTENTS

		page
Title		I
Abstract		II
Contents		III
Acknowledgements		VII
Chapter 1	Doped Semiconductors and Metal Non-metal Transition	
	1.1 Introduction	1
	1.2 Impurity band and metal non-metal transition in heavily doped semiconductors	2
	1.3 Alkali metal doped semiconductors	11
	1.4 Sodium tungsten bronze Na_xWO_3 and clathrate alkali-silicon compounds	13
Chapter 2	Crystal Structure of Sodium-Silicon Clathrate Compounds	
	2.1 Crystal structure of Na_8Si_{46} and Na_xSi_{136}	17
	2.1.1 A-type clathrate Na_8Si_{46} phase	17
	2.1.2 B-type clathrate Na_xSi_{136} phase	18
	2.2 Previous work on sodium-silicon clathrate compounds	22
Chapter 3	Preparation of Clathrate Na_xSi_{136} Compounds	
	3.1 Dry box system	25
	3.2 Sample preparation procedure	27
	3.2.1 Dissolution - first stage in making NaSi phase compound	28

3.2.2 Bomb method 28

3.2.3 Radio frequency (R.F.) induction furnace method 30

3.2.4 Thermal degradation of NaSi - second stage in making Na_xSi_{136} phase compounds 35

3.2.5 Final stage - sample purification and cleaning 37

3.3 Making high sodium concentration Na_xSi_{136} samples 37

3.4 Sample characterization 41

Chapter 4 Specific Heat Measurement by AC Method

4.1 Introduction 63

4.2 Experimental low temperature AC calorimetry 66

4.2.1 AC method 66

4.2.2 Low frequency limit : external time constant 69

4.2.3 High frequency limit : internal time constant 70

4.3 Modification of the calorimeter 71

4.3.1 Sapphire sample platform 74

4.3.2 Nichrome thin film heater 75

4.3.3 Thin slab carbon thermometer 76

4.4 Thermometer calibration 77

4.5 The addenda heat capacity 79

4.6 Technical problems in measuring the heat capacity of a compacted Na_xSi_{136} powder sample 83

4.7 Concluding remarks 86

Chapter 5 Low Temperature Magnetic Susceptibility of Na_xSi_{136}

5.1 Introduction 88

5.2 Experimental method 90

5.3 Presentation of results 95

5.4 Discussion and conclusions 104

Chapter 6 Electron Paramagnetic Resonance Studies on Na_xSi_{136}

6.1 Background theory 107

6.2 Experimental 112

6.3 Presentation of results 113

6.3.1 Resonance spectrum 113

6.3.2 Paramagnetic susceptibility 118

6.4 Simple model calculation of the electron density at the sodium nucleus 124

6.4.1 Muffin-tin potential model 125

6.4.2 Determination of the new wavefunction Q(r) by numerical integration 129

6.4.3 Calculation of the new energy E' by a self-consistent method 136

6.4.4 Computer program and calculated results 138

6.5 Conclusions 144

Chapter 7 Conclusions

7.1 Introduction 146

7.2 Conclusions 146

Appendix A - 1 Computer program : X-ray diffraction line intensity calculation for Na_xSi_{136} 150

Appendix A - 2	Computer program : X-ray diffraction line intensity calculation for Na_8Si_{46}	152
Appendix B	Specific heat of some cryogenics materials	153
Appendix C	Magnetic susceptibility experimental data	154
Appendix D	Slater's tenth order polynomial	164
Appendix E	Computer program for calculating a new wavefunction Q(r)	166
Reference		172

ACKNOWLEDGEMENTS

I would like to thank my supervisor, Dr. A. D. Caplin, for his guidance, suggestion and criticism.

I am greatly indebted to Drs. A. K. Grover and S. K. Dhar of Tata Institute of Fundamental Research for performing the measurements of X-ray diffraction line intensity, to Dr. P. Gilberd for his critical reading of the thesis, to the research students of the Metal Physics Group for their assistance and valuable discussion.

A student award from the British Council is gratefully acknowledged.

Finally, I would like to thank my wife Grace , without her constant encouragement and patience, this work would not be completed.

CHAPTER 1

DOPED SEMICONDUCTORS AND METAL NON-METAL TRANSITION

1.1 INTRODUCTION

A doped semiconductor provides a typical example of the metal non-metal transition in disordered systems. A material in which the electrical conductivity tends to a finite value as the temperature approaches zero is regarded as a metal; by 'non-metal' is meant that the conductivity tends to zero. The mechanism of this transition has been extensively investigated, particularly by the transport and magnetic properties associated with the electron correlation and disorder in the impurity band of the heavily doped semiconductors such as phosphorus doped silicon [1] and others. This transition also occurs in other compounds such as sodium tungsten bronze Na_xWO_3 [2,3] in which sodium is inserted in the cubic perovskite structure with the corner linked WO_6 octahedra. The metal non-metal transition occurs at sodium concentration of 10 to 30% [3]. In the mid-1960s, new type alkali-silicon (and germanium) clathrate compounds Me_xSi_{136}, where Me can be any alkali metal except lithium, have been synthesized by the Bordeaux group [4,5]. In this large(one hundred and thirty six silicon atoms) unit cell the silicon structure of a tetrahedral network contains regular cavities with distortion of bond angles and lengths from the usual diamond structure. The alkali atoms occupy partially the sites in the centres of the large clathrate cages. There has been considerable interest in the clathrate structure as possible models for amorphous semiconductors [2]. The structures are

remarkable in possessing the characteristics of the amorphous semiconductors [6] such as many five- and six- fold rings, distortion of bond angles and lengths, and large space or voids. This clathrate compound may appear to be an ideal material for investigating the magnetic properties related to the nature of alkali atoms in the compound and the metal non-metal transition[7].

1.2 IMPURITY BAND AND METAL NON-METAL TRANSITION IN HEAVILY DOPED SEMICONDUCTORS

Doping foreign atoms into semiconductors, the dopants make up as either the substitutional or interstitial impurities which depends on the properties of the dopants. In this section, we confine ourselves to discuss the substitutional impurity in the semiconductors.

Silicon and germanium are semiconductors which have an energy gap between the valence and conduction bands. The silicon atom has fourteen electrons ($3s^2 3p^2$). Every atom is bonded to four nearest silicon atoms by the sp^3 hybridization of the 3s-orbital and the three 3p-orbitals in which the electron charge density is greatest in the direction of the nearest neighbouring atoms. Each of these four equivalent orbitals directs toward the corners of a regular tetrahedron.

Substitution of the host atoms in silicon by elements from the fifth column of the periodic table leaves the tetrahedral coordination structure intact. The substitutional impurities of the fifth column have five valence electrons. Four of these will combine with the unpaired electrons from the four nearest host atoms to make up four valence bonds, with the fifth electron weakly bonded to the guest atom.

The impurity thus acts as a donor of an electron which is then available for conduction. Such a semiconductor is called n-type. The energy levels of the fifth electron of the guest atom occupy positions between the valence and conduction bands of the host crystal. For n-type material, the impurity energy level is close to the bottom of the conduction band within the energy gap, the separation being termed the ionization energy of the donors.

In lightly doped semiconductors, the interatomic separations of the impurities are large and the donors are essentially all isolated. As the density increases the donors are closer together but because of the completely random positioning of the donors, overlap of some wave-functions will be inevitably took place. Since the interactions between donors are short range, as the concentration increases, those donors come closer will be paired up and then tripled at higher densities. The effect of these short range interactions leads to the impurity energy levels being broadened and an allowed energy region (the impurity band) arises in the energy gap of the host crystal.

Impurity band semiconductors are thus of interest because, beside the ordered crystalline lattice of the host atoms, they contain a disordered lattice of substitutional impurity atoms whose intersite distances change with concentration. The combined effects of the disorder and the electron correlation of the donors in the impurity band have important rôles in the metal non-metal transition. The intrasite Coulomb repulsion of donor electrons leads to the impurity band being split into two Hubbard bands (Fig.1-1) separated by the Coulomb repulsion energy U. The lower Hubbard band consists of singly occupied impurity sites and the upper band consists of doubly occupied

sites in which the donor is negatively charged. This upper band is also called D^- band. For a compensated sample, the position of the Fermi level (E_F) is pinned at the level of the impurity band and it can be changed by changing the compensation ratio of the donor and acceptor concentrations. But for an uncompensated sample, the Fermi level lies at an energy half way between the donor and conduction bands.

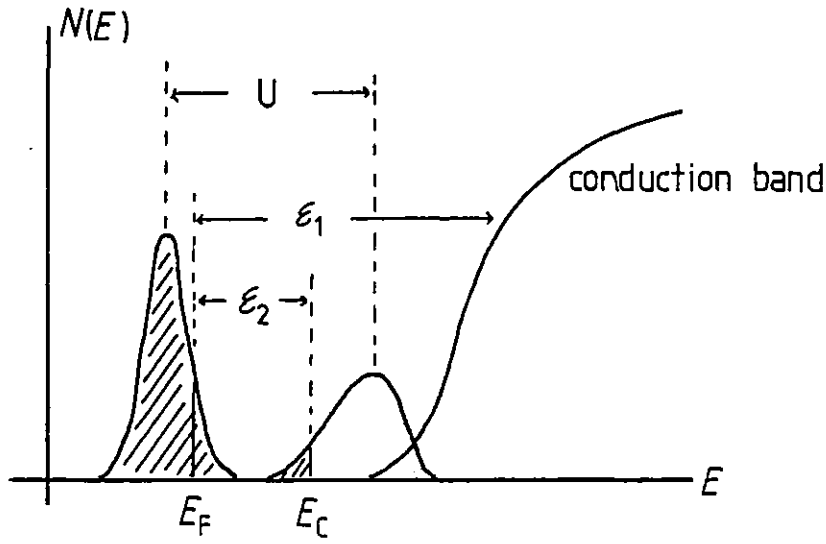

FIG. 1-1 Hubbard bands in doped semiconductor. Shaded regions are localized states.

The disorder in the impurity band causes an electron to be localised below the conduction band, hence, states in lower Hubbard band and the tail end of the upper band are localized. This form of localization is known as Anderson localization[2]. States above a critical energy E_C are non-localized; E_C is then called the 'mobility edge'.

At high temperatures, electron conduction takes place in the conduction band of the host atoms by ionizing the donor electrons with a thermal activation energy ε_1. The conductivity σ can be expressed

in the form

$$\sigma = \sigma_1 \exp\left(-\frac{\varepsilon_1}{K_B T}\right) \qquad \text{Eq.1-1}$$

There is one important conduction mechanism in doped and compensated semiconductors at low temperatures. A thermal activated hopping by electrons occurs between the ionized and neutral impurity centres, which are provided by compensation, in the localized states. The hopping activation energy ε_3 is caused by the random fields of the compensating impurities. The conductivity follows the form

$$\sigma = \sigma_3 \exp\left(-\frac{\varepsilon_3}{K_B T}\right) \qquad \text{Eq.1-2}$$

This form of electrical conduction has been extensively studied in gallium doped germanium (p-type) by Fritzsche[8](Fig.1-2). For low impurity concentration samples, a maximum of the Hall coefficient occurs at the temperature at which the two above conduction processes have equal magnitude.

As the impurity concentration increases the Hubbard bands will broaden, the upper band will merge into the conduction bands of the host atoms and then the two Hubbard bands will eventually merge. When the Hubbard bands have broadened, another form of conduction takes place. This is indicated by the presence of two Hall coefficient maxima as seen in Fig.1-2. For a compensated semiconductor the states near the Fermi level are localized. In this region, the electron is excited from a donor level to the mobility edge E_C in the upper band, the excitation energy ε_2 being $\varepsilon_2 = E_C - E_F$ [2]. This is the

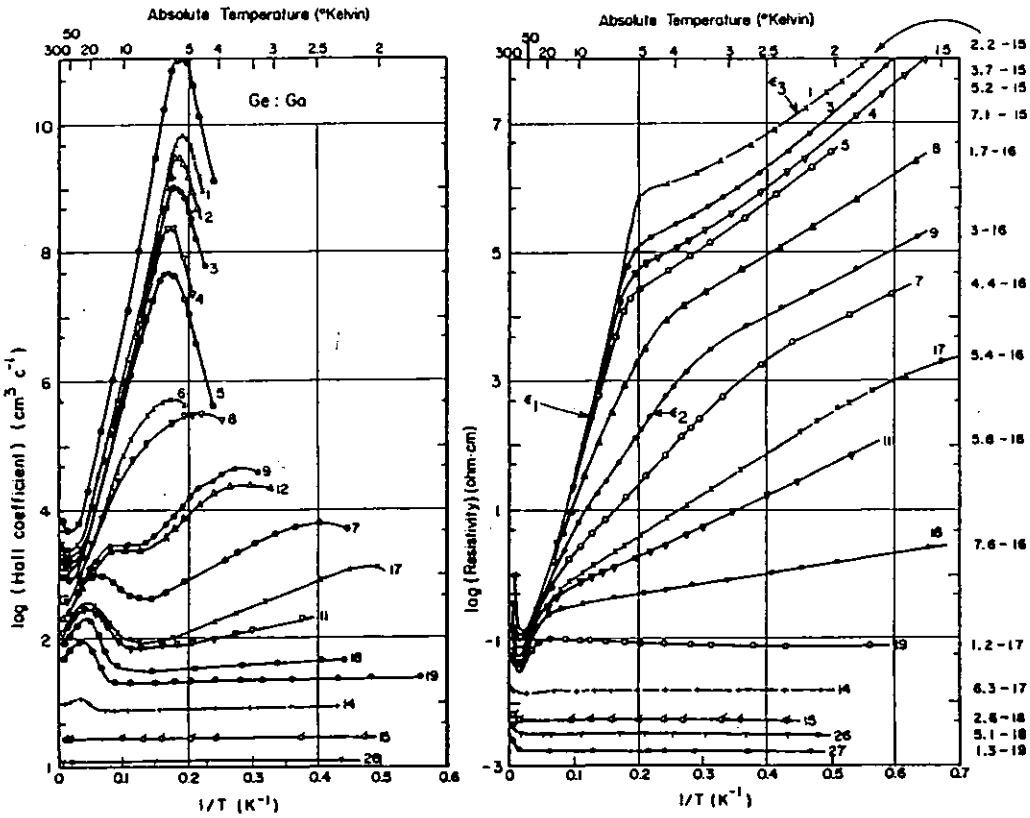

FIG. 1-2 Temperature dependence of Hall coefficient and resistivity of Ga doped Ge. Acceptor concentrations are marked on the right hand side using the code 1.2-17 = 1.2×10^{17} . (After ref. 8)

so-called impurity conduction, the conductivity has a form

$$\sigma = \sigma_2 \exp\left(-\frac{\varepsilon_2}{K_B T}\right) \qquad \text{Eq.1-3}$$

The change of impurity concentration can lead to a change of the positions of the Fermi level and the mobility edge. With increasing the concentration ε_2 decreases and finally becomes zero at certain concentration. A metal non-metal transition then occurs at this critical concentration n_c . At the impurity concentration below n_c, the density of states at E_F is sufficiently high, and all electrons are localized and they need thermal activation to move. In a limit of lower temperatures, conduction is governed by the variable range hopping. The conductivity σ is given by

$$\sigma = \sigma_0 \exp\left(-\frac{A}{T^{\frac{1}{4}}}\right) \qquad \text{Eq.1-4}$$

This is the Mott $T^{-\frac{1}{4}}$ law and A being a constant factor which depends upon the density of states at E_F . The impurity and variable range hopping conductions also occur in an uncompensated doped semiconductor only at the impurity concentration near the critical n_c. At this stage, the upper and lower bands have merged, the density of states at E_F is finite and the states are still localized. The metal non-metal transition occurs when $\varepsilon_2 = 0$. This has been observed in uncompensated phosphorus doped silicon[9,10]. The electronic specific heat coefficient γ (which is related to the density of states at the Fermi level) observed in phosphorus doped silicon[10 - 12] is shown to vary continuously over the metal non-metal transition region (Fig.1-3) and stays finite

even in the non-metallic region with the concentration $\simeq 0.5\,n_c$. The finite γ in non-metallic samples is evidence for the continuous spectrum of an ensemble of localized electrons. For samples with concentration $\geq n_c$, the coefficient γ varies as $n^{\frac{1}{3}}$ in agreement with the degenerate semiconductor picture[13] that the Fermi level lies inside the conduction band.

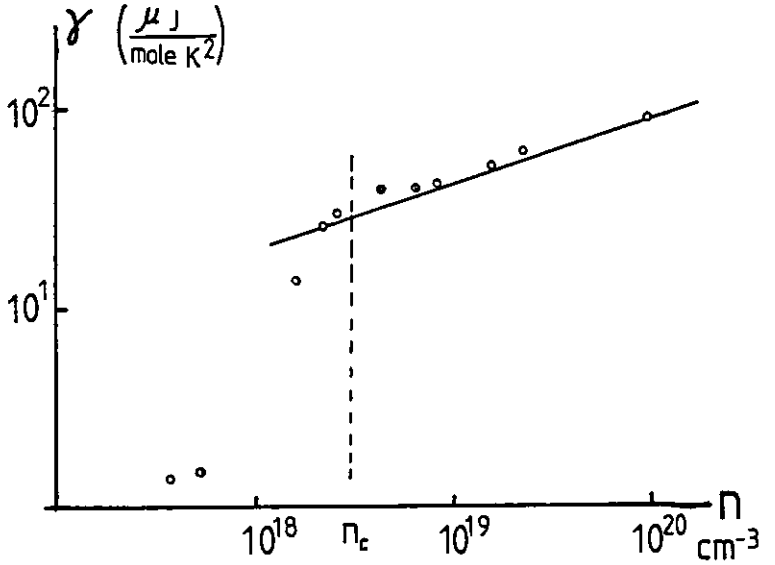

FIG. 1-3 Electronic specific heat coefficient as a function of donor concentration for phosphorus doped silicon.

For heavily doped semiconductors such as phosphorus doped silicon with impurity concentration higher than the critical concentration n_c ($\sim 4 \times 10^{18}$ cm^{-3}), the magnetic susceptibility is Pauli-like paramagnetic[10] and consistent with the experimental results of the specific heat and electrical resistivity: that a free-electron gas occupies the host conduction band. On the other hand, for concentrations $< n_c$, one observes a Curie-Weiss susceptibility but without any indication of a pure antiferromagnetic order transition

down to very low temperatures[14]. The reciprocal susceptibility plot curve goes to the origin as the temperature approaches zero (Fig.1-4).

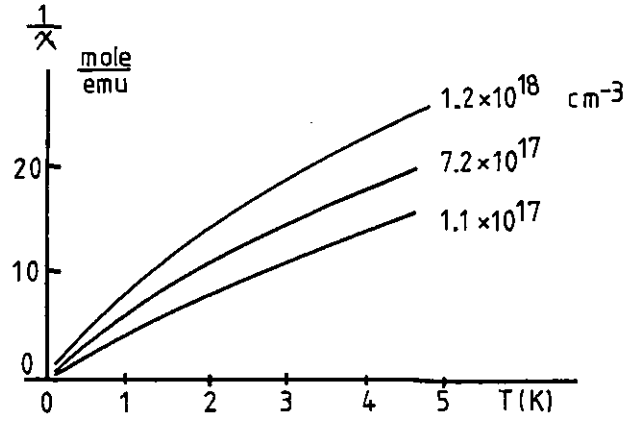

FIG. 1-4 Curie-Weiss plots of donor susceptibilities for the several concentrations of phosphorus doped silicon. (Ref.14).

Andres et al[14] interpret this characteristic downward curvature of the Curie-Weiss plots of phosphorus doped silicon as the combined effects of inter- and intra- cluster interactions. Because of random distribution of phosphorus atoms in silicon, the short range interaction of donors atoms leads to a very wide range of nearest neighbour interaction[15-18].

The features of the electron paramagnetic resonance spectrum for phosphorus doped silicon are extraordinary[19-28]. For very low phosphorus concentration ($\sim 10^{15}$ cm^{-3}) samples, the spectrum consists of two hyperfine split lines from the donor atoms (Fig.1-5(a)). In this region the donor electrons are well localized. When the impurity concentration increases to order 10^{17} cm^{-3}, the spectrum shows several extra resonance lines between the two hyperfine lines (Fig.1-5(b)). These resonance lines are formed because an electron can experience a

hyperfine interaction with two or more impurity nuclei. With a further increase in the donor concentration, the effect of dielectric screening due to the presence of the surrounding impurities also becomes stronger, the electrons start to be delocalized. As the result, the two hyperfine lines fade and the cluster resonance lines eventually merge and form a single sharp line (Fig.1-5(c)&(d)). At even higher concentration ($> 10^{18}$ cm^{-3}), that is, in the metallic region, the resonance lines becomes broader as all donor electrons completely delocalize and move freely throughout the entire crystal with metallic conduction as a result. Morigaki and Maekawa[20] have

FIG. 1-5 EPR SPECTRA FOR Si:P

(a) $n = 7 \times 10^{15}$ cm^{-3}. Localized states for hyperfine lines of phosphorus.

(b) $n = 3 \times 10^{16}$ cm^{-3}. Cluster centres of phosphorus atoms.

(c) $n = 5 \times 10^{17}$ cm^{-3}. Hyperfine lines fade and all the clusters merge to form one single line.

(d) $n = 1.7 \times 10^{18}$ cm^{-3}. One sharp resonance line.

(e) $n = 1.7 \times 10^{18}$ cm^{-3}. Two resonance lines as seen in high frequency (46 GHz).

reported that at the transition region from non-metallic to metallic type of impurity conduction (1.7×10^{18} cm^{-3}), the single line can be resolved into two sharp resonance lines (Fig.1- 5(e)) separated by 0.8 gauss (the resonance frequency being 46 GHz). They interpreted these being caused by the two different kinds of donor cluster which form in the non-metallic and metallic region of the crystal.

1.3 ALKALI METAL DOPED SEMICONDUCTORS

There have been few investigations on alkali metal doped silicon and germanimum over last two decades. The alkali metals such as lithium, sodium, potassium and cesium do not substitute the host atoms but diffuse interstitially in the host crystal. The ground state excitation of the alkali donor electron are well understood in terms of the effective mass approximation [29]. The behaviour of alkali donors in silicon and germanium is quite different from substitutional dopants in doped semiconductors, in that they may be either electrically active or neutral [30]. Pell[31], Reiss and Fuller[32] have found out that lithium is an electrically active interstitial impurity in silicon with the ionization energy being 0.03 eV. Lithium[33] is doped in silicon as a compensator to improve the radiation stability of charged-particle detectors. However, the extremely high diffusion mobility of lithium reduces the thermal stability of such device.

Sclar[40] reported that cesium could be doped by diffusion of cesium from the vapour into silicon at 1100 °C resulting in donor concentrations as high as 10^{19} cm^{-3}. McCaldin and Widmer[34,35] have doped silicon with cesium and sodium by ion injection into silicon

crystal with sufficient kinetic energy to overcome the surface barrier to solution. The donor concentration as high as 10^{20} cm^{-3} could be obtained by this method. For the case of sodium doped silicon[35], the donor concentration droped from 10^{20} cm^{-3} at the surface to 7 x 10^{17} cm^{-3} at 0.2 μcm depth. McCaldin et al[36] prepared sodium doped silicon by diffusion of sodium from the vapour into silicon wafer at 800 °C for a week. They found that the sodium concentrations were of the order of 10^{17} cm^{-3} and the sodium atoms penetrated inathin (<50μ) surface layer; in the interior of the specimen, sodium concentrations were below 10^{15} cm^{-3}. They also found out that sodium donors were electrically inactive. In contrast, sodium donors doped by ion injection method acted as an effective donor. They concluded that sodium atoms enter silicon as an interstitial donor, the electrical property of sodium depended strongly on the method of doping.

Zorin et al[37,38] studied the properties of sodium and potassium doped silicon in which the dopants were doped by ion implantation (energy = 50 keV). The majority of alkali ions was located in a thin surface layer and they were electrically inactive, only a fraction of alkali atoms behaved like the donors with the ionization energy of 0.04 eV. The duration of annealing the ion implantation silicon sample has an effect on the surface conductance (Fig.1-6).

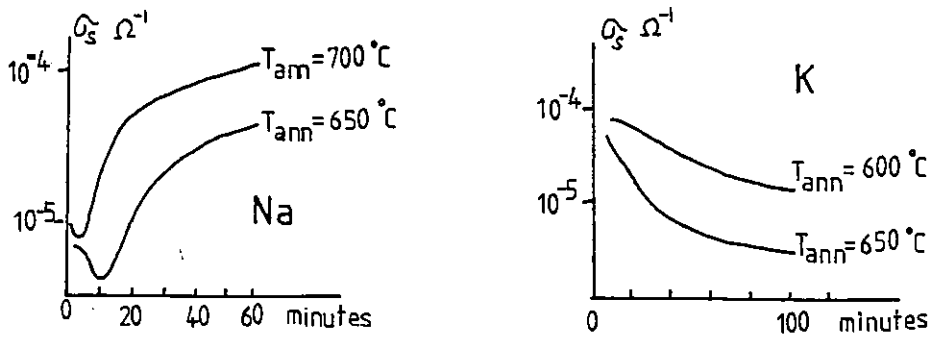

FIG. 1-6 Dependence on the surface conductance of sodium and potassium doped silicon of the duration of annealing t_{ann}.

The behaviour of surface conductance of sodium and potassium in silicon was quite different. Zorin et al considered that the decay of surface conductance with the duration of annealing in the case of potassium was probably due to the formation of electrically neutral potassium-vacancy complexes. In the case of sodium, annealing of radiation defects initially resulted in the formation of sodium-vacancy complexes, thus, surface conductance decreases. When the formation of sodium-vacancy complexes reached an equilibrium, the annealing of the remaining defects increased the surface conductance.

Alkali metal doped semiconductors are different in that the dopants do not form impurity band and show metal non-metal transition, contrary to substitutional doped semiconductors.

1.4 SODIUM TUNGSTEN BRONZE Na_xWO_3 AND CLATHRATE ALKALI-SILICON COMPOUNDS

Tungsten bronze, Me_xWO_3 where Me can be any alkali ion , bears a striking resemblance to heavily doped semiconductors such as phosphorus doped silicon which shows a metal non-metal transition[2,3]. There are many structural phases of the tungsten bronze, its structure depends on the nature and the concentration of Me[41]. Sodium can be introduced randomly into the vacant sites at the centre of WO_3 cages of the host material (Fig.1-7). The cubic phase crystal is stable at room

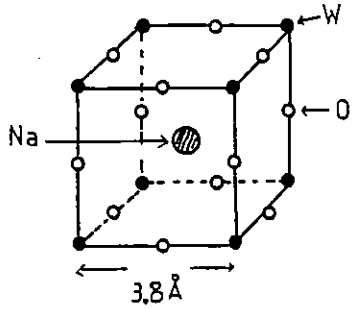

FIG. 1-7 A typical cubic lattice cell of Na_xWO_3 .

temperature only for $x > 0.5$. McNeil and Conroy[42] found that metastable cubic crystals can be prepared in the composition range between 0.2 and 0.45 by quenching from high temperatures.

The electrical resistivity as a function of x ($0.22<x<0.9$) has been measured at room temperature[42,43] . The resistivity is high, $\sim 10^3$ $\mu\Omega$ cm at $x \sim 0.22$ dropping to 10 $\mu\Omega$ cm for higher values of x . This indicates that metal non-metal transition may occur at sodium concentration near $x = 0.2$. The electronic specific heat coefficient γ is linearly dependent upon the sodium concentration [44] (Fig.1-8). The experimental result is in conflict with the calculated result based on the nearly free-electron model[13]. According to this model, the electronic specific heat coefficient γ is proportional

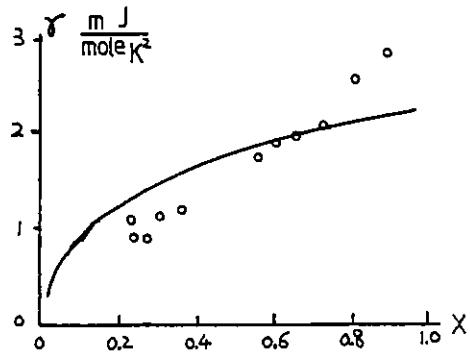

FIG. 1-8 Electronic specific heat coefficient γ versus concentration x. The solid line is predicted by the nearly free-electron theory.

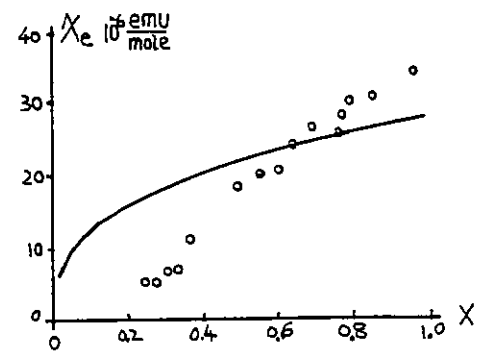

FIG. 1-9 Magnetic susceptibility χ_e versus concentration. The solid line is predicted by the nearly free-electron theory.

to $x^{\frac{1}{3}}$. The electronic specific heat coefficient of phosphorus doped silicon in metallic region also varies as $n^{\frac{1}{3}}$(donor concentration) in agreement with the nearly free-electron model. The paramagnetic

susceptibility χ_e due to the conduction electron in Na_xWO_3 as a function of the composition x (Fig.1-9) is in conflict with the predicted behaviour from the nearly free-electron model in which χ_e should be proportional to $x^{\frac{1}{3}}$. Zumsteg[44] interpreted the experimental result of a linear relationship between γ and x as follows. He considered that in Na_xWO_3 each unit cell contains a sodium atom being an isolated particle of metal with its Fermi energy the same despite the concentration of sodium. As the number of sodium atoms increases, the isolated cells form clusters. Eventually as the clusters grow larger with increasing concentration, they form a connected network of occupied neighbours. The Fermi energy remains constant with only the density of states at Fermi level increasing linearly with the composition x .

Clathrate alkali-silicon compounds are of interest because the structure possesses some remarkable characters such as distorted tetrahedral network contains regular large cavities; alkali atoms reside at the centres of the cages. There are two types of clathrate compounds. One consists of forty-six silicon atoms Me_8Si_{46} (A-type) and the other contains one hundred and thirty six silicon atoms Me_xSi_{136} (B-type). Both phases are cubic structure with big lattice spacing 10.19 Å and 14.62 Å respectively. In A-type clathrate, it contains the silicon structure of distorted tetrahedral network with regular cavities, the alkali atoms occupy all eight metallic sites. It is expected to be of metallic character[7]. B-type clathrate is more interesting because in many of the cages, most of the metallic sites are vacant, the alkali atoms are randomly distributed. The composition of alkali atoms varies from one to twenty four (fully

occupied) in a unit cell. The arrangement of silicon atoms in five- and six- fold rings with distorted bond angles and lengths looks disorderly but on the large scale the structure of the compound is truely periodic. The short range disorder and long range order are unique in the clathrate structure. These characters are different from the heavily doped semiconductors in which the structure being short range order but long range disorder. The clathrate compounds (B-type) may bear resemblance to heavily doped semiconductors in the metal non-metal transition character[7]. One might expect the electrons to move in extended orbits around the isolated alkali atoms, similar to the impurity band formed by heavily doped impurities in semiconductors.

CHAPTER 2

CRYSTAL STRUCTURE OF SODIUM - SILICON CLATHRATE COMPOUNDS

2.1 CRYSTAL STRUCTURE OF Na_8Si_{46} AND Na_xSi_{136}

Two alkali-silicon clathrate compounds, in which alkali atoms are enclosed in cages of silicon atoms, have been synthesized and their crystal structures have been characterized by the Bordeaux group [4,5]. Both phases are formed by thermal degradation of alkali-silicon compound MeSi (where Me = Na, K, Rb or Cs); one phase can be described by the formular Me_8Si_{46} (A-type) and the other as Me_xSi_{136} (B-type), where x is the composition of alkali atom in the compound. The maximum possible value of x in this Na_xSi_{136} compound is twenty-four, with the lowest value determined by the Bordeaux group being three. In both phases, the silicon atoms are fully bonded to each other in a tetrahedral network. The alkali atoms occupy either fully (A-type) or partially (B-type) the sites in the centre of the polyhedral cages.

The crystal structure of these two clathrate phases have been reported in great detail by Cros [48].

2.1.1 A-type clathrate Na_8Si_{46} phase

This Na_8Si_{46} compound has a cubic structure with a lattice parameter equal to 10.19 Å. The clathrate structure results from a periodic array comprising two pentagonal dodecahedra and six tetrakaidecahedra per unit cell. The former has twelve faces; the latter is composed of twelve pentagonal faces and two hexagonal faces on opposite sides (Figs. 2-1(a) & (b), Fig.2-2). Each silicon atom is tetrahedrally bonded with considerable distortion of bond angles which range between

$106^{\circ}15'$ and $125^{\circ}12'$ (cf. the undistorted tetrahedral angle is $109^{\circ}28'$). The silicon-silicon bond lengths are between 2.36 and 2.37 Å (in the elemental silicon bonding length is 2.35 Å)(TABLE 2-1). There are forty-six silicon atoms in a unit cell; the sodium atoms occupy the sites at the centre of the pentagonal dodecahedral, and tetrakaidecahedral cages. The former type of cage is smaller and the sodium atom contained within it (Me_1) is at a distance of 3.23 Å from eight of the silicon atoms (Si_2) and 3.37 Å from twelve others (Si_3). In the large cage (Me_2), the sodium atom is at a distance of 3.6 Å from four silicon atoms (Si_1), 3.79 Å from another eight (Si_2) and 4.41 Å from twelve others (Si_3).

2.1.2 B-type clathrate Na_xSi_{136} phase

This B-type clathrate compound also has a cubic structure with a lattice parameter equal to 14.62 Å. The clathrate structure results from a periodic array comprising sixteen pentagonal dodecahedra and eight hexakaidecahedra per unit cell; the latter has twelve pentagonal faces and four hexagonal faces (Figs. 2-1(a) & (c), and Fig. 2-3). There are one hundred and thirty-six silicon atoms per unit cell, each tetrahedrally bonded with angles which range between $105^{\circ}15'$ and $121^{\circ}47'$. The silicon-silicon bond lengths are between 2.32 and 2.40 Å (TABLE 2-2). The sodium atoms partially occupy the sites Me_1 and Me_2, shown in Fig.2-3, up to a maximum occupancy per unit cell of twenty-four. Kasper et al [5] have reported that , for $Na_{9.5}Si_{136}$, the ratio of distribution of sodium atoms in Me_1 and Me_2 sites is 1:4. The sodium atom in the small cage (Me_1) is at distance of 3.16 Å from two of the silicon atoms (Si_1), 3.26 Å from another six (Si_2) and 3.35 Å from

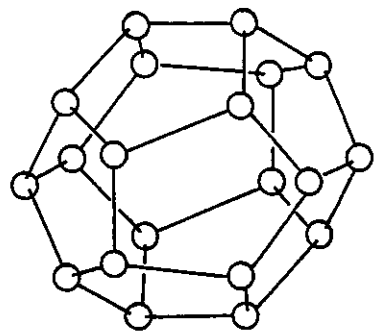

(a) Pentagonal dodecahedra - twelve pentagonal faces

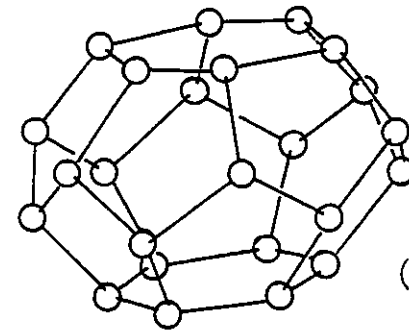

(b) Tetrakaidecahedra - two hexagonal faces and twelve pentagonal faces

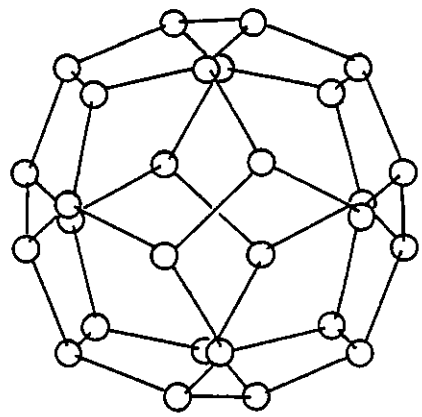

(c) Hexakaidecahedra - four hexagonal faces and twelve pentagonal faces

FIG. 2-1 BASIC ELEMENTS OF CLATHRATE STRUCTURES

TABLE 2-1 Na_8Si_{46} Phase Crystallography Data

Cubic			a = 10.19 ± 0.02 Å		
Space group			Pm3n		
Density			2.27 ± 0.01 g/cc		
Atomic positions :					
6	Si_1	(c)	1/4	0	1/2
16	Si_2	(i)	0.183	0.183	0.183
24	Si_3	(k)	0	0.310	0.116
2	Na_1	(a)	0	0	0
6	Na_2	(d)	1/4	1/2	0

Interatomic distances

d_1	$Si_1 - Si_3$	2.37 Å
d_2	$Si_2 - Si_3$	2.37
d_3	$Si_3 - Si_3$	2.36
d_4	$Si_2 - Si_2$	2.36
	$Na_1 - Si_2$	3.23
	$Na_1 - Si_3$	3.37
	$Na_2 - Si_1$	3.60
	$Na_2 - Si_2$	3.79
	$Na_2 - Si_3$	3.41
	$Na_1 - Na_1$	8.83
	$Na_1 - Na_2$	5.70
	$Na_2 - Na_2$	5.10
	$Na_2 - Na_2$	6.24

Bonding angles

α	$Si_3 - Si_3 - Si_2$	106°45'
β	$Si_3 - Si_2 - Si_3$	111°06'
γ	$Si_3 - Si_1 - Si_3$	109°36'
δ	$Si_1 - Si_3 - Si_3$	125°12'
ε	$Si_3 - Si_1 - Si_3$	109°24'
φ	$Si_1 - Si_3 - Si_2$	106°15'
θ	$Si_3 - Si_2 - Si_2$	107°46'

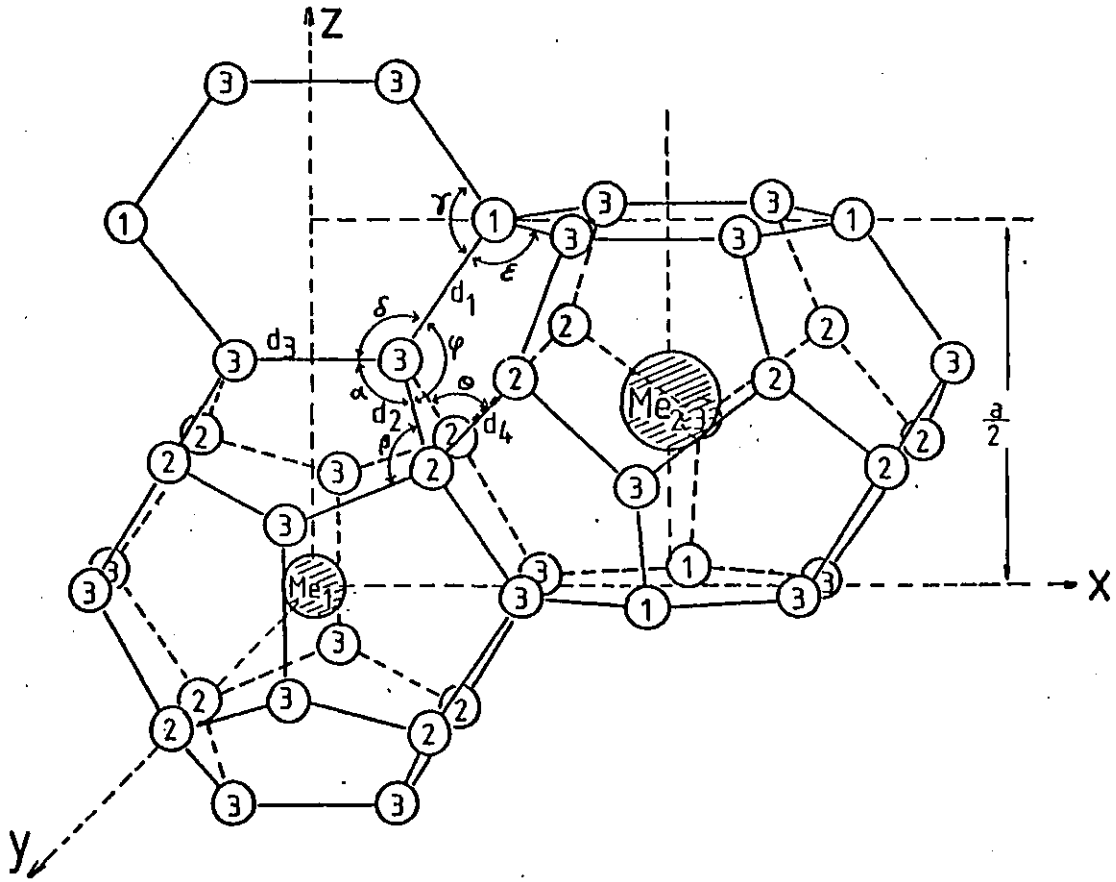

FIG. 2-2 Na_8Si_{46} Clathrate structure

TABLE 2-2 Na_xSi_{136} Phase Crystallography Data

Cubic		a = 14.62 ± 0.02 Å	
Space group		Fd3m (O_h^7)	
Density		2.03 ∿ 2.26 g/cc	
Atomic positions : (000),$(\frac{1}{2}\frac{1}{2}0)$,$(\frac{1}{2}0\frac{1}{2})$,$(0\frac{1}{2}\frac{1}{2})$ +			
8	Si_1	(a)	0 0 0 , 1/4 1/4 1/4
32	Si_2	(e)	x x x , x = -0.094
96	Si_3	(g)	x x z , x = -0.058 , z =-0.264
16	αNa_1	(c)	1/8 1/8 1/8 , 3/8 1/8 3/8 , 1/8 3/8 3/8, 3/8 3/8 1/8
8	βNa_2	(b)	1/2 1/2 1/2 , 3/4 3/4 3/4

α & β are the probabilities of occupancy of the sodium atoms in the cages

Interatomic distances

$d_1 = Si_1 - Si_2$	= 2.38 Å
$d_2 = Si_2 - Si_3$	= 2.34
$d_3 = Si_3 - Si_3$	= 2.40
$d_4 = Si_3 - Si_3$	= 2.32
$Na_1 - Si_1$	= 3.16
$Na_1 - Si_2$	= 3.26
$Na_1 - Si_3$	= 3.35
$Na_2 - Si_2$	= 3.95
$Na_2 - Si_3$	= 3.97
$Na_2 - Si_3$	= 3.85
$Na_1 - Na_1$	= 5.17
$Na_1 - Na_2$	= 6.06
$Na_2 - Na_2$	= 6.33

Bonding angles

$\alpha = Si_2 - Si_1 - Si_2$	= 109°27'
$\beta = Si_1 - Si_2 - Si_3$	= 106°45'
$\gamma = Si_2 - Si_3 - Si_3$	= 108°31'
$\delta = Si_3 - Si_2 - Si_3$	= 112°03'
$\varepsilon = Si_2 - Si_3 - Si_3$	= 105°15'
$\varphi = Si_3 - Si_3 - Si_3$	= 108°44'
$\theta = Si_3 - Si_3 - Si_3$	= 117°42'
$\eta = Si_3 - Si_3 - Si_3$	= 121°47'

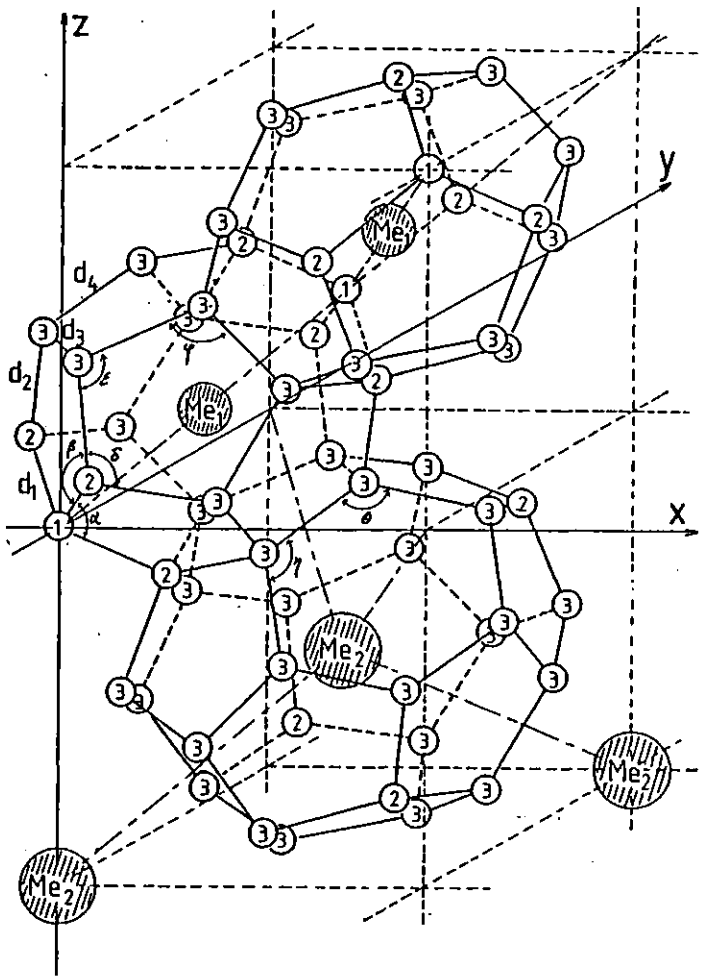

FIG. 2-3 Na_xSi_{136} CLATHRATE STRUCTURE

twelve others (Si_3). In the large cage (Me_2), there are four silicon atoms (Si_2) at a distance of 3.95 Å with another twenty-four (Si_3) distant by 3.85 and 3.97 Å .

2.2 PREVIOUS WORK ON SODIUM - SILICON CLATHRATE COMPOUNDS

There has been little experimental work on the sodium-silicon clathrate compounds since the Bordeaux group synthesized them. They measured the electrical conductivity of the compressed powder, the thermoelectric power, and the magnetic susceptibility of the compounds over a limited temperature range from 80 to 600 K [45].

Figure 2-4(a) shows the electrical conductivity measured by this group as a function of reciprocal temperature for Na_8Si_{46} and Na_xSi_{136} . They argued that Na_8Si_{46} had a zero activation energy and thus was a metallic compound; for the Na_xSi_{136} phase, they maintained the behaviour was like that of a doped semiconductor, the activation energy δE_D decreasing with increasing sodium concentration. Those interpretations are questionable. The conductivity of a compressed powder sample cannot be considered simply as a crystalline semiconductor with an impurity conductivity. Since these compounds are in the form of a powder, Mott [7] argues that the variable activation energy is due to the defects between grains of the material creating sufficient disorder to cause Anderson localization so that the conduction is by thermally activated hopping.

At high temperatures the thermopower becomes more negative with increasing temperature (Fig. 2-4(b)). Mott interprets this as a result of Anderson localization, therefore a small activation energy

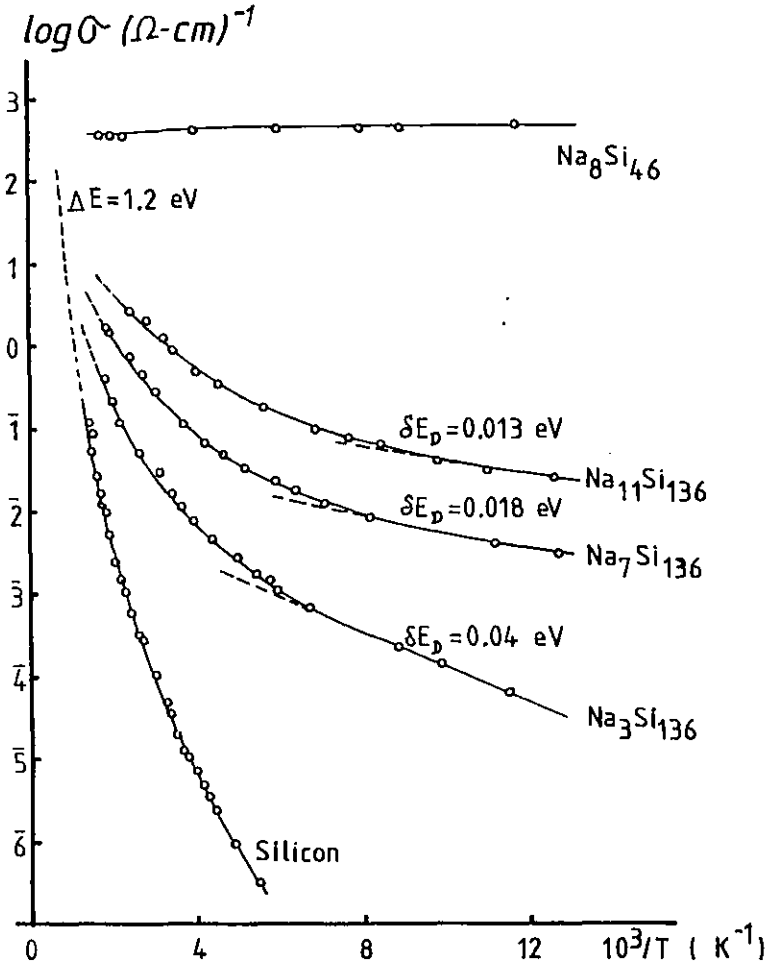

FIG. 2-4(a) Electrical conductivity of compacted Na_xSi_{136} samples (Bordeaux)

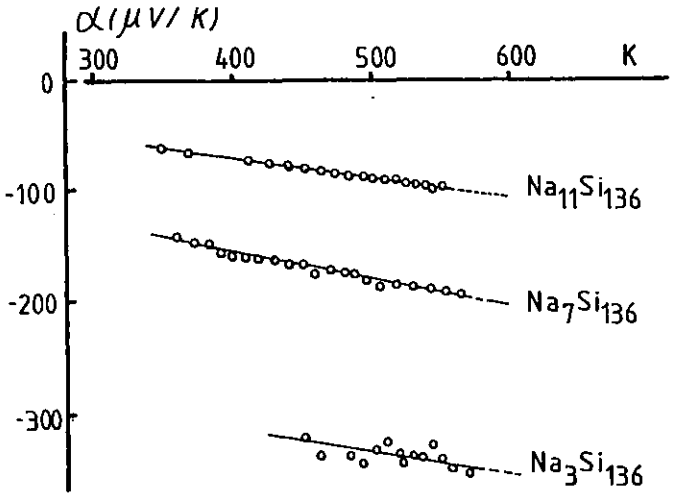

FIG. 2-4(b) Coefficients of Seebeck effect of Na_xSi_{136} (Bordeaux)

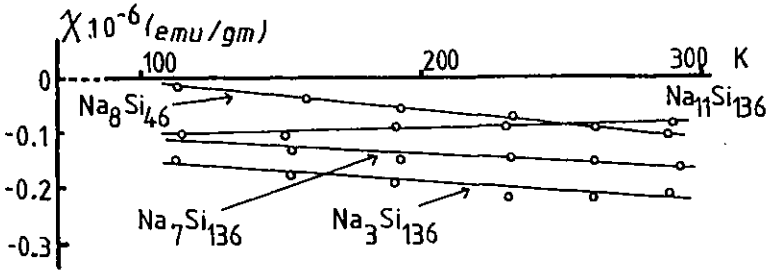

FIG. 2-4(c) Magnetic susceptibility of Na_xSi_{136} (Bordeaux)

and the associated thermally activated hopping will be observed in the conductivity.

The form of the sample does not matter in interpreting the magnetic susceptibility. The magnetic susceptibility of the clathrate compounds, which is of the form of a powder, in the temperature region 100 to 300 K is small and diamagnetic, with a value of around -10^{-7} emu-gram^{-1}. With the exception of $Na_{11}Si_{136}$, it decreases with increasing temperature (Fig. 2-4(c)). The susceptibility of Na_8Si_{46} is also diamagnetic.

Bundy and Kasper [49] have measured the electrical resistance of Na_3Si_{136} and $Na_{11}Si_{136}$ powder sample under high pressure up to 200 kbar. The resistance drops abruptly above 100 kbar. Under decompression it increases again although not to its original value, however, because Na_xSi_{136} materials lose their original crystalline clathrate structure during the process. The new crystal structure(s) have not yet been determined.

On the theoretical side, Henderson [50] has used the A-type clathrate structure as a simple model of amorphous germanium to calculate the radial distribution function and the electronic density of states. He considered that both amorphous germanium and A-type clathrate structure have distorted tetrahedral bonds, and five- and six-atoms rings. He found that the electronic density of states was similar to that measured for amorphous germanium. Weinstein [51,52] has reported that a statistical mixture of 60% Si III (a high-pressure metastable polytype of silicon) and 40% B-type clathrate structure provides a good fit to both the density of states and X-ray diffraction data of amorphous germanium and silicon. The latter also has distorted tetrahedral bonds with five- and six- atoms rings. Their works suggest similarities between the amorphous semiconductors and clathrate compounds.

CHAPTER 3

PREPARATION OF CLATHRATE Na_xSi_{136} COMPOUNDS

3.1 DRY BOX SYSTEM

The preparation of Na_xSi_{136} compounds is a straightforward but rather slow process. Since sodium reacts readily with water vapour, precautions have to be taken while handling it and, therefore, a dry box is essential equipment (Fig.3-1). Dry nitrogen gas was collected from a fifty-litre liquid nitrogen dewar, and stored in a gas reservoir (volume = 0.3 m^3). A twenty-Watt heater was installed in the dewar to increase the boiling rate of liquid nitrogen and build up a pressure of three and a half bars so that the nitrogen gas could pass through the relief valve (A) to the glove box. A regulator (B) could be opened when it was necessary to increase the flow. In order to maintain a low relative humidity, it was necessary to flush the dry box with nitrogen gas continuously for forty-eight hours before doing work in the box.

The glove box contains two parts : on the left is an air-lock compartment with an access door; on the right is the working area. Between them is a sliding door which must be closed when opening the access door. When materials such as sodium, silicon etc. were transferred to the air-lock compartment from the atmosphere, this compartment was quickly flushed with nitrogen gas by opening the solenoid valve (C) and adjusting the needle valve (D) to a suitable flow rate (normally twenty-five litres per minute). This flow was maintained for at least five minutes before moving the materials to

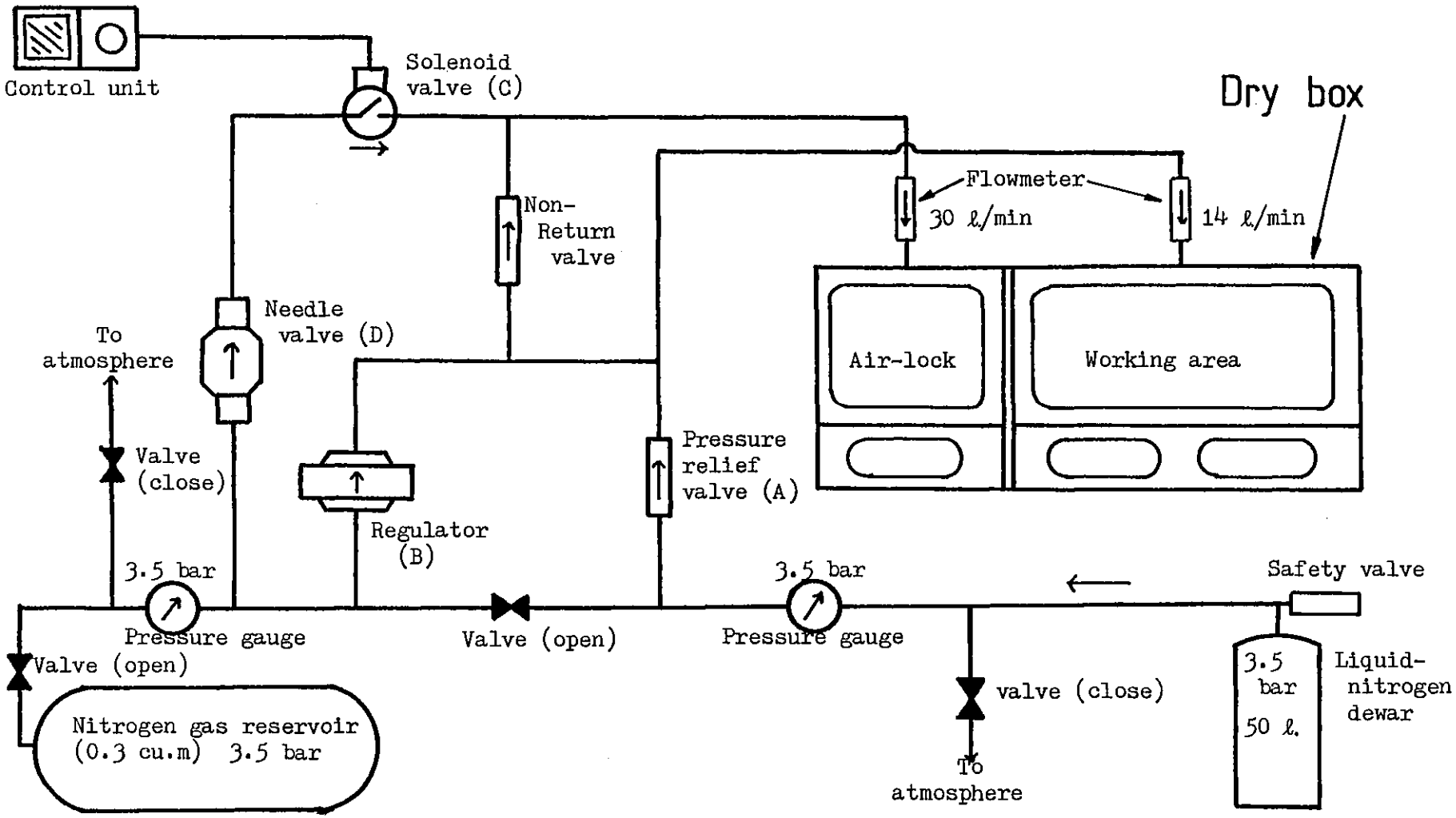

FIG. 3-1 DRY NITROGEN GAS GLOVE BOX SYSTEM

the working area and closing the sliding door. At this stage, the regulator was adjusted to allow more gas to flush the box at the rate of ten litres per minute. The humidity in the dry-box was measured with a hair-hygrometer, an instrument which is really designed to measure atmospheric humidity and is therefore rather insensitive in the low humidity conditions in which it was being used. Thus a typical reading of 4% relative humidity actually corresponded to 0.01% (as determined by a much more sensitive dew point meter). Sodium metal itself is a very good indicator of the humidity in the dry-box. If the metal quickly tarnishes from a silver-white colour, this indicates that the metal is reacting with water vapour in the air and hence that the humidity is too high.

3.2 SAMPLE PREPARATION PROCEDURE

A large lump of sodium (purity 3N) was removed from a beaker filled with paraffin oil and washed with low boiling-point (40 ^{o}C) petroleum ether which would evaporate quickly in the dry box. A small piece of high purity (6N, n-type) silicon wafer (about 3 grams) was washed with dilute hydrofluoric acid and distilled water and crushed into smaller fragments in a clean plastic bag with a heavy brass hammer. The clean silicon fragments and sodium were packed together in a tantalum pot and then covered with a tantalum cap. The advantages of using tantalum is that this material has a very high melting point, and sodium and silicon do not react with it. The amount of sodium was at least three to one by weight in favour of sodium for, during the process of solution to form NaSi phase at 700 ^{o}C, some sodium was lost by evaporation.

3.2.1 Dissolution - first stage in making NaSi phase compound

Two alternative methods - bomb method [46-48] and radio frequency (R.F.)induction method - were employed at the first stage to make NaSi compound. Silicon is dissolved in molten sodium at 700 °C to form NaSi phase, i.e.

$$Na_{(excess)} + Si \xrightarrow[\text{normal pressure}]{700\ ^{\circ}C} NaSi + Na_{(excess)}$$

Figure 3-2 shows the flow chart of the Na_xSi_{136} compound preparation procedure. Details of the method will be described in the following sections.

3.2.2 Bomb method

From the early experience in preparing NaSi compound, when the silicon and sodium were packed in a stainless steel bomb without using any sample pot, we found that the sample was contaminated with Si-Fe ferromagnetic alloy. The iron impurity was picked up obviously through contact with the walls of the bomb, therefore the sample must keep in a pot so that it would not contact the steel walls.

The clean silicon fragments and sodium were packed in a tantalum pot and covered with a tantalum cap. The pot rested upon a short length of stainless steel tube within a stainless steel inner

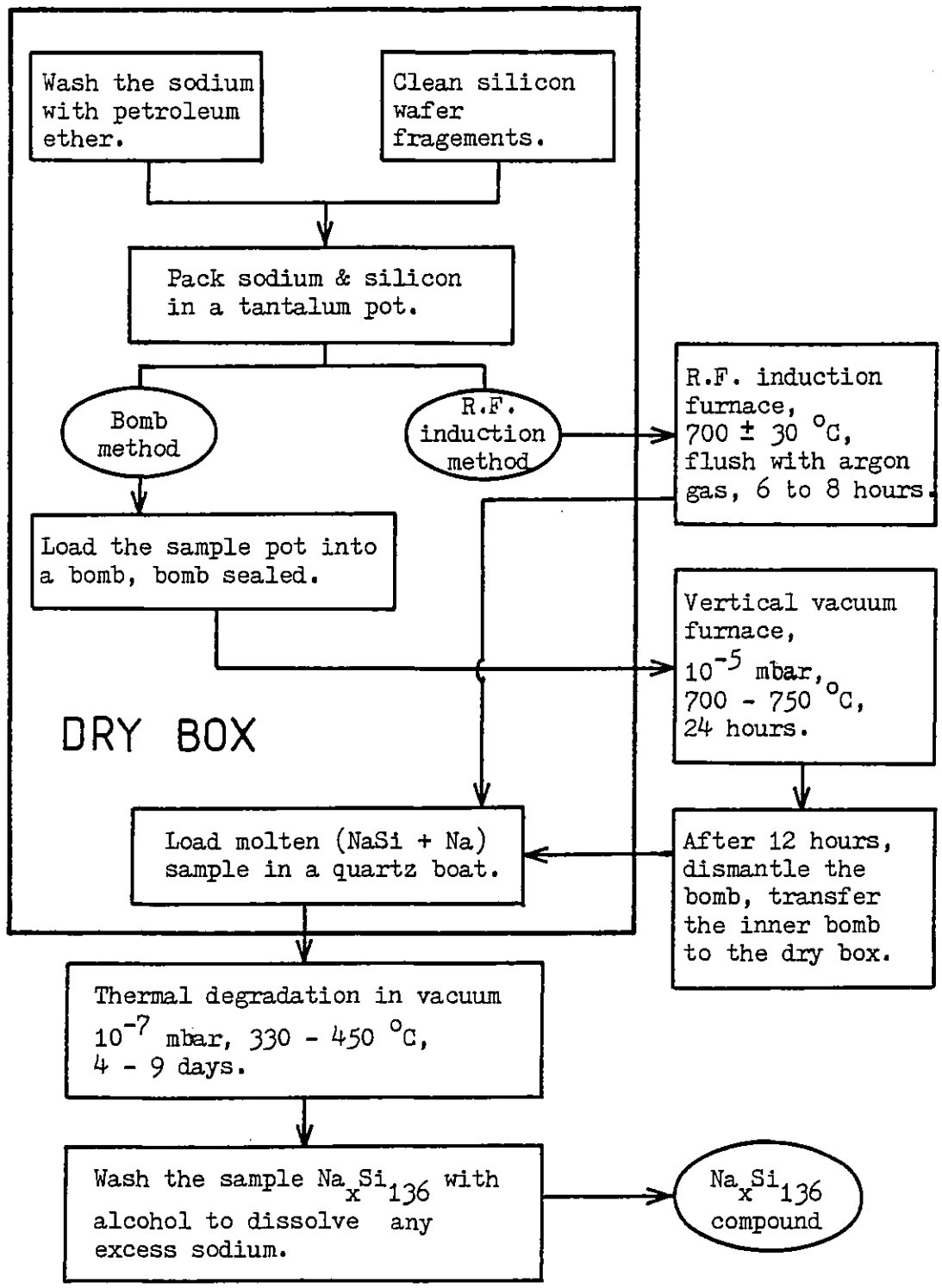

Fig. 3-2 Na_xSi_{136} sample preparation procedure.

bomb (Fig. 3-3). This tube thus created a cavity underneath the pot in which was collected the evaporated sodium that might otherwise re-enter the pot. This sodium had to be separated from the sample as it was contaminated with iron which was picked up through contact with the walls of the inner bomb.

The inner bomb was then loaded into an outer steel bomb and then locked in place by three pieces of steel at the tail of the outer bomb (Fig. 3-3). The inner bomb was then sealed by tightening the cap onto a soft nickel O-ring which had been annealed at 900 ^{o}C in vacuum for a couple of hours. The sealed bomb was removed from the dry-box and transferred to a vertical vacuum furnace (Fig. 3-4) for baking at 700 - 750 ^{o}C in a vacuum of 10^{-5} mbar for twenty-four hours. The quartz tube was maintained at a lower pressure than the bomb so that any sodium leaking from the bomb would not return and would, in fact, condense on the coolest part of the tube. After twenty-four hours the silicon and sodium solution formed NaSi compound. This NaSi is very sensitive to water vapour and therefore the tantalum pot had to be unloaded from the inner bomb in the dry-box.

3.2.3 Radio frequency (R.F.)induction furnace method

The tantalum pot, packed with sodium and silicon, was transferred quickly to the R.F. induction furnace from the dry-box. The tantalum pot was arranged so as to sit on a piece of quartz tube which supported it at the hottest part of the R.F. coil. The top of the pot again was covered by a tantalum cap (Fig. 3-5).

The furnace chamber was pumped by a rotary pump and flushed

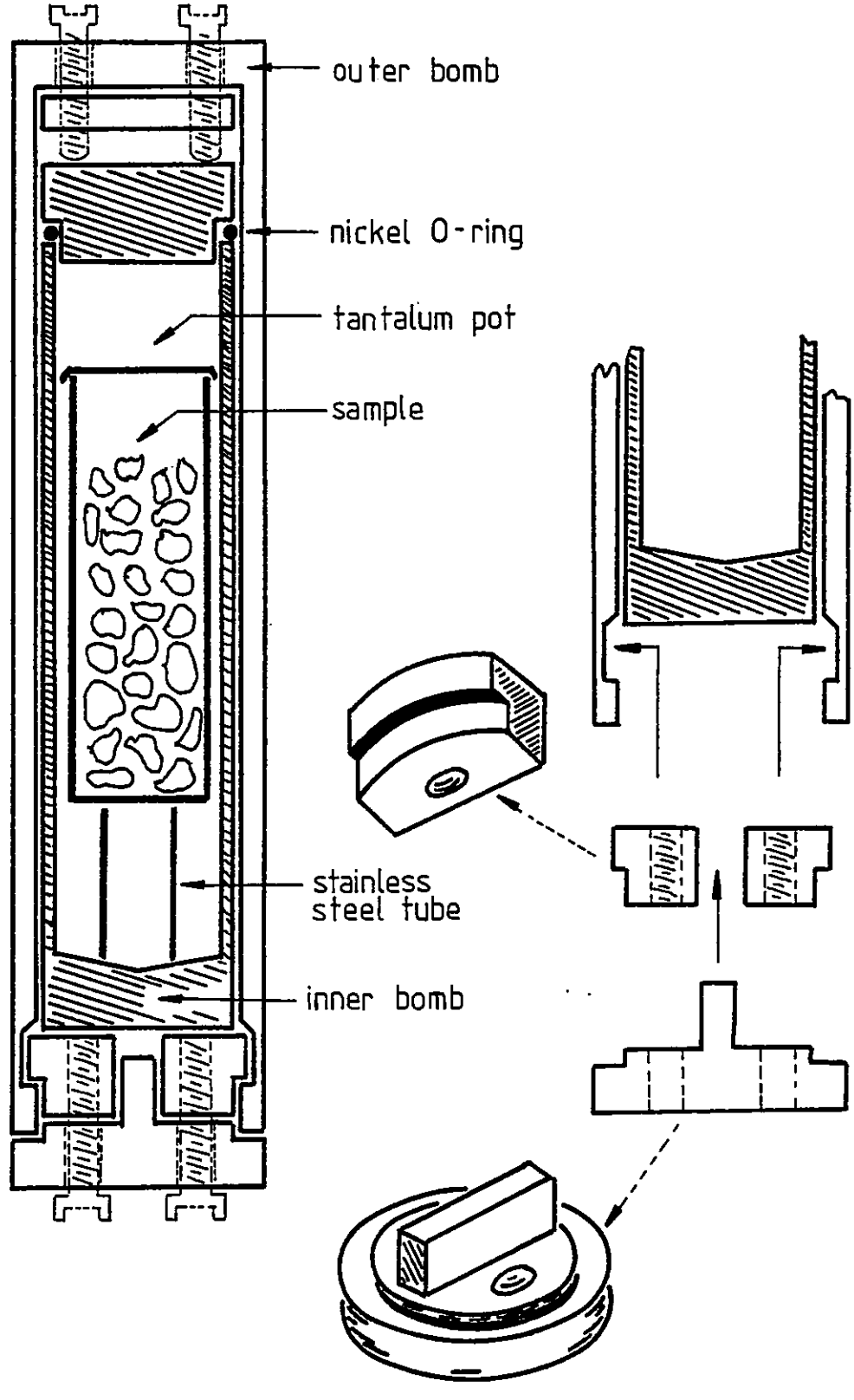

FIG. 3-3 STAINLESS STEEL BOMB AND TANTALUM POT

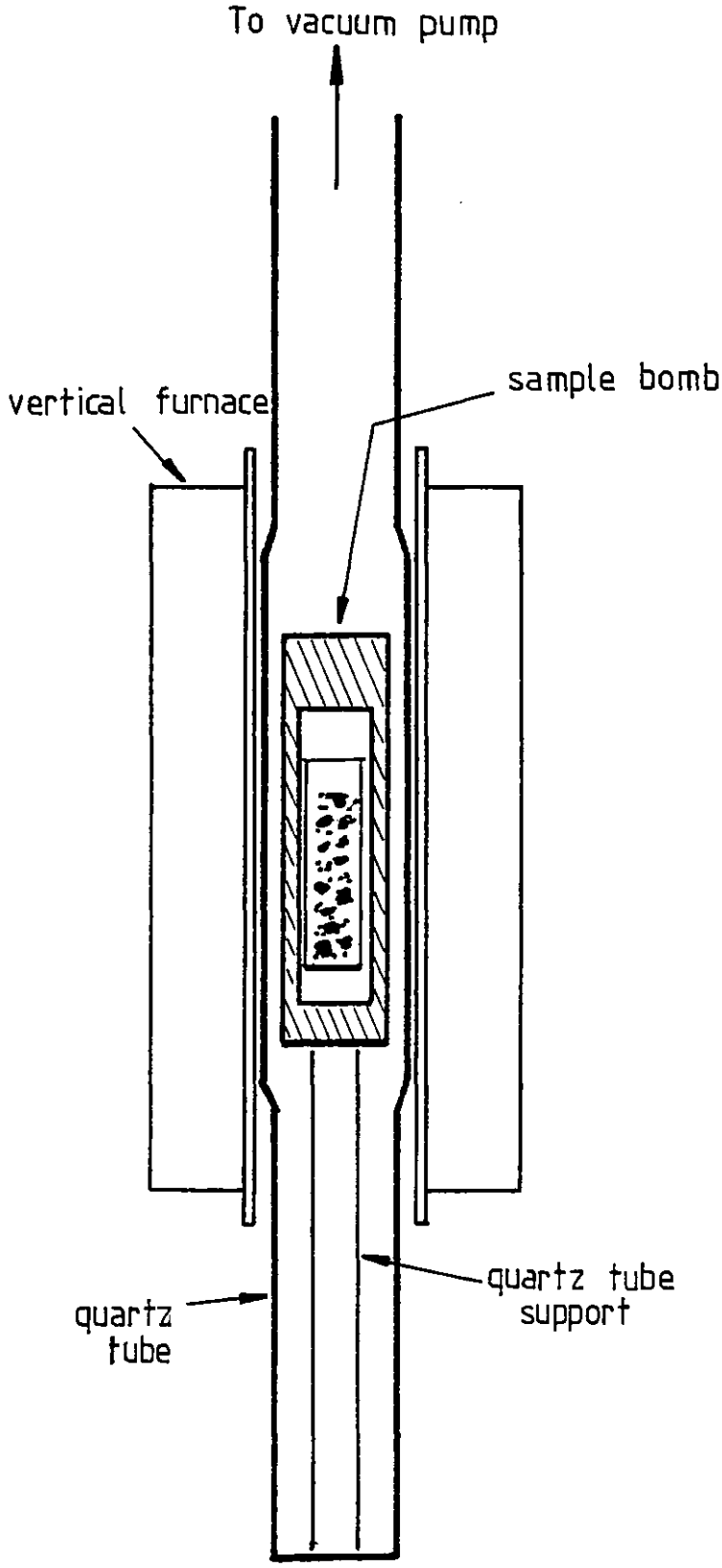

FIG. 3-4 VERTICAL FURNACE SYSTEM FOR PREPARING NaSi COMPOUND

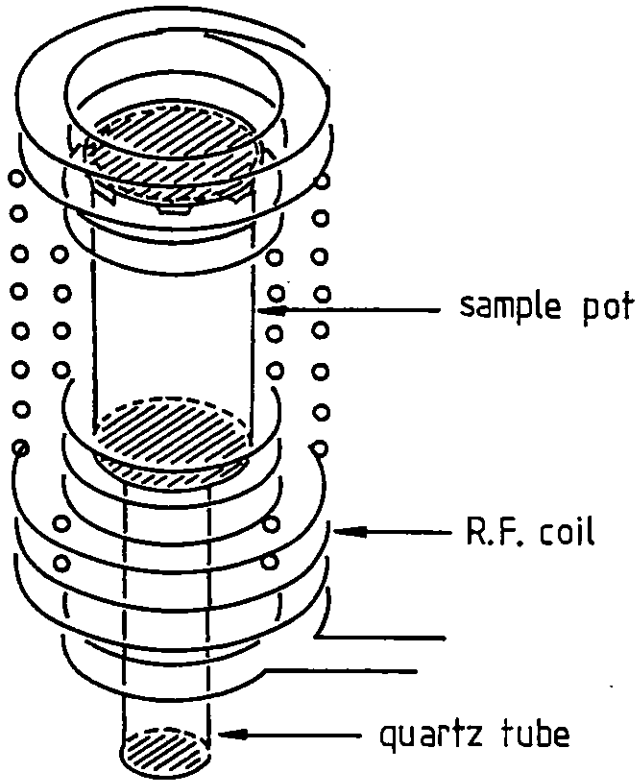

FIG. 3-5 RADIO FREQUENCY (R.F.) INDUCTION FURNACE

with argon gas four or five time to expel any residual water vapour from the furnace. Thereafter, the flow of argon was maintained at the rate of five cubic feet per hour. The furnace chamber wall was continuously water-cooled.

It took six to eight hours to complete the process of solution to form NaSi compound at 700 ^{o}C. The working frequency of the furnace was between 1 MHz and 0.5 MHz. The temperature was monitored by an optical pyrometer and controlled by adjusting the power supply current. During the process, it was necessary to adjust the current frequently in order to maintain a stable temperature because the coupling capacity between the sample pot and the R.F. coil changed due to loss of sodium. Nevertheless the temperature was kept at 700 $\pm$ 30 ^{o}C. The evaporated sodium condensed on the cold wall of the furnace.

After the solution process was completed, the pot was left to cool down in the furnace for three hours and then it was transferred quickly to the dry-box to unload the sample NaSi + Na (excess).

In the bomb method, the sample was secure from being contaminated by water vapour when the bomb was transferred to and from the dry-box and the furnace. The process of forming NaSi phase was slow, and it was quite inconvenient to use great force in the limited space of the dry-box in order to open the cap of the inner bomb after processing because sodium wet the cap and the bomb from within. The second method (R.F.) had the advantage of being fast but needed intensive labour to monitor and stablize the temperature. The sample pot had to be exposed to the atmosphere when it was loaded and unloaded from the furnace, so that it was more susceptible to contamination by water vapour. We considered the bomb method was the best.

3.2.4 Thermal degradation of NaSi - second stage in making Na_xSi_{136} phase compounds

NaSi compound is very reactive with water vapour but it is stable at normal temperaturesup to 300 °C in a water vapour free environment or a vacuum. This compound itself is in the form of a powder. Because a lot of excess sodium accompanied it and wet the tantalum pot, in order to unload the sample the pot was heated on a hot plate to 150 °C (at which temperature the sodium metal melts). The molten sample was poured out into a 150 mm long quartz boat.

The sample boat was then removed from the dry-box and transferred quickly to a high vacuum horizontal furnace (Fig. 3-6). In the vacuum quartz tube, there was a protecting quartz tube with one end closed except for a small hole (~3 mm diameter). This tube protected the outer quartz tube from being attacked by the sodium vapour, thus preventing cracking. It also provided a cold surface onto which the vapour could condense, in this way protecting the vacuum pump.

The Stanton Redcroft low mass horizontal furnace had a very constant temperature over a central region of 200 mm within which the sample boat could be comfortably situated. The temperature variation with time of the furnace was not more than 2 °C.

The sample was kept at the desired temperature for four to nine days to complete the thermal degradation process :

$$NaSi + Na_{(excess)} \xrightarrow[10^{-7}\ mbar]{330\ -\ 450\ ^{\circ}C} Na_xSi_{136} + Na_{(distilled\ off)}$$

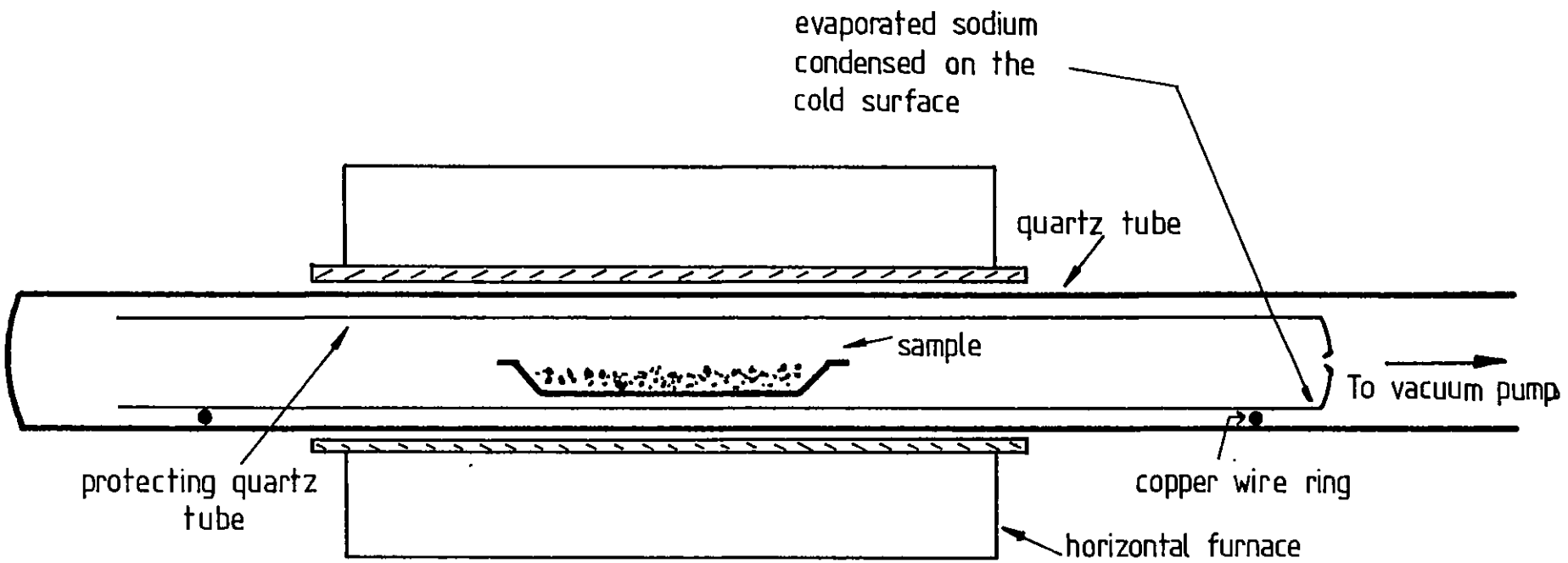

FIG. 3-6 HIGH VACUUM HORIZONTAL FURNACE SYSTEM FOR PREPARING Na_xSi_{136} COMPOUNDS BY DISTILLING EXCESS SODIUM FROM NaSi

The degradation temperature was an important factor which determined the composition of sodium in the compound (see §3-4); a lower temperature would cause a higher concentration of sodium. The Na_xSi_{136} thus obtained was in the form of a powder.

3.2.5 Final stage - sample purification and cleaning

The chemical properties of the Na_xSi_{136} compounds are similar to those of ordinary silicon [4,5]. At temperatures above 450 °C, the compound decomposes gradually to pure silicon phase [48]. With these stable properties when exposed to the atmosphere, the purification process could be performed without using the dry-box.

Absolute alcohol (C_2H_5OH) was used to wash the Na_xSi_{136} sample in a quartz tube after the thermal degradation process was completed. This procedure dissolved any excess sodium which might have remained in the sample. The Na_xSi_{136} sample precipitated and then a pipette was used to suck away most of the alcohol. The sample tube under vacuum was gently warmed by a hot-air blower, so that the remaining alcohol was boiled off. The dry sample was poured out and any undissolved silicon wafer was removed. The undissolved wafer was the remains of big silicon fragment which could not be completely dissolved in sodium to form NaSi within twenty-four (by the bomb method) or eight hours (by R.F. method), it probably needed longer time to complete the process.

3.3 MAKING HIGH SODIUM CONCENTRATION Na_xSi_{136} SAMPLES

By thermal diffusion, it was possible to reintroduce sodium

back into the vacant metallic sites in the Na_xSi_{136} compound so that the concentration of sodium would increase. This was done with two samples for which the initial values of x were 2.8 and 18.7 (see §3-4).

An outline of the procedure is shown in Fig. 3-7. About one gram of the Na_xSi_{136} compound was packed in a 14 mm bore closed end quartz tube. Valve (A) was connected to the tube. A vacuum pump was connected to this valve and the tube was pumped and, at the same time, heated up to 150 °C in order to bring about outgassing. The whole tube including valve (A) was transferred to the dry-box. Here the valve was temporarily disconnected and about two grams of sodium metal were also inserted in the tube, the two compounds being kept apart by a constriction (Fig. 3-8). Valve (A) was then reconnected and the sample tube removed from the dry-box and connected to the horizontal furnace vacuum pump. It was necessary to rough pump initially through the needle valve in order to prevent the powder sample from being sucked into the sodium compartment or the pump. The tube was heated at 200 °C for a period of six hours at about 10^{-7} mbar in order to outgas so that the vapour pressure in the tube was very low. This reduced the scattering rate of sodium atoms with other molecules/residual in the tube. The tube was then sealed. It was left in the horizontal furnace at 310 °C for twenty-four hours and the tube rotated about its axis occasionally. This ensured that the sodium entered the sample evenly.

The amount of sodium which diffused into the compound was found to depend on the residual pressure, the temperature, the length of time and most importantly, the diameter of the constriction. If the constriction was too small, insufficient sodium vapour would diffuse into the compound section. This had the additional disadvantage that

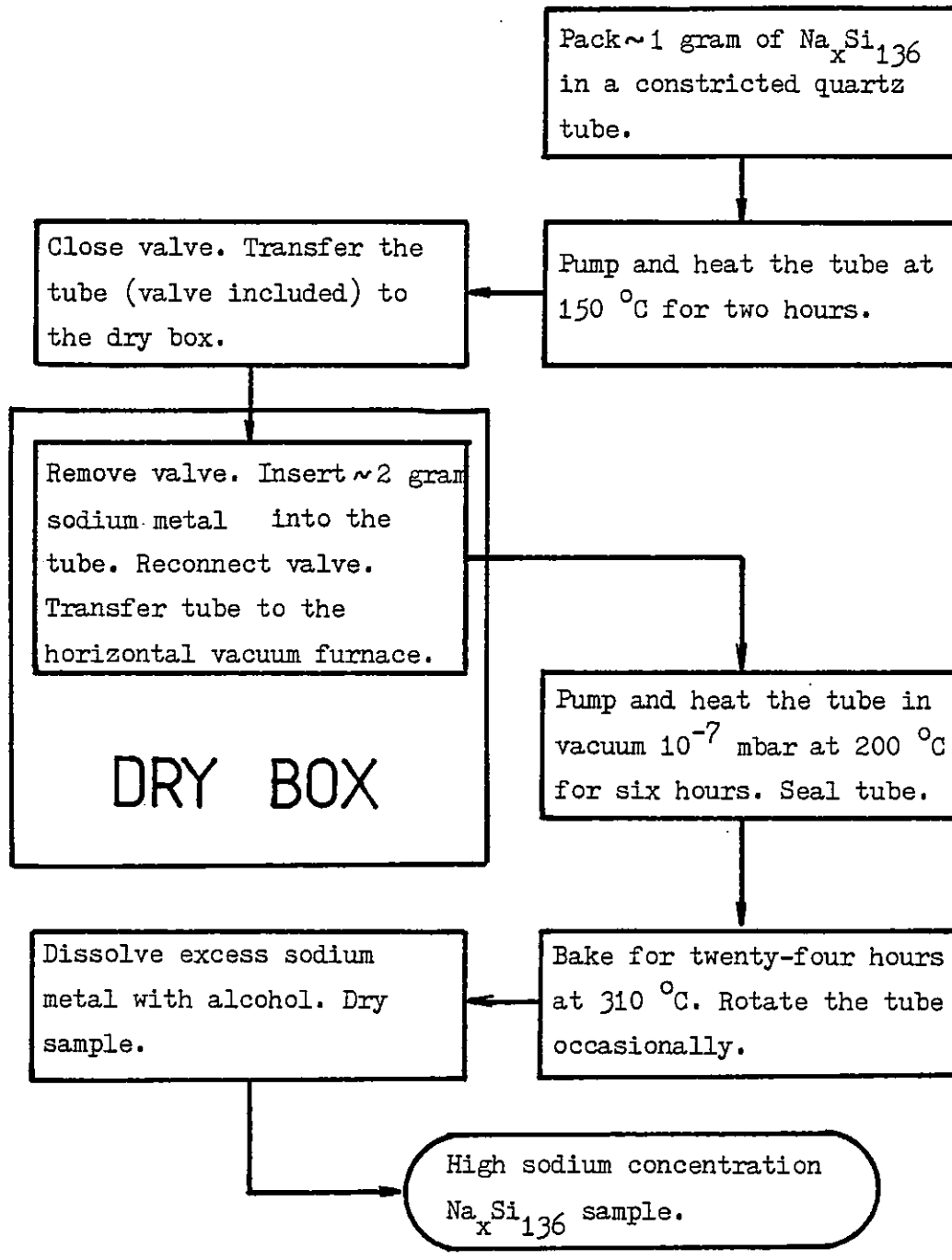

FIG. 3-7 PROCEDURE FOR PREPARING HIGH SODIUM CONCENTRATION Na_xSi_{136} BY THERMAL DIFFUSION METHOD

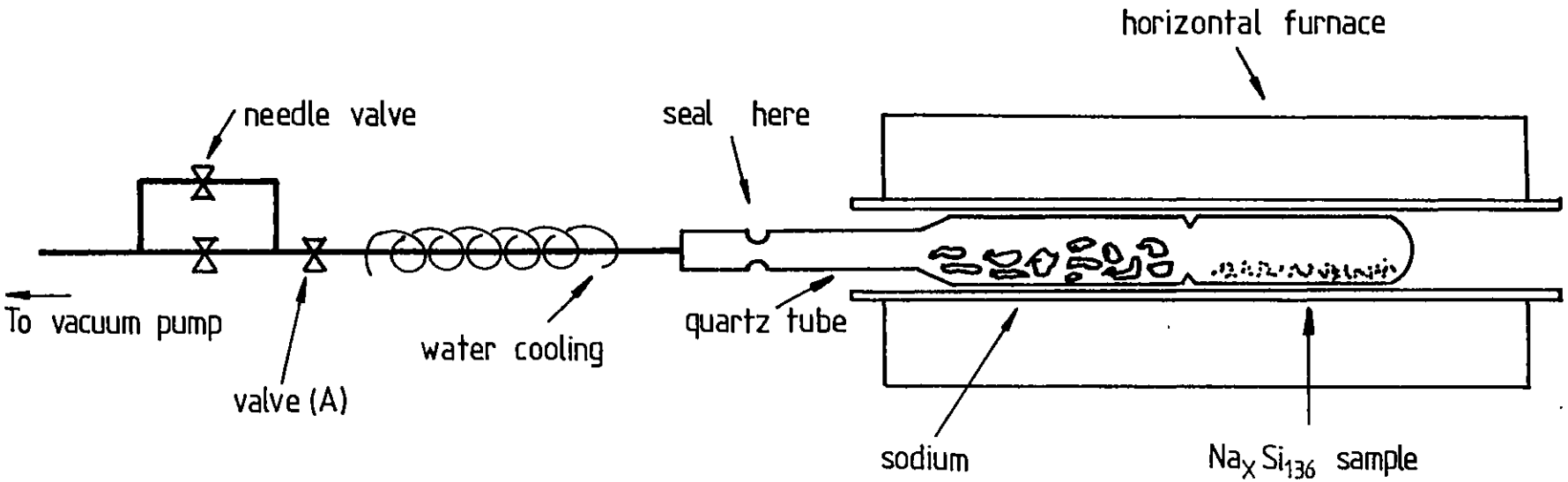

FIG. 3-8 APPARATUS FOR DIFFUSING SODIUM BACK INTO $Na_X Si_{136}$ SAMPLE TO INCREASE ITS SODIUN CONCENTRATION

most of the sodium was available to attack the quartz tube wall and cause cracking. After several attempts, it was found that a diameter of 10 mm was sufficient to allow most of the sodium vapour to diffuse into the sample.

The sample was then purified and cleaned as described in §3.2.5.

3.4 SAMPLE CHARACTERIZATION

Ten Na_xSi_{136} samples were prepared with different concentrations of sodium. Eight of them were prepared by thermal degradation at various temperatures (TABLE 3-1). Two samples (Nos. 20-D and 25-D)were prepared, beginning with samples 20 and 25 with initial x values 2.8 and 18.7 respectively, by thermally diffusing sodium back into the samples.

Each sample was examined by X-ray diffraction (Cu Kα radiation) using a Guinier camera and, in order to measure the line intensities, a diffractometer. X-ray diffraction analysis revealed that five of the samples (Nos. 20,20-D,26,25,25-D) were single phase - Na_xSi_{136} . Four of the remaining five (Nos. 9, 11, 13 and 15) contained a second phase - Na_8Si_{46} , with sample 13 also containing a pure silicon phase. Sample 12 was Na_xSi_{136} phase but also contained silicon phase. This sample was prepared at 450 °C, the contaminant silicon phase being due to decomposition of Na_xSi_{136} and, perhaps, remnants of undissolved silicon wafer. Since sample 13 was prepared at 425 °C which was below the decomposition temperature 450 °C of Na_xSi_{136} , the presence of silicon phase was probably brought about by remnants of undissolved silicon wafer. According to the Bordeaux group, single phase Na_xSi_{136}

TABLE 3-1 DETAILS OF Na_xSi_{136} SAMPLES, LISTED IN ORDER OF INCREASING SODIUM CONCENTRATION

Sample No.	Method of preparation of NaSi	Degradation temperature (°C)	Duration of degradation (days)	Vacuum pressure (10^{-7} mbar)	Composition (x) of Na_xSi_{136}	Other phases Si , Na_8Si_{46}
12	Bomb	450	8	2	1.5	Si
20	R.F. induction	445	4	4	2.8	
13	Bomb	425	9	4	4.5	Si, Na_8Si_{46}
15	Bomb	410	7	4	5.3	Na_8Si_{46}
20-D		Diffusion, 310	1	10	7.5	
26	Bomb	345	4	3	13	
9	Bomb	340	7	4	14	Na_8Si_{46}
11	Bomb	360	9	2	17	Na_8Si_{46}
25	R.F. induction	330	4	3	18.7	
25-D		Diffusion, 310	1	7	22	

compound is obtained by thermal degradation of NaSi under a vacuum of 10^{-5} torr; on the other hand, Na_8Si_{46} phase can only be prepared by thermal degradation of NaSi in an argon atmosphere at 410 °C for 200 hours. If the degradation temperature was increased to higher temperatures (420 to 455 °C), again in an argon atmosphere, a second phase - Na_xSi_{136} - would appear in the Na_8Si_{46} phase compound. The compound would eventually decompose to silicon phase at still higher temperatures. The reason for two clathrate phases coexisting in the samples prepared in vacuum is not fully understood. Perhaps portions of Na_xSi_{136} in which the available metallic sites are fully occupied by sodium can transform into Na_8Si_{46} phase after a long period of thermal treatment (7 to 9 days, for example, in the case of samples 9 and 11). It does seem from TABLE 3-1 that, in order to have a single Na_xSi_{136} phase sample, the distilling time should not be longer than seven days.

The concentration of sodium in the samples (Na_xSi_{136} phase) was determined by measuring the X-ray diffraction line intensities. Figure 3-9 shows the diffraction line intensity spectra of ten Na_xSi_{136} samples. The observed line intensities were obtained by measuring the areas under the diffraction lines (TABLE 3-2). The line intensities depend not only on the concentration of sodium in the sample but also on the distribution of sodium between the two types of cages in the Na_xSi_{136} clathrate compound. If α represents the number of Na_1 atoms per unit cell of Na_xSi_{136} (i.e. the occupancy of the Me_1 cages) and β the corresponding number of Na_2 atoms (the occupancy of the Me_2 cages), then

$$16\,\alpha + 8\,\beta = x \qquad \text{Eq.3-1.}$$

Hence the structure factor of Na_xSi_{136} is

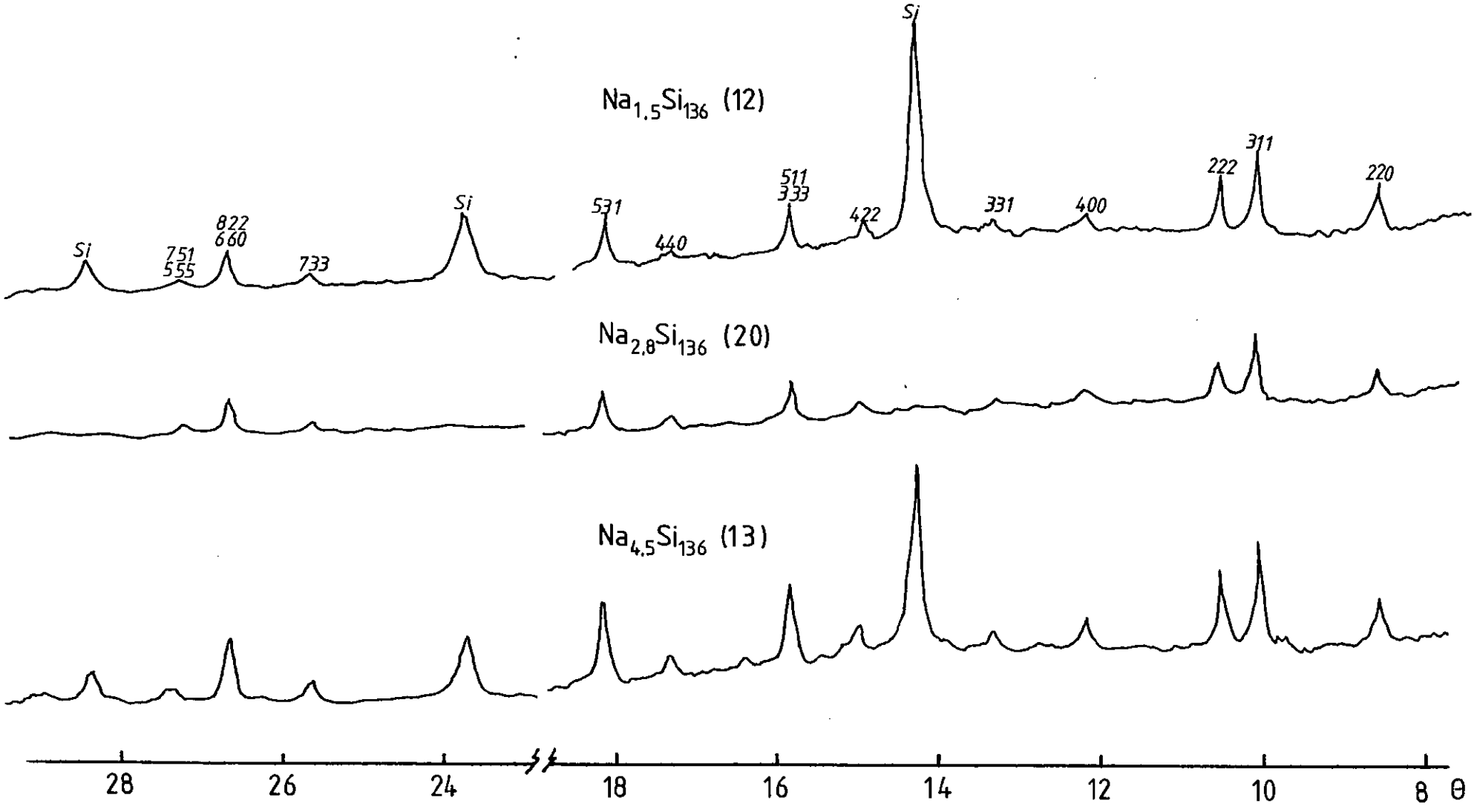

FIG. 3-9 X-RAY DIFFRACTION SPECTRA FOR Na_XSi_{136} (Si_{46} → Na_8Si_{46} phase; Si → silicon phase)

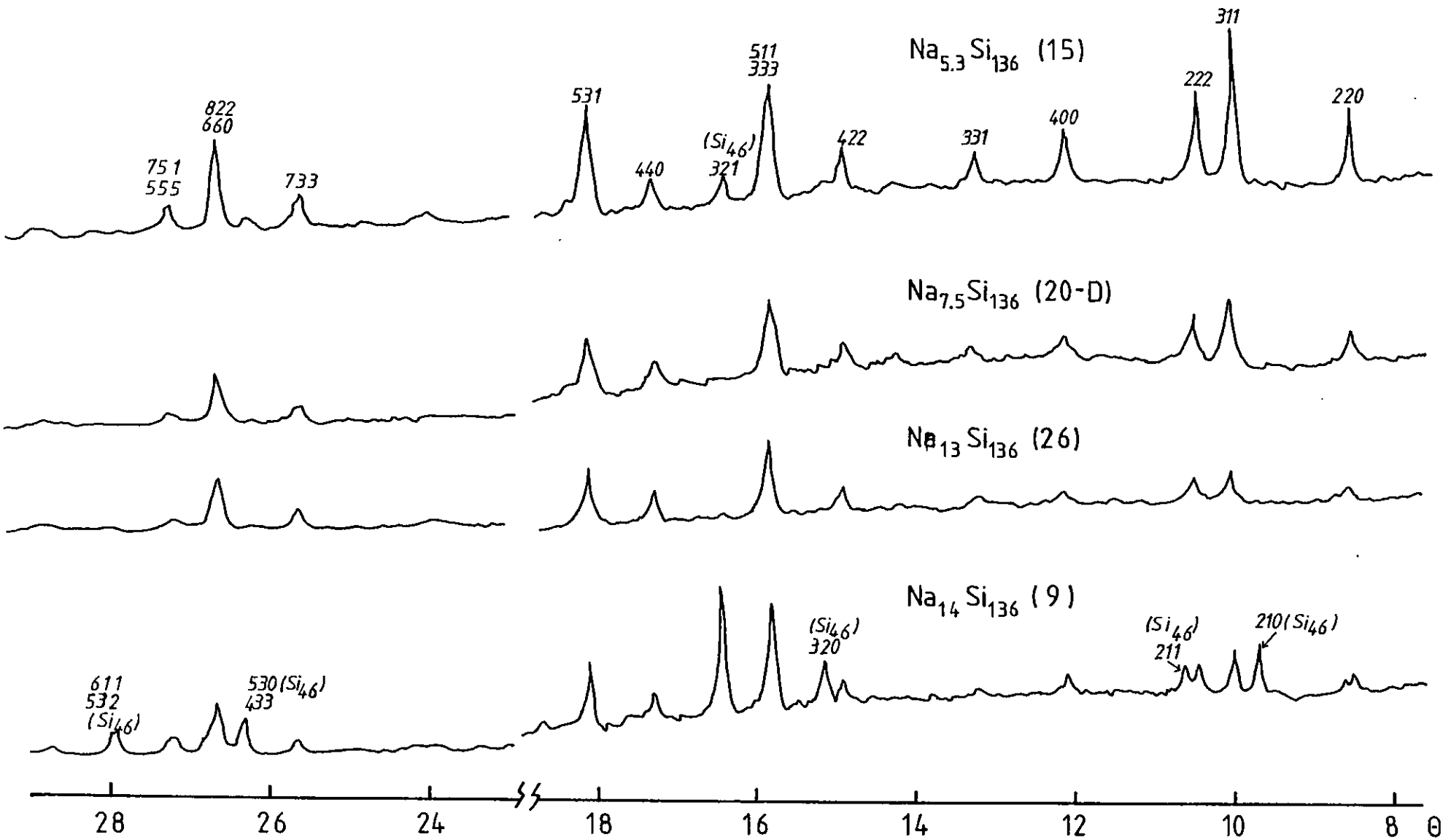
$Na_{5.3}Si_{136}$ (15)
$Na_{7.5}Si_{136}$ (20-D)
$Na_{13}Si_{136}$ (26)
$Na_{14}Si_{136}$ (9)
751
555
822
660
733
531
440
(Si_{46})
321
511
333
422
331
400
222
311
220
611
532
(Si_{46})
530 (Si_{46})
433
(Si_{46})
320
(Si_{46})
211
210 (Si_{46})
28
26
24
18
16
14
12
10
8
θ

FIG. 3-9 (cont.)

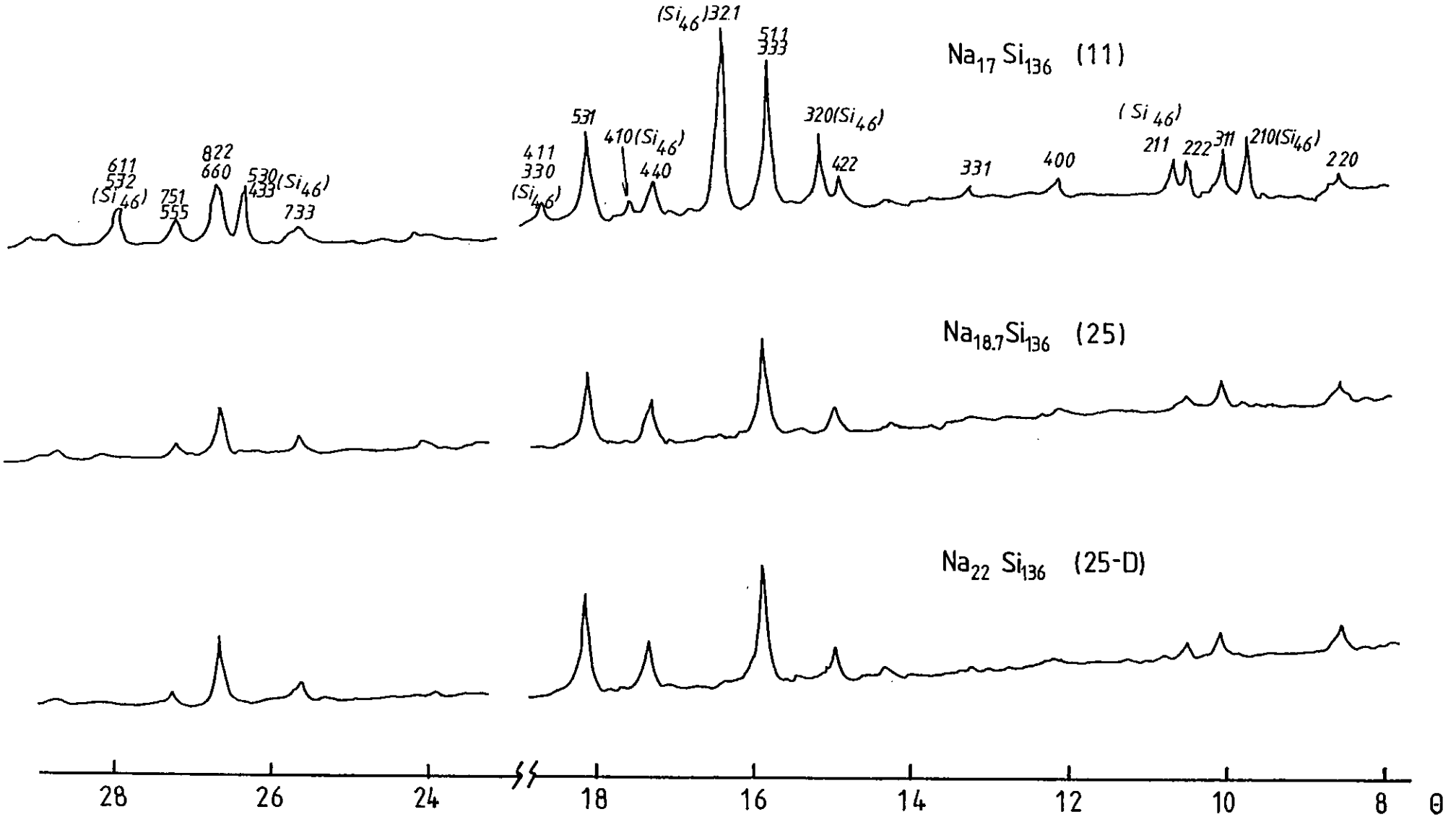
$Na_{17}Si_{136}$ (11)
$Na_{18.7}Si_{136}$ (25)
$Na_{22}Si_{136}$ (25-D)
611
532
(Si_{46})
751
555
822
660
530
433
(Si_{46})
733
411
330
(Si_{46})
531
410(Si_{46})
440
(Si_{46})321
511
333
320(Si_{46})
422
331
400
(Si_{46})
211
222
311
210(Si_{46})
220
28
26
24
18
16
14
12
10
8
θ

FIG. 3-9 (cont.)

$$F(hkl) = F_{Si_1} + F_{Si_2} + F_{Si_3} + \alpha F_{Na_1} + \beta F_{Na_2}$$

Eq.3-2

where F_{Si_1}, F_{Si_2} and F_{Si_3} are the structure factors for the three types of silicon in the compound, and F_{Na_1} and F_{Na_2} are the structure factors for the sodium (Fig. 2-3). The calculated intensity (53) is

$$I_{Cal} = |F(hkl)|^2 \times m \times L(\theta) \times A_o \times \exp\left[-2B\left(\frac{\sin(\theta)}{\lambda}\right)^2\right]$$

$$= I(\theta) \times \exp\left[-2B\left(\frac{\sin(\theta)}{\lambda}\right)^2\right] \qquad \text{Eq.3-3}$$

where m is the multiplicity factor, $L(\theta)$ the Lorentz polarization factor, A_o the absorption factor and the exponential term the Debye-Waller factor. The quantity B, which is called the temperature factor, depends on the amplitude U of thermal vibration of the atom :

$$B = 8\pi^2 \langle U^2 \rangle \qquad \text{Eq.3-4}$$

where $\langle U^2 \rangle$ is the mean displacement of the atom. The exact calculation of B as a function of temperature is extremely difficult. Debye has given an approximate expression :

$$B = \frac{1.15 \times 10^4}{A\ \theta_D^2} T \left[\Phi(X_D) + \frac{X_D}{4}\right] \qquad \text{Eq.3-5}$$

where $X_D = \frac{\theta_D}{T}$, θ_D being the Debye temperature of the substance,

A is the atomic weight of the element and

$$\Phi(x_D) = \frac{1}{X_D} \int_0^{X_D} \frac{\xi}{e^{\xi} - 1} d\xi$$

The function $\Phi(x_D)$ is tabulated in "International Tables for X-ray Crystallography", volume II [54]. Equation 3-5 applies only to elements with cubic crystal structure. It is impossible to calculate the temperature factor for the clathrate compound by using equation 3-5 because the Debye temperature θ_D is not known. The temperature factor B can be determined empirically as follows :

The observed line intensity is

$$I_{obs}(hkl) = K \times I(\theta) \times \exp\left[-2B\left(\frac{\sin(\theta)}{\lambda}\right)^2\right] \quad \text{Eq.3-6}$$

Taking logarithms of both sides

$$\log\left[\frac{I(\theta)}{I_{obs}(hkl)}\right] = \log\frac{1}{K} + 2B\left(\frac{\sin(\theta)}{\lambda}\right)^2 \log e \quad \text{Eq.3-7}$$

Therefore a plot of $\log[I(\theta)/I_{obs}(hkl)]$ versus $(\sin(\theta)/\lambda)^2$ should be a straight line. The slope of the line gives B, and the intercept provides the scale factor K which is proportional to $C\, I_o/v^2$ (where I_o is the intensity of incident X-ray beam, v the volume of unit cell, C the volume fraction of that phase in the compound). If the sample is single phase then C equal one.

A series of $I(\theta)$ for several important diffraction lines of Na_xSi_{136} was computed with the sodium component, x, varying from zero to twenty-four. The computer program for calculating the line intensity of Na_xSi_{136} listed in Appendix A-1. For each value of x, a series of possible values for α and β were chosen (according to Eq.3-1). The parameter B was obtained from a best linear fit of Eq.3-7 (Fig.3-11) by the iterative procedure as outlined in Fig.3-10. It was found that the temperature factor B was 6.5 $Å^2$. With this value of B, the calculated intensities were then normalised to line (511)-(333) (TABLE 3-2). Contrary to the results of the Bordeaux group [4,5,48], in none of the samples was the line (822)-(660) the most intense (TABLE 3-4). In fact, line (311) was the strongest for the low concentration samples (Nos. 12, 20,13,and 15); for the high concentration samples, line (511)-(333) became the strongest (Fig. 3-9 and TABLE 3-2).

The observed and calculated line intensities for Na_8Si_{46} phase in samples 9 and 11 were also calculated (TABLE 3-3). The computer program for calculating the line intensity of Na_8Si_{46} is listed in Appendix A-2. The temperature factor B was again approximately 6.5 $Å^2$, once more quite different from the Bordeaux group who obtained 1 $Å^2$ in both cases. The strongest intensity line was (321) which this time agreed with them.

A large temperature factor for our samples indicated that it might be caused by defects in the crystal so that the mean displacement of the atoms was bigger than that of the samples from the Bordeaux group. The cubic lattice parameters of Na_8Si_{46} and Na_xSi_{136} as determined by the X-ray measurements are 10.19 Å and 14.62 Å respectively which agree with the results of the Bordeaux group (see TABLES 2-2 and 2-3).

FIG. 3-10 ITERATIVE PROCEDURE FOR EMPIRICALLY DETERMINING THE TEMPERATURE FACTOR B AND THE DISTRIBUTION OF SODIUM BETWEEN THE $Me_1(\alpha)$ AND $Me_2(\beta)$ CAGES

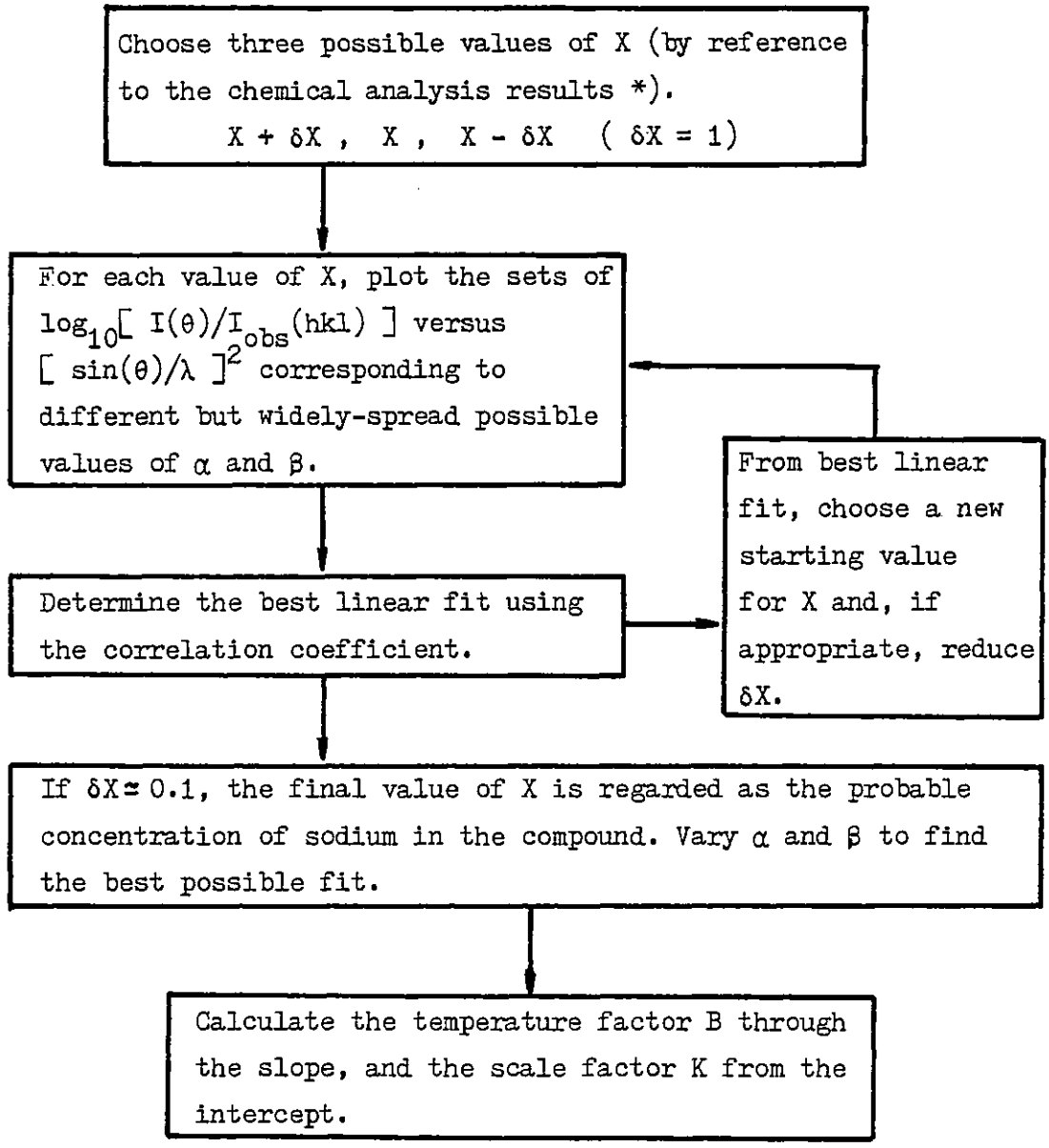

* Chemical analysis of sodium concentration were performed by the Analytical Service Laboratory of Imperial College.

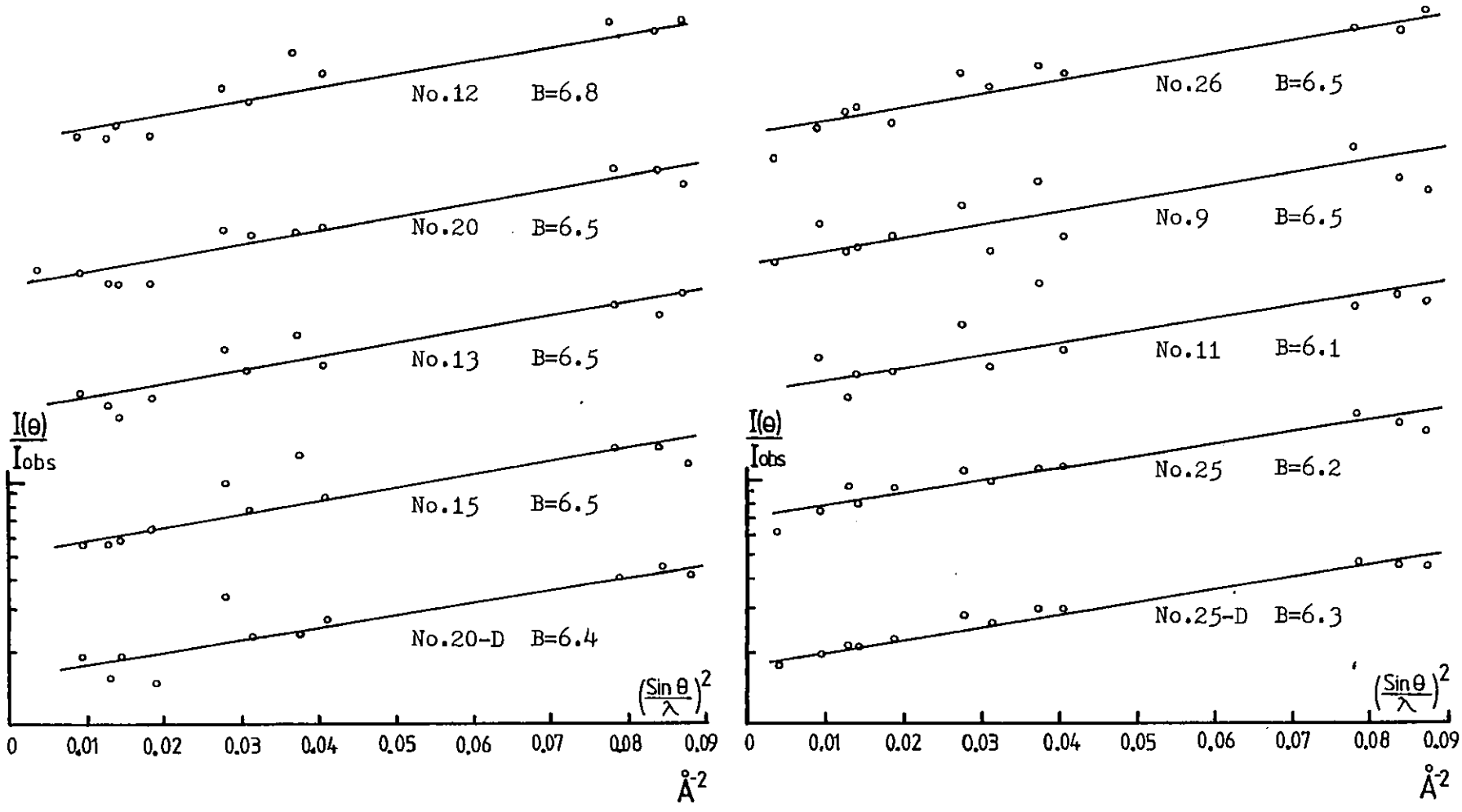

FIG. 3-11 EMPIRICAL DETERMINATION OF DEBYE-WALLER TEMPERATURE FACTOR FOR Na_xSi_{136} (For clarity, some of the plotted curves have been offset.)

TABLE 3-2 OBSERVED AND CALCULATED X-RAY DIFFRACTION INTENSITIES FOR Na_xSi_{136}

Sample No.	12		20		13		15		20-D	
h k l	I_{obs}	I_{cal}	I_{obs}	I_{cal}	I_{obs}	I_{cal}	I_{obs}	I_{cal}	I_{obs}	I_{cal}
* 1 1 1		41.1	28.7	29.8		22.6		19.7		12.7
2 2 0	94.1	87.3	76.2	70.1	51.7	56.8	55.4	50.9	32.6	36.8
3 1 1	165.0	145.8	157.0	127.0	116.3	106.6	109.0	97.0	89.1	76.4
2 2 2	85.2	84.3	101.0	80.7	91.5	73.9	76.8	70.9	59.8	63.7
4 0 0	39.5	33.4	47.0	35.5	39.3	35.6	37.1	35.6	49.6	35.9
4 2 2	30.9	36.3	35.7	39.5	32.2	41.8	31.5	42.8	33.6	45.7
511 - 333	100.0	100.0	100.0	100.0	100.0	100.0	100.0	100.0	100.0	100.0
4 4 0	26.0	37.7	39.4	38.1	29.4	38.7	25.4	39.0	42.3	39.7
5 3 1	106.0	118.7	105.7	104.4	101.7	93.3	90.2	88.6	75.8	76.3
7 3 3	32.2	36.5	41.8	35.7	35.5	34.3	35.3	33.6	34.5	32.0
822 - 660	100.0	94.9	101.1	92.5	106.6	89.1	96.5	87.6	87.1	83.7
751 - 555	28.0	29.2	35.5	27.4	25.9	25.4	34.0	24.6	27.0	22.4

(Relative intensities are normalized to line (511)-(333) , B~6.5 $Å^2$)

TABLE 3-2 OBSERVED AND CALCULATED X-RAY DIFFRACTION INTENSITIES FOR Na_xSi_{136}

Sample No.	26		9		11		25		25-D	
h k l	I_{obs}	I_{cal}	I_{obs}	I_{cal}	I_{obs}	I_{cal}	I_{obs}	I_{cal}	I_{obs}	I_{cal}
1 1 1	39.5	21.3	17.0	23.0		28.6	49.7	45.3	38.2	37.5
2 2 0	35.5	30.0	15.7	28.9	10.6	26.1	31.3	31.4	21.9	22.1
3 1 1	52.0	47.5	33.1	43.0	34.2	32.0	22.7	28.7	17.8	18.5
2 2 2	40.3	38.2	25.7	34.5	21.6	24.9	17.2	17.6	13.3	13.6
4 0 0	30.2	22.9	22.0	20.8	14.4	15.6	9.0	9.9	9.0	9.4
4 2 2	34.3	40.6	23.5	39.8	23.1	37.3	27.5	32.3	29.6	33.9
511 - 333	100.0	100.0	100.0	100.0	100.0	100.0	100.0	100.0	100.0	100.0
4 4 0	40.7	43.3	23.7	43.9	23.3	45.7	44.6	47.7	45.2	48.4
5 3 1	78.6	75.0	70.9	74.7	72.7	74.7	81.9	84.0	85.5	73.7
7 3 3	30.2	25.7	16.8	24.7	22.4	22.0	19.2	18.6	18.1	18.2
822 - 660	86.5	72.8	69.6	70.9	66.2	65.9	73.4	62.3	66.5	58.9
751 - 555	21.0	19.2	21.8	18.7	29.4	17.3	22.0	16.9	19.1	15.5

(Relative intensities are normalized to line (511)-(333) , B~6.5 $Å^2$)

TABLE 3-3 Observed and Calculated X-ray diffraction intensities for Na_8Si_{46} phase in samples 9 and 11.

h k l	2 1 0	2 1 1	3 2 0	3 2 1	4 1 0	4 1 1 3 3 0	5 3 0 4 3 3	6 1 1 5 3 2
Sample--9	26.3	19.2	34.4	100.0	10.3	14.8	34.8	26.8
Sample--11	27.5	15.7	37.5	100.0	19.0	13.2	36.6	24.5
I_{cal}	21.6	12.2	39.8	100.0	22.6	11.5	34.3	22.0

(Relative intensities are normalized to line (321). B $\sim$6.5$\AA^2$)

TABLE 3-4 COMPARISON BETWEEN THE X-RAY ANALYSIS OF Na_xSi_{136} AND Na_8Si_{46} COMPOUNDS BY THE BORDEAUX GROUP AND THE PRESENT WORK.

	Bordeaux group	Present work
Strongest X-ray diffraction line for Na_xSi_{136}.	*(822)-(660)* line for X from 3 to 11.	*(311)* line for X from 1.5 to 6, *(511)-(333)* line for X from 7 to 22.
Strogest line for Na_8Si_{46}	*(321)* line	*(321)* line
Lattice parameter Na_8Si_{46} (Å)	10.19	10.19
Na_xSi_{136} (Å)	14.62	14.62
Temperature factor B	1 $Å^2$ for both phases	6.5 $Å^2$ for both phases

The composition (Na_xSi_{136} phase) for all ten samples determined by X-ray analysis are listed in TABLE 3-5. As expected, samples 20-D and 25-D had their concentration of sodium increased by the thermal diffusion process. Sample 20-D greatly increased its concentration of sodium from 1 at.% to 5 at.% whereas in sample 25-D it increased from 12 at.% to 14 at.%.

An exploration of the sodium distribution between Me_1 and Me_2 sites indicates preference for the large cage (Me_2); in high concentration samples(for example, samples 25 and 25-d) the distribution is more or less equal as it fills up the vacant sites (TABLE 3-5 and Fig.3-12). The composition of the Na_xSi_{136} samples as a function of the degradation temperature is plotted in Fig.3-13. The higher degradation temperature causes lower concentration.

As stated at the beginning of this section that some samples contained a second clathrate phase (Na_8Si_{46}) and a pure silicon phase. It is possible to determine the composition of two (or three) phases in a mixture sample from the X-ray diffraction intensity analysis by the direct comparison method [53] in which the line intensities of different phases in the same sample are compared. The advantage of this method is that it does not require another standard pure phase sample in order to determine the proportion of that phase in the mixture sample. The line intensity of Na_xSi_{136} phase is strongly dependent on the sodium distribution, it is therefore impossible to obtain a standard pure phase sample with same sodium distribution for comparison.

Assume that a sample contains two clathrate phases, A-type Na_8Si_{46} and B-type Na_xSi_{136} . Both phases have different crystal structure and lattice parameter. It should be recalled from Eq.3-6 that

TABLE 3-5 COMPOSITION AND DISTRIBUTION OF SODIUM IN Na_xSi_{136}

Sample No.	Concentration of sodium at.%		Na_xSi_{136} : x	Distributions of sodium $16\alpha + 8\beta = x$	
	Chem. analy.	X-ray analy.	(X-ray)	Na_1 : α	Na_2 : β
12	1.96	1.09	1.5	0.054	0.08
20	3.87	2.02	2.8	0.04	0.27
13	3.38	3.20	4.5	0.06	0.44
15	4.23	3.75	5.3	0.07	0.52
20-D	9.68	5.23	7.5	0.094	0.75
26	10.9	8.7	13	0.41	0,80
9	13.0	9.3	14	0.47	0.81
11	12.3	11.1	17	0.65	0.83
25	14.4	12.1	18.7	0.85	0.64
25-D	15.7	13.9	22	0.94	0.87

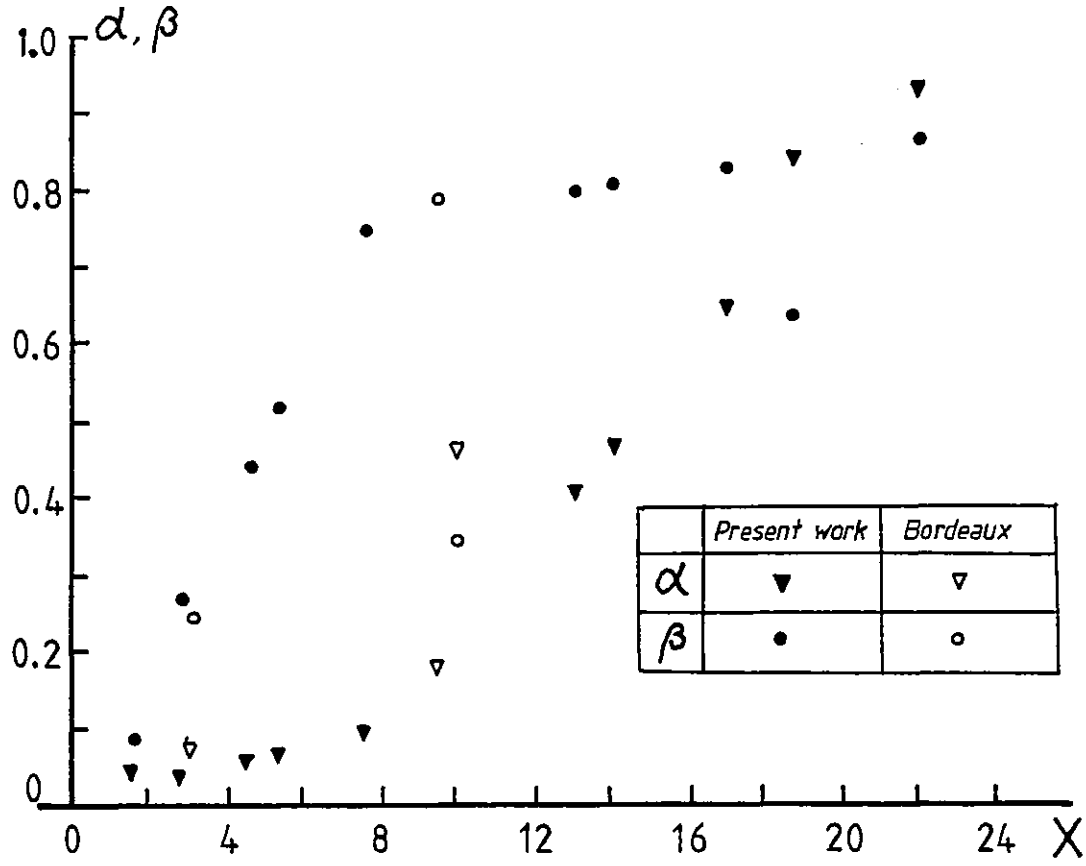

FIG. 3-12 DISTRIBUTION OF SODIUM IN Na_XSi_{136} AS A FUNCTION OF THE COMPOSITION

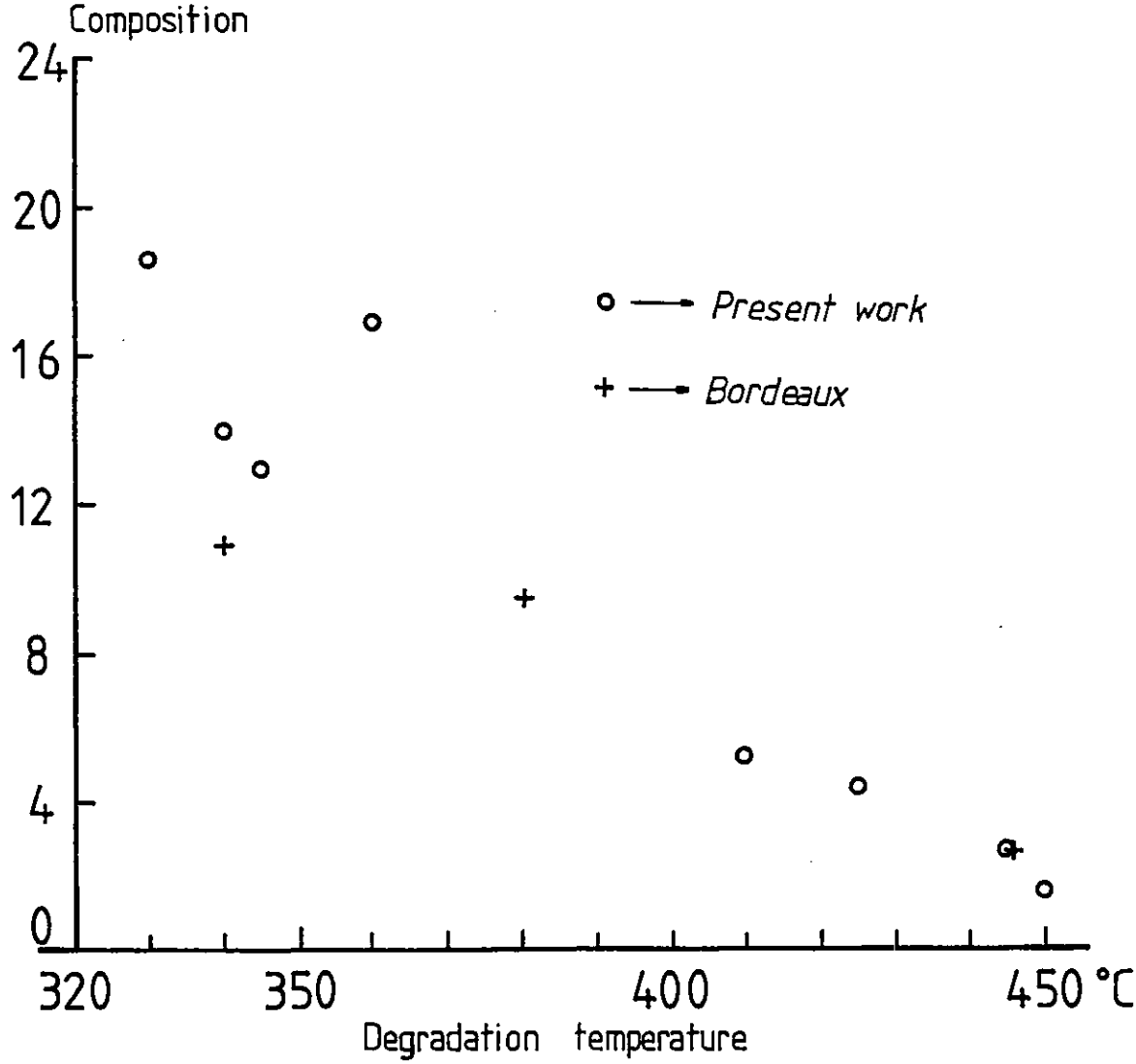

FIG. 3-13 COMPOSITION (as determined by X-ray analysis) AS A FUNCTION OF DEGRADATION TEMPERATURE FOR Na_XSi_{136}

the scale factor K is proportional to $C\, I_o/v^2$, hence

$$K = K_1 I_o \frac{C}{v^2}$$

and $$R(\theta) = I(\theta) \exp\left[-2B\left(\frac{\sin(\theta)}{\lambda}\right)^2\right]$$

therefore $$I_{obs}(hkl) = K_1 I_o \frac{C}{v^2} R(\theta) \qquad \text{Eq.3-8}$$

where $K_1 I_o$ is a constant which depends on the X-ray instrument but independent of the kind and amount of the diffracting substance, $R(\theta)$ depends on hkl , and the kind of substance, v the volume of unit cell of the substance, C the volume fraction of the substance in the sample. Hence, for A-type clathrate phase, the observed intensity of a particular line

$$I_{obs}(hkl) = I_A = K_1 I_o \frac{C_A}{v_A^2} R_A(\theta)$$

for B-type

$$I_B = K_1 I_o \frac{C_B}{v_B^2} R_B(\theta)$$

Division of these equations yields

$$\frac{I_A}{I_B} = \frac{C_A}{C_B} \times \left(\frac{v_B}{v_A}\right)^2 \times \frac{R_A(\theta)}{R_B(\theta)} \qquad \text{Eq.3-9}$$

The value of C_A/C_B can therefore be obtained from the observed line intensities of two phases, I_A and I_B , in one sample, and the calculation of $(v_B/v_A)^2$ and $R_A(\theta)/R_B(\theta)$. In a two phase sample

$$C_A + C_B = 1$$

the value of C_A and C_B can be obtained. Similarly, in three phases sample, for example a third phase is pure silicon, its volume fraction being C_S, the values of C_A/C_S and C_B/C_S can be obtained, hence, the value of C_S is then found from the relation

$$C_A + C_B + C_S = 1$$

Volume concentration of different phases contained in samples 12, 13, 15, 9 and 11 are listed in TABLE 3-6.

TABLE 3-6 VOLUME FRACTION (%) OF THREE PHASES CONTAINED IN THE SAMPLES

Sample No.	12	13	15	9	11
Na_xSi_{136}	48	60	91	60	54
Na_8Si_{46}		5	9	40	46
Si	52	35			

The reported results of chemical analysis of sodium concentration for all ten samples by the Analytical Service Laboratory of Imperial College were slightly higher than the X-ray analysis results (TABLE 3-5). It needs to be understood that chemical analysis includes all sodium contained in the sample, rather than part that in the Na_xSi_{136} phase compounds. If the sodium concentration of the second phase (Na_8Si_{46}) is taken into account, the X-ray analysis value is still lower than the chemical analysis. We believe that the chemical analysis values tended to be higher than they should be. If we consider that the chemical analysis value of sample 25 (14.4 at.%) was true, then there were 23 sodium atoms per unit cell. The analysis result of sample 25-D (in which the sodium concentration has been increased by thermal diffusion process) shows that the number of sodium atoms per unit cell should be 26. This is impossible, because the maximum metallic sites are twenty-four.

CHAPTER 4

SPECIFIC HEAT MEASUREMENT BY AC METHOD

4.1 INTRODUCTION

From a crystallographic point of view, the sodium atom is thought to be isolated within the silicon polyhedral cage of the Na_xSi_{136} phase. The shortest interatomic distance between a sodium and silicon atom is 3.15 Å in the small cage (Me_1) and 3.85 Å in the large cage (Me_2). It seems to be impossible for any two nearest neighbour sodium atoms being bonded directly at such a distance of 6 Å apart. The rôle of sodium atoms in stablizing the clathrate structure is obscure; the structure is stable even with only 8% of the available metallic sites being occupied. The specific heat measurement should give information about the interactions between the 'guest' sodium and the 'host' silicon atoms. If the sodium and silicon atoms are weakly coupled, this will give rise to a local vibrational mode. The Einstein theory of specific heat describes this kind of local vibrational mode very well indeed; for example, such a local mode exists in $Al_{10}V$[56]. The theory assumes that all atoms within a crystal vibrate at the same frequency, ω_E . Thus the contribution from a local mode to the heat capacity is

$$C_{lm} = 3NK_B\left(\frac{\Theta_E}{T}\right)^2 \frac{\exp(\Theta_E/T)}{[\exp(\Theta_E/T)-1]^2} \qquad \text{Eq.4-1}$$

where $\Theta_E = \hbar\omega_E/k_B$ is the Einstein temperature.

In general, the heat capacity of a solid includes a lattice contribution and an electronic contribution. The Debye model of lattice heat capacity assumes that the lattice vibrates as if it is an elastic continuum, but the vibration frequencies cannot exceed a certain maximum value. Therefore the frequency distribution function is given by

$$f(\omega) \propto \omega^2 \qquad \text{for} \qquad \omega < \omega_D = \omega_{max}$$

$$f(\omega) = 0 \qquad \text{for} \qquad \omega > \omega_D$$

and the lattice contribution to the heat capacity in the Debye theory is

$$C_{lat} = 9NK_B\left(\frac{T}{\Theta_D}\right)^3 \int_0^{\frac{\Theta_D}{T}} \frac{Z^4 \exp(Z)}{[\exp(Z)-1]^2}\, dZ \qquad \text{Eq.4-2}$$

where $Z = \hbar\omega / K_B T$, and $\Theta_D = \hbar\omega_D / K_B$ is the Debye temperature.

In the low temperature range $(T/\Theta_D) \ll 1$ and, only the low frequency normal modes with the energy $\hbar\omega \leq K_B T$ are excited, and the lattice heat capacity is

$$C_{lat} = \frac{12}{5}\pi^4 NK_B\left(\frac{T}{\Theta_D}\right)^3 = \beta T^3 \qquad \text{Eq.4-3}$$

whilst in the high temperature range

$$C_{lat} \simeq 3NK_B = 25 \quad \text{J mole}^{-1}\,\text{K}^{-1} \qquad \text{Eq.4-4}$$

The contribution of the electron gas to the heat capacity is

$$C_{el} = \frac{1}{3}\pi^2 K_B^2 n(E_F) T = \gamma T \qquad \text{Eq.4-5}$$

where $n(E_F)$ is the density of states at the Fermi energy. As indicated before, the total heat capacity of a solid can be expressed as

$$C = C_{lat} + C_{el} \qquad \text{Eq.4-6}$$

so that in the low temeprature range

$$C = \gamma T + \beta T^3 \qquad \text{Eq.4-7}$$

Also, if there is a local vibrational mode heat capacity, then this must be included to give

$$C = \gamma T + \beta T^3 + C_{lm} \qquad \text{Eq.4-8}$$

There were two main objectives in investigating the heat capacity of Na_xSi_{136} compounds :

1) To investigate whether there is a well-defined local vibrational mode; that is, is the sodium atom isolated in the clathrate cage? If the local mode frequency is independent on the occupancy distribution of sodium atoms in the compound then this indicates that there exists some kind of interaction (or coupling) between the adjacent sodium atoms. If no such dependence is found then the sodium atoms must be well isolated within the cage.

2) If there is a metal non-metal transition in Na_xSi_{136} compound, does the electronic heat capacity coefficient, γ, or the density of states at the Fermi level vary continuously over the transition region?

An existing low temperature AC calorimeter[55] in this laboratory was constructed by Nicholson[56] and later modified by Dawes[57]. The heart (sample holder platform, etc.) of the calorimeter was constructed from copper foil. Its addenda heat capacity was thermally equivalent to 1.7 grams of copper. It was considered that the addenda heat capacity might be too large for measuring the heat capacity of Na_xSi_{136} compounds. Some further modifications of the sample platform, heater and thermometer were made in order to reduce the addenda heat capacity, and to give a better resolution (§4.3). Whilst the addenda heat capacity has been reduced to about half of its original value (§4.5), unresolved technical problems prevented any useful measurements of heat capacity of Na_xSi_{136} compounds (§4.6).

4.2 EXPERIMENTAL LOW TEMPERATURE AC CALORIMETRY

In this section, we shall briefly describe the basic principle of AC calorimetry. The general features and operation of the apparatus are presented in great detail in the thesis of Dawes[57].

4.2.1 AC method

The basic principle of AC calorimetry is that, by applying a low frequency (usually 1 Hz to 0.01 Hz) oscillatory heat input to

a small specimen which is connected thermally to a heat reservoir, the heat capacity can then be obtained from the resulting temperature oscillation of the specimen. The heat reservoir is normally a helium bath which ensures a rapid return to thermal equilibrium after any heat input. An AC voltage V_h , of frequency ω applied across a heater R_h (Fig.4-1), provided an oscillatory AC thermal power at a frequency of 2ω and a DC heat input to the sample:

$$\dot{Q} = \frac{V_h^2}{R_h} \sin^2 \omega t = \dot{Q}_o (1 + \cos 2\omega t) \qquad \text{Eq.4-9}$$

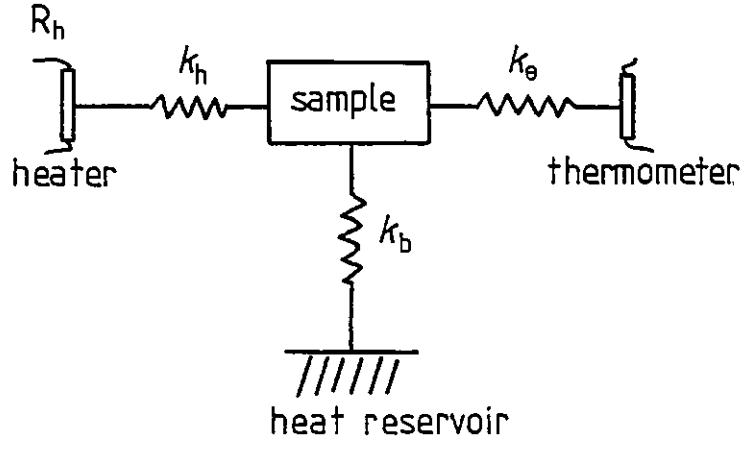

FIG. 4-1 Schematic model of an AC calorimeter. k_b , k_h and k_e are respectively the thermal conductance of the thermal weak link, the heater, and the thermometer.

The heat flows through the specimen and out to the heat reservoir via the thermal link. The resulting temperature oscillation of the specimen[55]

is

$$T = T_b + T_o + T_{AC}\cos(\omega t - \phi) \qquad \text{Eq.4-10}$$

where T_b is the heat reservoir temperature, T_{AC} the sinusoidal temperature oscillations from which the heat capacity can be calculated , ϕ the phase shift with respect to the input power. T_o is the sample/resultant temperature which is independent of input power frequency. Its magnitude is just sufficient to maintain a heat flow through the thermal link equal to the time-averaged heat input:

$$T_o = \frac{1}{2}\frac{\dot{Q}_o}{k_b}$$

where k_b is the thermal conductance of the heat link. If the heat capacity of the sample is much bigger than that of the heater and thermometer, and the internal thermal relaxation time (τ_{int} , associated with the thermal diffusion) of the sample is much shorter than the period of the applied heat oscillations, and is much shorter than the sample-to-bath (external) relaxation time ($\tau_{ext} = \frac{C}{k_b}$, where C is the heat capacity of the sample), then the magnitude of T_{AC} can be reduced to [55]

$$T_{AC} \simeq \frac{\dot{Q}_o}{2\omega C}\left[1 + \frac{1}{4\omega^2\tau_{ext}^2} + 4\omega^2\tau_{int}^2\right]^{-\frac{1}{2}} \qquad \text{Eq.4-11}$$

Within a certain frequency limitation, $\tau_{ext} \gg \frac{1}{\omega} \gg \tau_{int}$, the expression Eq.4-11 can be simplified; valid to 1% accuracy:

$$T_{AC} \simeq \frac{\dot{Q}_o}{2\omega C} \qquad \text{Eq.4-12}$$

The frequency ω of the input heat voltage should be limited to the range [57] :

$$\frac{\sqrt{2}}{5}\,\tau_{ext} > \frac{1}{\omega} > 10\sqrt{2}\,\tau_{int} \qquad \text{Eq.4-13}$$

In practice, for good temperature resolution T_{AC}/T_o should be 5% or less, that is,

$$\frac{2\hat{\imath}}{\omega} \leq \begin{cases} \tau_{ext} & \text{for} \quad T_o \gg T_b \\ 2\tau_{ext} & \text{for} \quad T_o \sim T_b \end{cases} \qquad \text{Eq.4-14}$$

4.2.2 Low frequency limit : external time constant

The external time constant, τ_{ext} , can be experimentally determined by applying an DC thermal power $\dot{Q}_1$ to the sample (at present temperature T_o) until the sample has reached equilibrium at new temperature T_1 . If the thermal power is stepped abruptly to $\dot{Q}_o$ by a small amount ΔQ ($= \dot{Q}_1 - \dot{Q}_o$) , then the temperature of the sample would decay exponentially to the original temperature T_o .

The resultant change in temperature is

$$\Delta T = (T_1 - T_o)\exp\left(-\frac{K_b t}{C}\right) = \Delta T_o \exp\left(-\frac{t}{\tau_{ext}}\right) \qquad \text{Eq.4-15}$$

where $$\tau_{ext} = \frac{C}{K_b}$$

Hence, the external time constant is determined by measuring the rate at which the DC temperature of the sample returned to equilibrium upon

a change in the rate of heat imput.

4.2.3 High frequency limit : internal time constant

Consider the system where the thermal resistance of the heater, thermometer and sample are finite. If the frequency of the input AC power is comparable to the internal relaxation time of the sample, the amplitude of T_{AC} decreases non-linearly with increasing frequency. The high frequency limit therefore may be deduced from measurements of the non-linear change of the frequency dependence of T_{AC} .

In order to estimate the internal relaxation time τ_{int} , it is possible to obtain a temperature response in which the amplitude of first harmonic response is frequency independent, and the second harmonic term being neglected. By coupling a small AC thermal power capacitively to a large DC thermal power [56], it is possible to get a temperature response with frequency independent amplitude because the coupled impedance of the capacitor decreases with the frequency so that it is frequency independent. The large DC power will maintain the sample at average sample temperature T_0 . The AC component is

$$T_{AC} \propto 2 V_{DC} V_{AC} (1 + \omega^2 \tau_{int}^2)^{-\frac{1}{2}}$$

thus τ_{int} effects show up as frequency dependent at high frequencies, and T_{AC} is frequency independent at low frequencies. Hence, the time constant τ_{int} can be experimentally determined by gradually increasing the input AC power frequency from low frequencies until the T_{AC} amplitude has fallen to one half of its frequency independent

values. We define this frequency as $\omega_{\frac{1}{2}}$ at which the T_{AC} amplitude being one half, hence, we have

$$\omega_{\frac{1}{2}} \tau_{int} \simeq \sqrt{3}$$

for 1% accuracy (Eq.4-12), the condition $\omega \tau_{int} \leq \frac{1}{10\sqrt{2}}$ must be satisfied, therefore

$$\frac{1}{\omega} \geq \frac{10\sqrt{6}}{\omega_{\frac{1}{2}}} \qquad \text{Eq.4-16}$$

so that $$\frac{2\pi}{\omega} = t_p \geq 25\, t_{p/2} \qquad \text{Eq.4-17}$$

where $$t_{p/2} = \frac{2\pi}{\omega_{\frac{1}{2}}}$$

Eq.4-17 indicates that the upper frequency limit of the input AC heat voltage must be limited to periods $\geq 25\, t_{p/2}$ for 1% accuracy in measuring the heat capacity.

4.3 MODIFICATION OF THE CALORIMETER

The original sample platform of the AC calorimeter in this laboratory was constructed from copper foil with an Allen-Bradley carbon thermometer glued with G.E.7031 varnish onto a tab (Fig.4-2(a)). The heater was a thin film metal oxide resistor cemented to a piece of copper foil with a smear of thinned G.E.7031 varnish. The addenda heat capacity of this assembly was thermal equivalent to 1.7 grams of copper. The main sources of large addenda heat capacity were the carbon thermometer, G.E.varnish and the copper foil (Appendix B lists

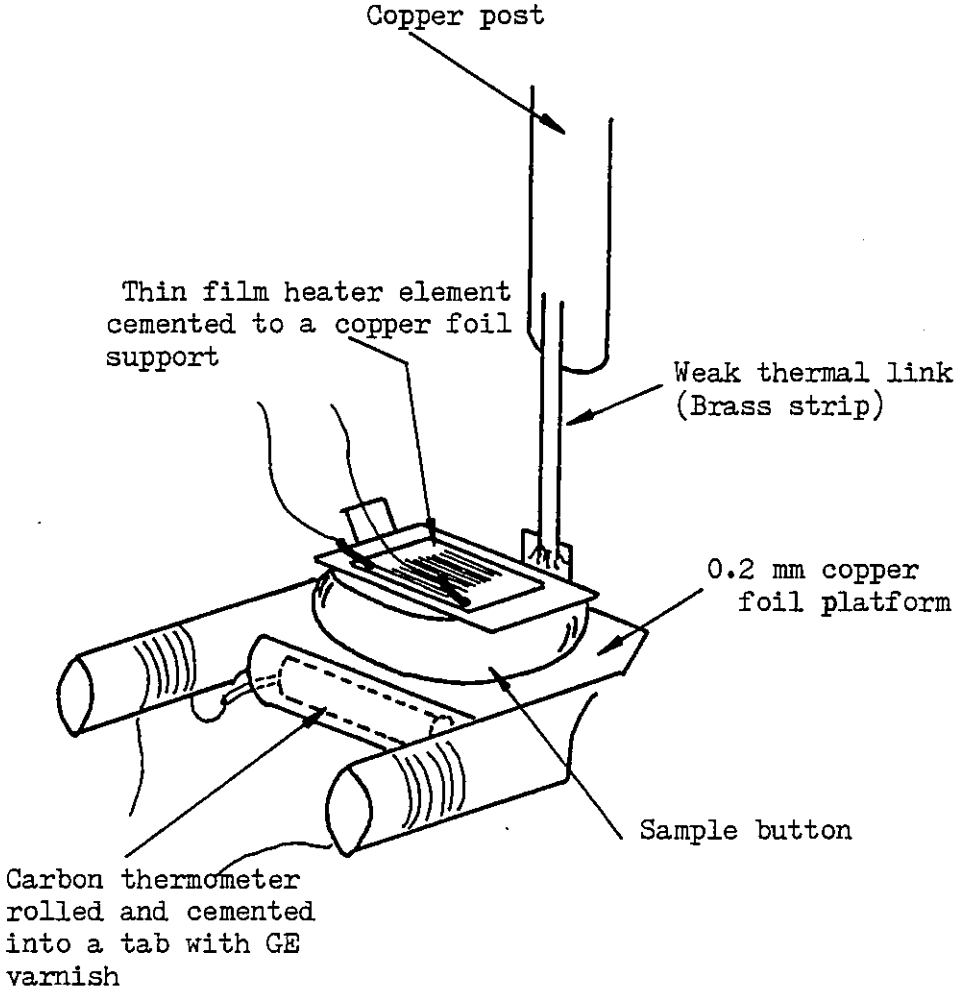

FIG. 4-2(a) OLD SAMPLE PLATFORM

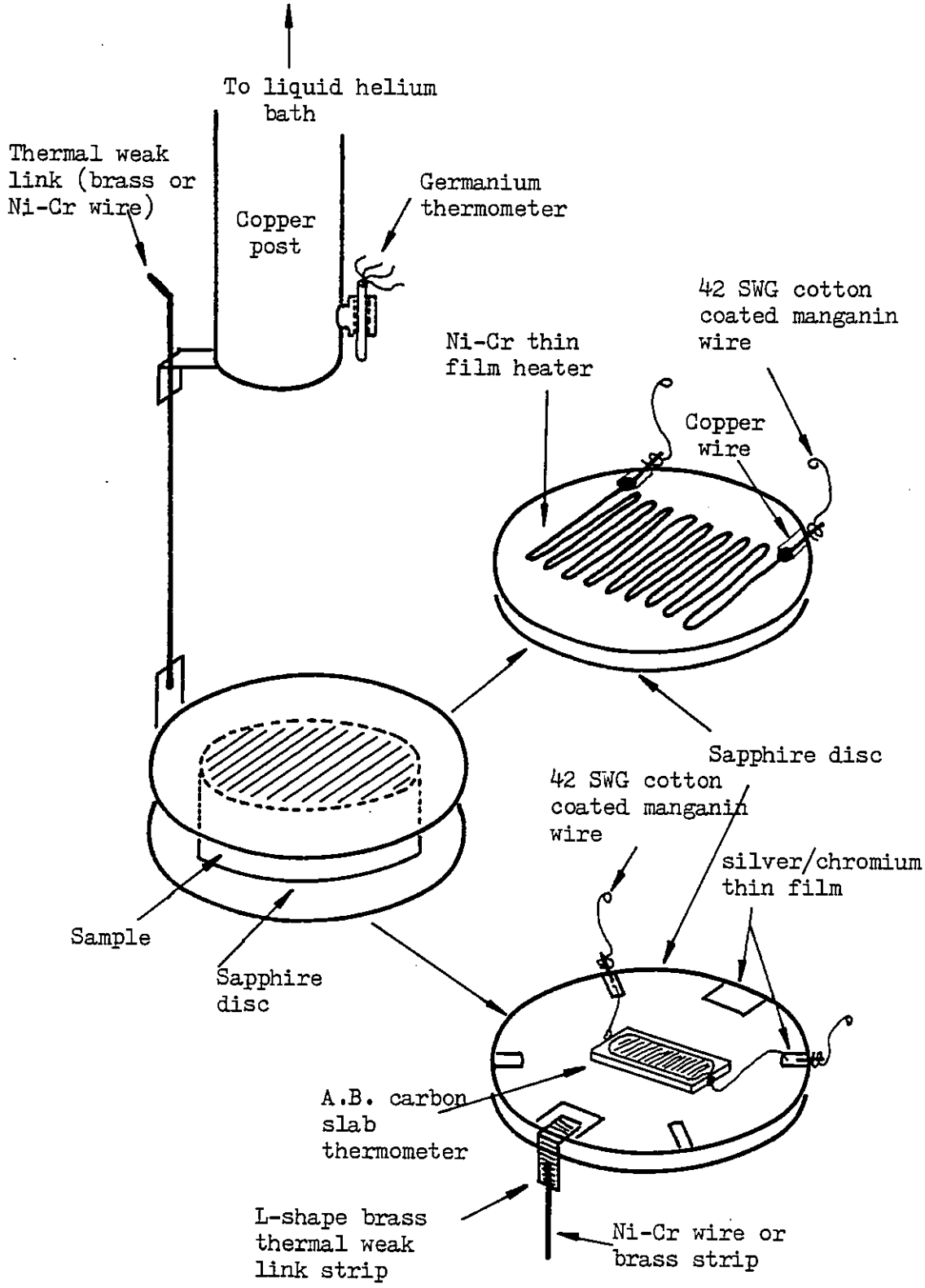

FIG. 4-2(b) MODIFIED SAMPLE PLATFORM AND HEATER

the heat capacities of some cryogenics materials). We will describe how the modifications were made in order to reduce the addenda heat capacity in the following subsections.

4.3.1 Sapphire sample platform

A new sample platform was constructed from a sapphire disc with 20 mm diameter, 0.5 mm thickness (weight = 434.5 mg). The advantage of using sapphire disc is that it has a very high Debye temperature Θ_D=1042 K[69,70] so that its lattice heat capacity is small. The thermal conductivety of the sapphire is big[71]. Thus the internal thermal relaxation time of the sapphire disc is very short.

It was found from a series of tests of the adhesion of silver film on the sapphire that it was necessary to first evaporate a chromium layer in order to improve adhesion of silver contact film on the sapphire. A set of six silver chromium contacts were evaporated onto the sapphire disc (Fig. 4-2 (b)). The thickness of the film contacts were about 3000 Å. The total weight of these was 0.12 mg and the heat capacity of these film was estimated $\sim 2 \times 10^{-8}$ J K^{-1} at 4.2 K. A L-shape brass strip (10mm x 2.5mm x 0.3mm) was permanently soldered to one of the contacts. A piece of nichrome wire was then spot welded to the brass as a weak thermal link to the helium bath. This thermal link wire can be easily interchanged, depending on the conditions of the experiment. A slice of an Allen Bradley carbon thermometer, which was ground to a thickness of 0.5 mm (see §4.3.3), was attached to the disc by using Apiezon 'N' grease as

a thermal contact agent. Two short copper wire (13 mm, SWG41) as the leads were Pb/Sn soldered to the silver/Chromium contacts.

4.3.2. Nichrome thin film heater

It was intended to avoid using G.E. varnish to glue a thin film heater to a disc because of its big heat capacity, therefore, a nichrome thin film heater was evaporated on a second sapphire disc (same size as the sample platform).

Two silver / chromium thin film contacts as the electrical terminals were evaporated on the sapphire disc before hand. An ohm meter was connected to these two terminals that it was used to monitor the resistance of the nichrome thin film during the evaporation. The resistance of the heater should be approximately 900 Ω. The heater had a zig-zag length 120 mm with width 0.4 mm covered a 100 mm^2 area (Fig.4-2(b)). The sapphire disc was heated to 200 ^{o}C during the evaporation of nichrome thin film, and after the evaporation was completed the disc was left at this temperature for five hours in the vacuum. This process would improve the adhesion of the film as well as prevent it being further oxidised after exposure to the atmosphere. The weight of the thin film was 0.15 mg. The resistance was about 900 Ω. Two short copper wire (2.5 mm long, 26 SWG) were Pb/Sn soldered to the electrical terminals. Another two 10 mm long cotton coated manganin wires(SWG 42) were soldered to the copper wire as the heater leads.

4.3.3. Thin slab carbon thermometer

Some brands of carbon composition resistors are useful as low temperature thermometers, however, their heat capacity is quite big at low temperatures (Appendix C), and high thermal resistance of their coating causes a slow thermal response. The heat capacity can be reduced and the thermal response improved by grinding the resistor to a thin slab.

An 47 Ω, 1/8-Watt Allen-Bradley carbon resistor was set in plastic in a metallographic mounting press die. It was ground on both side parallel to its axis to a desired thickness by a fine carbondum paper. The resistance increased to about 80 Ω with its thickness of 0.5 mm, its weight was reduced to 30% of its original weight ($\sim$25 mg). The end copper leads of the resistor were also cut away leaving 0.5 mm length. 13 mm long copper leads (SWG 41) were Pb/Sn soldered to the copper terminals at each end of the slab resistor. The newly ground slab thermometer was thermally cycled to liquid nitrogen temperature several times to check its resistance response with the temperatures and the reproducibility.

The slab resistor was attached to the sample platform sapphire using 0.5 mg of Apiezon 'N' grease as a thermal contact agent, and the two copper leads were then soldered to the silver / chromium contact terminals.

The thin slab thermometer has several advantages:

1) It reduces its heat capacity.
2) It increases the thermal contact area because of its flat surface so that it has a fast thermal response.

3) The flat contact surface minimizes the amount of thermal contact agent (Apiezon 'N' grease) which has big heat capacity.

4.4 THERMOMETER CALIBRATION

In the present new designed calorimeter, a germanium thermometer was permanently attached to the lower end of the copper post of the helium bath (Fig.4-3). The germanium thermometer has been calibrated to ± 0.1% accuracy over the range 4.2 to 100 K by CrysCal . it / Also has been calibrated against another calibrated germanium thermometer (CCG 344) below 4.2 down to 1.14 K by the author.

After every experimental run, the slab carbon thermometer was calibrated between 1.5 and 20 K against the germanium thermometer; it was calibrated also against the helium vapour pressure below 4.2 K. The procedure of temperature calibration above 4.2 K is as follows. The top of the sample chamber was ^a risen slightly above the liquid helium level, the can temperature was controlled by passing current through the metal resistor heaters which were attached to a copper rod screwed into the brass flange on the top of the sample chamber. Steady temperatures were set up by applying an appropriate power to the can heater. If a high temperature was required, the can may rise a little bit higher but the lower end part of it should still be ^immersed in the liquid helium. The germanium thermometer resistance was determined by an DC four-terminal measurement. The carbon resistance was read from the scale on the Dekastat variable resistor at the DC bridge balance point. The calibration points were then smoothed by fitting a 3rd degree polynomial:

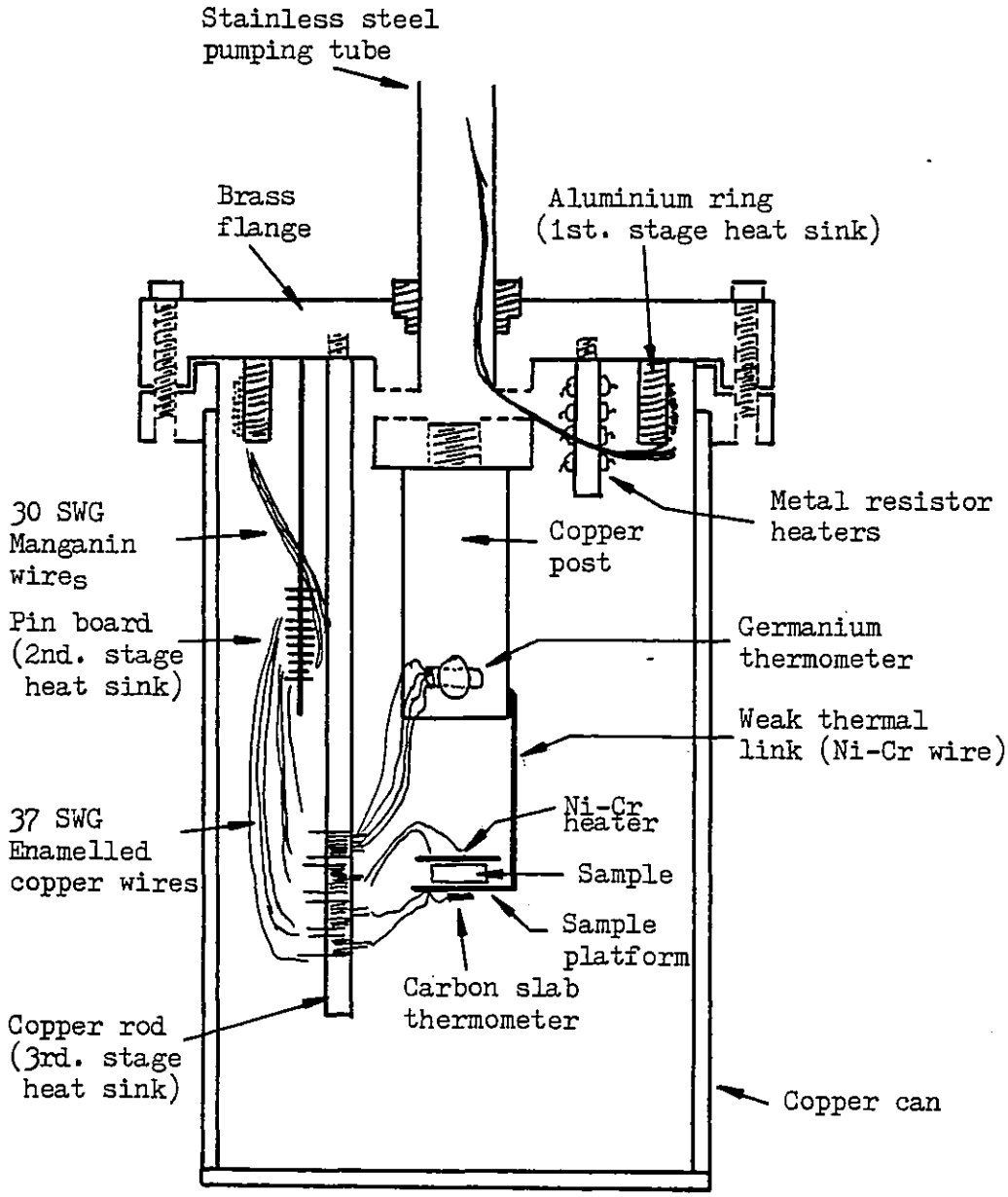

FIG. 4-3 SAMPLE CHAMBER

$$\frac{1}{T} = \sum_{n=0}^{3} a_n (\ln R)^n \qquad \text{Eq.4-18}$$

The quality of specific heat measurements depends critically on the accuracy of the thermometry and its temperature sensitivity. The temperature sensitivity of the thermometer was derived by differentiating of Eq.4-18 with respect of T:

$$\left(-\frac{1}{R}\frac{dR}{dT}\right) \sum_{n=1}^{3} n\, a_n (\ln R)^{n-1} = \frac{1}{T^2} \qquad \text{Eq.4-19}$$

4.5 THE ADDENDA HEAT CAPACITY

The specific heat measuring procedure by the AC method has been fully described by D.G. DAWES in his thesis[57]. The basic working formula for calculating the specific heat is given by Eq.4-12 :

$$C = \frac{\dot{Q}_o}{2\omega T_{AC}} \qquad \text{Eq.4-12}$$

The external and internal time constants were estimated by the method described in §4.2. The working frequency, $\omega \left(= \frac{2\pi}{t_p}\right)$, was chosen to satisfy the conditions of Eqs.4-14 and 4-17. The AC temperature oscillation traces were recorded on a chart recorder. The resistance change ΔR of the thermometer corresponding to defection Δy on the chart recorder was calibrated

$$\beta = \frac{\Delta R}{\Delta Y} \qquad \text{Eq.4-20}$$

hence the AC temperature T_{AC} could be calculated from

$$T_{AC} = \frac{\Delta R}{\Delta Y} Y_{pp} \frac{\Delta T}{\Delta R} \qquad \text{Eq.4-21}$$

where Y_{pp} is the peak to peak oscillation trace value; $\frac{\Delta T}{\Delta R}$ is the sensitivity of thermometer which has been calibrated (§4.4). From Eq.4-12, it is known that the amplitude of T_{AC} is proportional to the working time period $t_p (= \frac{2\pi}{\omega})$. Define

$$\alpha = \frac{Y_{pp}}{t_p} \qquad \text{Eq.4-22}$$

therefore the heat capacity is given by

$$C = \frac{\dot{Q}_o}{4\pi\alpha\beta} \frac{\Delta R}{\Delta T} \qquad \text{Eq.4-23}$$

The gradient factor, α, was measured by choosing several different t_p (which must satisfy the conditions of Eqs. 4-14 and 4-17), so that a plot of t_p against the corresponding T_{AC} amplitude was a straight line passing through the origin with a slope equal to the gradient α. If a deviation from linearity was observed at high frequency, and the straight line did not pass through the origin, this indicated the working time period, t_p was either too close to the internal time constant τ_{int}, or τ_{int} was too long.

The collective heat capacities of sapphire platform, heater, carbon thermometer, and thermal contact agent, etc. were measured in

the temperature range 4.2 to 18 K. A 0.7 mm diameter nichrome wire with length 50 mm (length adjustable according to the requirement of the exteral time constant limitation) was spot welded to the platform sapphire (§4.3.1, Fig.4-2(a)) as the weak thermal link to the helium bath. 1.8 mg Apiezon 'N' grease was smeared as a thermal contact agent of the platform and heater sapphire (A techinique of expelling air bubbles out of the grease will be described in next section,§4.6). The result of the addenda heat capacity, C/T, of the modified sample platform and heater is shown in Figure 4-4, and in terms of heat capacity was thermally equivalent to about one gram of copper. Table 4-1 lists various contributions to the addenda heat capacity. The estimated total heat capacity excluding the weak link nichrome wire was about 4.5×10^{-5} J K^{-1} at 4.2 K . The measured addenda heat capcaity was 6.8×10^{-5} J K^{-1} at 4.2 K. The contribution of nichrome wire must be included and it was estimated that the wire contributed about 30% to the addenda heat capacity. Tin-lead solder contributed 35% to the addenda heat capacity.

TABLE 4-1 Various contributions to addenda heat capacity

Material	Heat capacity at 4.2 K (J K^{-1})
Pb/Sn solder	2.4×10^{-5}
sapphire	5.4×10^{-6}
copper wire & Ag/Cr film	1.8×10^{-6}
carbon thermometer	1.4×10^{-6}
Ni - Cr heater	1.7×10^{-7}
Apiezon grease	4.7×10^{-6}
brass (L-shape)	5.9×10^{-6}
manganin wire	1.6×10^{-6}
Ni - Cr wire	1.8×10^{-4}

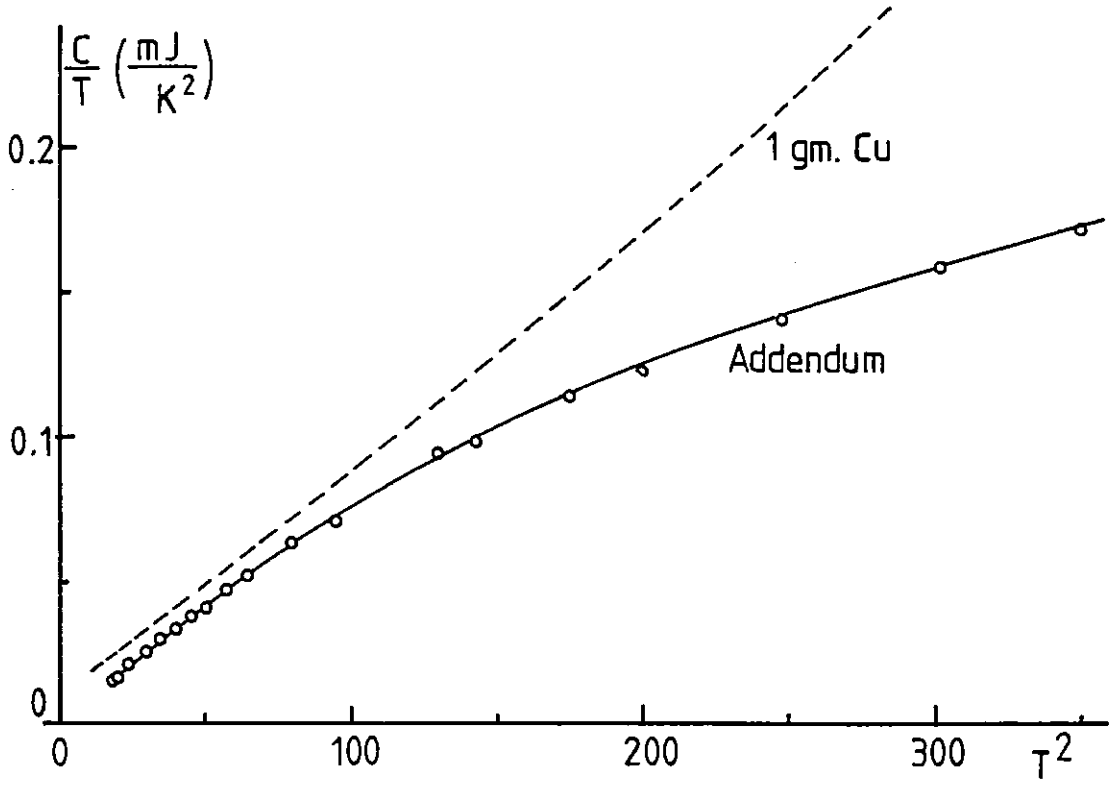

FIG. 4-4 ADDENDA HEAT CAPACITY

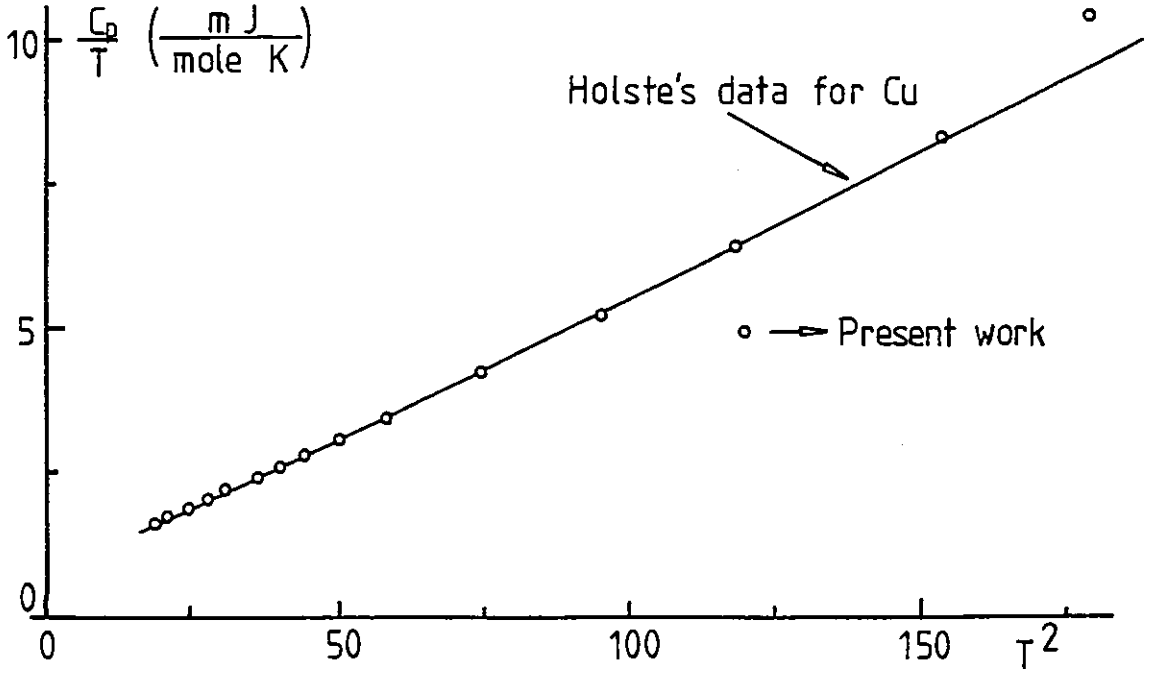

FIG. 4-5 SPECIFIC HEAT OF COPPER

A calibration of the apparatus has been checked by measuring the heat capacity of pure (5N) copper (2.032 grams). The results agreed within one percent uncertainty with Holste's data[77] in a limited temperature range (4.2 to 14 K). Fig.4-5 shows the results of copper sample and Holste's result.

4.6 TECHNICAL PROBLEMS IN MEASURING THE HEAT CAPACITY OF A COMPACTED Na_xSi_{136} POWDER SAMPLE

The thermal bonding of a specimen to platform and heater is crucial in measuring heat capacity by the AC method. Poor thermal contact between them results in a longer internal time constant which leads to invalidity of Eq.4-12. The specimen was sandwiched between the sapphire heater and platform discs, and it was placed horizontally between two warm brass disc plates ($\sim$35 °C at which temperature the thermal grease would melt) as shown in Fig.4-6. The air bubbles in the molten grease were squeezed out by the weight of the brass disc. This also ensured the thin grease layer bonded the specimen properly. Any air bubbles remaining in the grease would create problems when the calorimetry chamber was evacuated by expanding and breaking the bond or

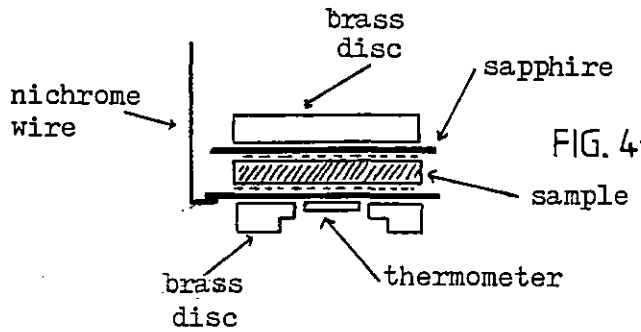

FIG. 4-6 Expel air bubbles out of grease.

tunnelling out and creating channel in the grease layer.

In measuring the heat capacity of copper, different kinds of thermal agents such as silicon oil, silicon vacuum grease, and Apiezon 'N' grease were tried as bonding agents but none of these provided a good bond for the copper sample on cooling down to helium temperature. The internal time constant τ_{int} $(= \frac{C}{K_{int}})$ and the time constant of exponential decay of temperature were unreasonably long (Table-4-2); these indicated the internal thermal resistance $1/K_{int}$ was too big. A check on the thermal contact bond after every experimental run showed some of the bonded surface area was not properly bonded by the grease. It normally took three hours to cool down to 77 K from room temperature as well as from 77 to 4.2 K. Thus, there was no chance of severe thermal shock. Probably the differential thermal expansion between the sapphire and copper sample caused the bond break. However, it was found that a mixture of 50% of fine copper powder (70 μm) and 50% of Apiezon 'N' grease lowered the thermal resistance but did not improve

TABLE 4-2 Comparison of two different thermal agents used to bond copper sample (2.032 grams). Note. $C = C_{Cu} + C_{grease}$

thermal agent	T K	τ_{ext} sec.	τ_{int} sec.	C J K^{-1}	$1/K_{int}$ K cm W^{-1}
silicon vacuum grease, 3.2 mg	4.2	15	0.4	2.4×10^{-4}	2.0×10^{3}
	6.0	26	0.8	6.0×10^{-4}	1.8×10^{3}
	10	58	1.8	2.7×10^{-3}	8.4×10^{2}
	15	100	3.1	1.1×10^{-2}	4.0×10^{2}
50% copper powder + 50% Apiezon 'N' grease mixture, 16.5 mg	4.2	12	0.1	2.1×10^{-4}	6.0×10^{2}
	6.0	22	0.2	5.1×10^{-4}	4.3×10^{2}
	10	47	0.3	1.9×10^{-3}	2.0×10^{2}
	15	80	0.47	6.5×10^{-3}	9.1×10^{1}

the strength of the bond. The measurement of the heat capacity of copper described earlier used 16.5 mg of the mixture to bond the specimen.

It was found much more difficult to bond a compacted Na_xSi_{136} specimen to the sample platform. This prevented any useful measurement of the heat capacity of Na_xSi_{136}.

Na_xSi_{136}, as prepared here, is a powder of grain size about 50 μm. The specimen used to attempt a heat capacity measurement was cold pressed into a disc of diameter 12.7 mm and about 1 mm thick. The compressing pressure was 2 kbar. The density of compacted specimen was 1.6 gm cm^{-3}. Note that the density of Na_xSi_{136} compound is 2.1 gm cm^{-3}. Because the specimen had some space between the grains some grease flowed into the specimen when bonding the sample to the holder. At least 20 mg of grease was used to bond the specimen. The thermal bonding of the specimen could be checked during cool-down the calorimetry by applying a step DC thermal power to the specimen (§4.2). If there is a good thermal bonding between the specimen and the platform and the heater, the internal time constant is negligible short compared to its external time constant, $\tau_{ext} \gg \tau_{int}$. When heat power is cut off suddenly, the trace of the specimen temperature on a chart recorder decays exponentially (Fig.4-7(a)). Thus the specimen temperature will be

$$T_s = T_o + \frac{\dot{Q}_o}{k_b} \exp\left(-\frac{t}{\tau_{ext}}\right) \qquad \text{Eq.4-24}$$

where T_o is the original specimen temperature. If, on the other hand, the internal relaxation time constant is long because of poor

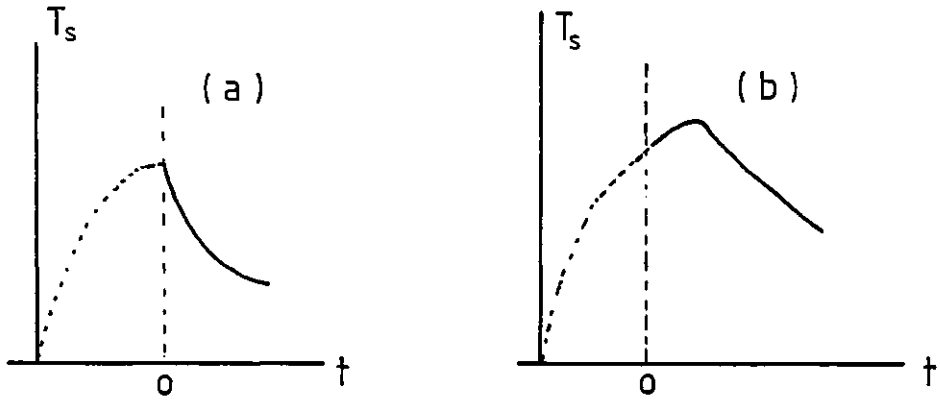

FIG. 4-7 Temperature decay trace: (a) good thermal contact; (b) poor thermal contact.

thermal contact as the result the internal thermal resistance is big, when the input heat power is cut off, the decay temperature trace would show a flat decay (Fig.4-7(b)),and it takes very long time to reach its original temperature T_0 . This trace is no longer a true exponential decay.

4.7 CONCLUDING REMARKS

The performance of the modified sample platform and heater was excellent compared to the original copper foil platform. The addenda heat capacity was greatly reduced to thermal equivalent of 0.7 gm of copper at 4.2 K. The experimental error was well within 2% for the heat capacity of 2.032 grams copper sample.

Unfortunately poor thermal bonding of the Na_xSi_{136} compacted specimens prevented any useful measurement of heat capacity. several

kinds of thermal agents such as silicon vacuum grease, Apiezon 'N' grease, mixture of copper powder and vacuum grease compound were tried. None of these could provide a small enough thermal resistance to reduce the internal time constant to acceptable values. We have tried to mix fine silver powder or aluminum powder with Na_xSi_{136} sample that it might prevent the grease flowing into the compacted sample, but this did not improve the situation.

CHAPTER 5

LOW TEMPERATURE MAGNETIC SUSCEPTIBILITY OF Na_xSi_{136}

5.1 INTRODUCTION

Determination of the magnetic properties has been found to be of great value in the study of the electronic structure of doped semiconductors. Phosphorus doped silicon (Si:P) is a well known example. This material undergoes a transition from metallic to non-metallic behaviour at an impurity concentration below some critical value ($n_c \sim 4 \times 10^{18}$ donor-cm^{-3}) (15). Recent experiments on the magnetic susceptibility of Si:P of donor concentration less than n_c indicate that it may be considered as an amorphous antiferromagnet. At low temperatures, the reciprocal susceptibility in Curie-Weiss plots shows a downward curvature towards the origin as the temperature approaches zero. This system has spins $S = \frac{1}{2}$, the interactions are purely antiferromagnetic. In an ordered antiferromagnet, the susceptibility has a maximum value at the Néel temperature. In Si:P system, no ordered transition to an antiferromagnetic state has been found at temperatures down to 3 mK. The phosphorus donors randomly substitute on the lattice sites, the effective Bohr radius of donor electrons is about 20 Å which is so much greater than the lattice spacing, it leads to broad distribution of the exchange interaction between donors, hence in this respect Si:P exhibits no ordered magnetic transition.

Na_xSi_{136} compounds could have some common features with doped semiconductors although, from the point of view of crystallography, they are different. For example, in Si:P, four of the valence electrons

of the phosphorus atom form covalent bonds with the nearest silicon neighbours, the fifth electron being loosely bound to it at low temperatures. This donor electron can be considered to be a hydrogenic 1s-orbital around the impurity centre. In clathrate compounds, sodium atoms do not substitute for the silicon but have their own specific sites in silicon clathrate cages. The silicon atoms are tetrahedrally bonded to each other (§2.1.2). The distance between two nearest sodium sites is 6 Å, and the distance between sodium and silicon is 3 Å. Sodium has one valence electron (3s), its energy being changed because of the screening effect of the silicon cage. In fact the binding of 3s-electron to the sodium ion will be weakened, and the electron will start moving in an orbit of greater radius.

Electrical resistivity measurements of doped semiconductors provide some useful information about the electronic properties of the donor - their ionization energy, effective Bohr radius, etc. However, there are many difficulties inherent in interpreting the electrical properties of a compressed powder sample. One example is the requirement of a detailed knowledge of grain contact resistance. On the other hand, analysis of the magnetic susceptibility does not given such difficulty. The limited range magnetic susceptibility results of Cros et al [45] provided insufficient information to interpret the physical behaviour of the sodium 3s-electrons in Na_xSi_{136} compounds. Therefore low temperature measurements of the magnetic susceptibility are necessary. There are several interesting points to investigate :

1) How does the localization of the 3s-electron of sodium atom depend on concentration ? Do the electrons become conduction electrons at high concentration ?

2) If nearest cages are occupied, what kind of interactions will take place between the 3s-electrons ? Are they purely antiferromagnetic or disordered antiferromagnetic (ie. showing only short range order) ?

5.2 EXPERIMENTAL METHOD

The experimental magnetic susceptibility studies of ten Na_xSi_{136} samples were carried out using a Faraday balance which measures the force exerted on a small cylindrial specimen in an applied inhomogeneous magnetic field. The force on a magnetic moment $\vec{\mu}$ in such a field is given by

$$\vec{F} = (\vec{\mu} \cdot \vec{\nabla}) \vec{B} \qquad \text{Eq.5-1}$$

If the thin specimen is aligned along the z-direction (perpendicular to field direction x), the two components of force F_x and F_y can be neglected. Then the vertical component of force exerted on the specimen is given by

$$F_z = m \chi B_x \frac{\partial B_x}{\partial z} \qquad \text{Eq.5-2(a)}$$

where m is the mass of the specimen, χ is the susceptibility per unit mass, B_x is the applied magnetic field. The strength of the gradient is related to the field B_x .

Because a higher magnetic field was required in other experiments, the electromagnet was replaced by a superconducting

solenoid and an antiparallel pair of Helmholtz coils. In this arrangement, the field, B_z , is in z-direction, and the gradient field $\partial B_z^o/\partial z$ is supplied by the Helmholtz coils, the equation for the force is

$$F_z = m\chi B_z \frac{\partial B_z^o}{\partial z} \qquad \text{Eq.5-2(b)}$$

The gradient field is independent from the main field B_z .

The force on the specimen is measured by a microbalance (of resolution one μ-gram),

$$F_z = Wg \qquad \text{Eq.5-3}$$

where W is the apparent increase in weight due to the field, and g is the gravitational acceleration.

In the early stages of the work, an electromagnet with the truncated conical pole tips driven by a 2-kWatt power supply was used to provide a maximum field of 8.5 kG. The region of constant within $\pm$ 1% and maximum $B_x(\partial B_x/\partial z)$ was found to be from 23 mm to 33 mm above the centre of the pole (Fig.5-1(a)), and, accordingly, the sample was positioned in the middle of this region. The maximum value of $B_x(\partial B_x/\partial z)$ was checked and calibrated by measuring the force exerted on a high purity (4N) tantalum specimen at room temperature. A Delrin cylinder (open at one end) was used as a sample holder for the Na_xSi_{136} specimens. It was 15 mm long with a diameter 4 mm. Its susceptibility was calibrated from liquid nitrogen temperature down to 1.5 ^oK and was found to be constant at -3.4×10^{-7} emu $gram^{-1}$. The Na_xSi_{136} samples, of about 100 mg, were packed into the cylinder which was suspended from a quartz

fibre in a suspension tube (detailed description of the Faraday balance can be found in Male's thesis [58]). A gold rod (mass=1 gram, length = 22 mm) was attached to the bottom of the cylinder in order to stabilize the suspension. This gold rod was located at the centre of the magnetic poles (Fig.5-1(a)) so that the net force exerted on the gold rod was zero.

At every temperature point (from 1.5 to 20 ^{o}K), the force was recorded by varying the applied field (which varied also the strength of the field gradient). Therefore a plot of $F_z/(\partial B_x/\partial z)$ versus the field B_x gives a slope equal to the total measured moment :

$$\frac{F_z}{\left(\frac{\partial B_x}{\partial z}\right)} = m_I \sigma + M \chi_T B_x \qquad \text{Eq.5-4(a)}$$

and

$$M \chi_T = m_s \chi_s + m_b \chi_b \qquad \text{Eq.5-5}$$

where χ_s is the susceptibility of the specimen, χ_b is the background susceptibility of the sample holder. χ_b is known, so the apparent susceptibility of the sample can be found from Eq.5-5. The intercept at zero field $m_I\sigma$ gives the magnetization due to the presence of any foreign ferromagnetic particles.

Care has been taken to minimize the amount of foreign impurity from falling into the powder samples, it estimated less than 20 ppm for most of the samples.

The superconducting solenoid can provide a magnetic field up to 40 kG., but the maximum field used in the present work was 10 kG. The gradient field, always 88 G cm^{-1}, was provided by an antiparallel

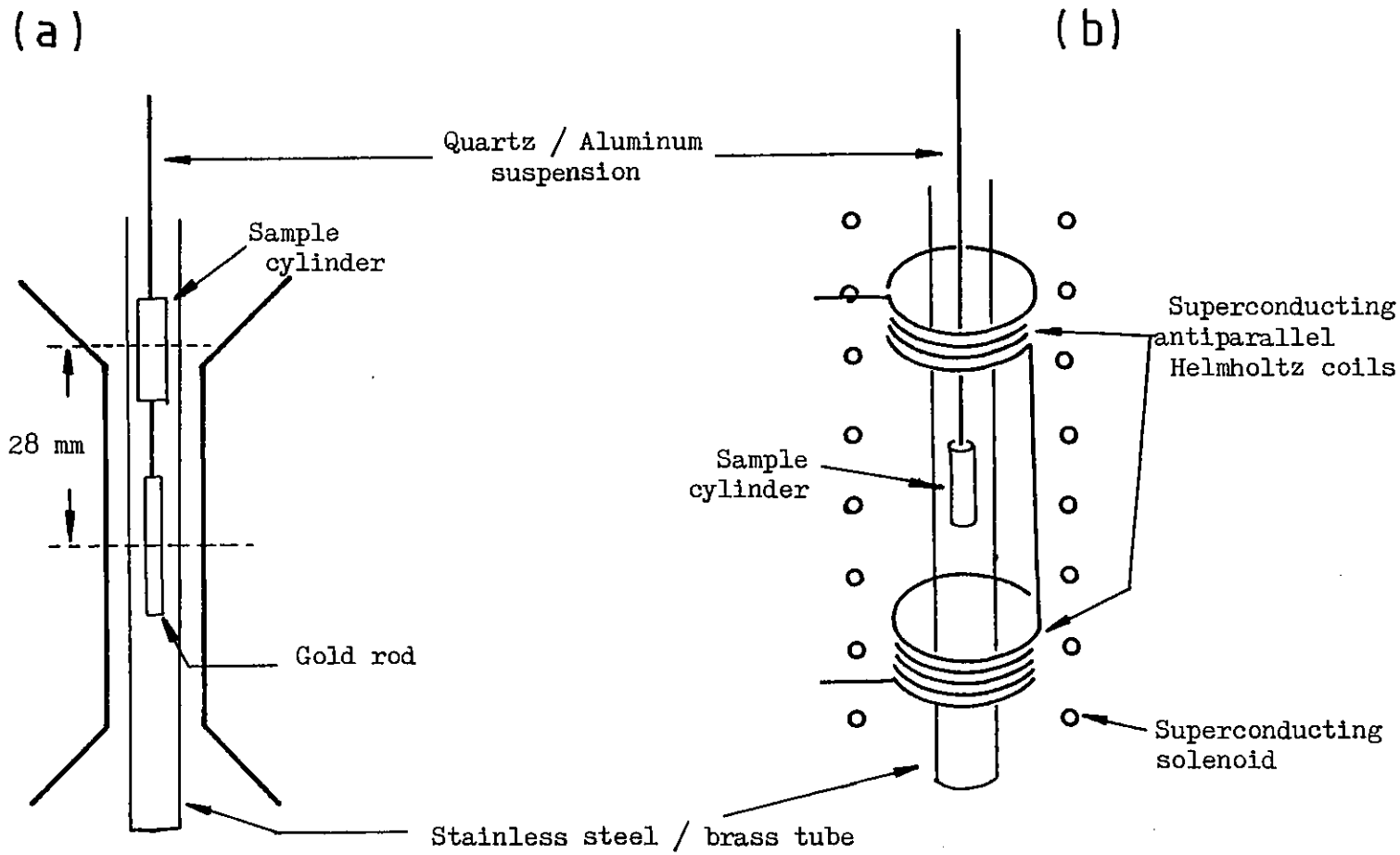

FIG. 5-1 ARRANGEMENT OF SPECIMEN IN THE SUSPENSION TUBE OF THE FARADAY BALANCE : (a) IN A FIELD SUPPLIED BY ELECTROMAGNET CONICAL POLES ; (b) IN A SUPERCONDUCTING SOLENOID

pair of Helmholtz coils (Fig.5-1(b)). The gold rod could not be attached to the sample holder because the Gouy force (tends to pull the gold rod downwards) would be significant compared with the force on the specimen. In order to overcome the lateral problem of the stability of the specimen in the field, a 30 cm long high purity alumimum wire (diameter $\simeq$ 0.5 mm) was glued to the tail end of the quartz fibre. The alumimum wire is more rigid than the quartz fibre, so that it restricts the lateral movement of the specimen in the magnetic field. Another advantage of using alumimum wire is that its magnetic susceptibility is small and almost constant with temperature. The sample holder was hung from the alumimum wire. Again, the background susceptibility of the sample holder in this arrangement was calibrated from 77 K down to 1.5 K. It was temperature independent but its value, $m_b \chi_b$ = -6.6×10^{-8} emu, was reduced, reflecting the paramagnetic contribution of the alumimum.

Experimentally, the field (supplied by the solenoid) and the field gradient (supplied by the Holmholtz coils) were applied separately. At each temperature point, the field B_z was varied from zero to 10 kG. in steps of one kG. At each step, the gradient field was switched from zero to a constant value (88 G cm^{-1}), and the net force due to the application of the gradient was read. Plotting the force in the same way as before gives the susceptibility of the sample :

$$\frac{F_z}{\left(\frac{\partial B_z}{\partial z}\right)} = m_I \sigma + M \chi_T B_z \qquad \text{Eq.5-4(b)}$$

For low temperature susceptibility measurements, it is sufficient to consider the experimental susceptibility χ_s to be composed of two components. The localized sodium 3s-electrons will contribute to the temperature dependent term χ . The silicon atoms and the sodium nuclear core will contribute diamagnetism which is temperature independent. This may consist of the Pauli paramagnetism which is the contribution of the delocalized 3s-electrons in the high sodium concentration sample. Hence

$$\chi_s = \chi + \chi_0 \qquad \text{Eq.5-6}$$

where $$\chi = \frac{N\mu^2}{3k_B(T+\theta)} = \frac{C}{T+\theta} \qquad \text{Eq.5-7}$$

χ is the Curie-Weiss susceptibility, χ_0 is the temperature independent term, N is the number of sodium atoms per mole, μ is the magnetic moment and C is the Curie constant. By plotting χ_s against 1/T, χ_o could be obtained by extrapolating to 1/T = 0. For all samples, was of order $\pm 10^{-8}$ emu gm^{-1} (except sample 12 which had a value of 6×10^{-7} emu gm^{-1}).

5.3 PRESENTATION OF RESULTS

The magnetic susceptibilities of ten Na_xSi_{136} samples with different sodium concentrations were measure from approximately 1.5 K up to 20 K (Appendix C lists the experimental data). The reciprocal susceptibilities in mole unit for all samples were plotted against temperature and are shown in Fig.5-2. The straight line is the linear

fit to the Curie-Weiss law (Eq. 5-7) with a positive Curie-Weiss temperature θ (Table 5-1). The positive θ for all Na_xSi_{136} samples indicates the presence of spin-spin interactions which give a tendency to antiferromagnetic alignment.

For low sodium concentration samples, such as $Na_{1.5}Si_{136}$, $Na_{2.8}Si_{136}$, $Na_{4.5}Si_{136}$ and $Na_{5.3}Si_{136}$, their susceptibilities at 4.2 K decreased as the sodium concentration decreased except $Na_{1.5}Si_{136}$. It needs to be stated that $Na_{1.5}Si_{136}$ was the most dilute sample, having 1.09 at.% sodium, but the sample contained 52% (volume) of pure silicon. The susceptibility of silicon is known to be diamagnetic, therefore it does not account for the value of the Curie constant of this sample. The average magnetic moment μ per sodium atom in these low concentration samples decreased from 0.37 μ_B to 0.17 μ_B as the sodium concentration increases. At temperatures down to 1.5 K, the reciprocal susceptibility of these samples has not shown any upturn which is characteristic of an ordered antiferromagnet.

$Na_{7.5}Si_{136}$ (sample 20-D) was the sample prepared by the thermal diffusion method that had its sodium concentration increased from 2 at.% (sample 20) to 5.2 at.%. The susceptibility reduced and its magnetic moment reduced from 0.37 μ_B to 0.13 μ_B .

On further increasing the sodium concentration, for example, $Na_{13}Si_{136}$, $Na_{18.7}Si_{136}$ and $Na_{22}Si_{136}$, the magnetic moment decreased to about 0.05 μ_B per sodium atom. It should be pointed out that $Na_{14}Si_{136}$ and $Na_{17}Si_{136}$ (samples 9 and 11 respectively) contained 40% and 46% (volume) Na_8Si_{46} phase respectively. The susceptibility of

FIG. 5-2 Reciprocal susceptibilities plotted against temperature for Na_xSi_{136}

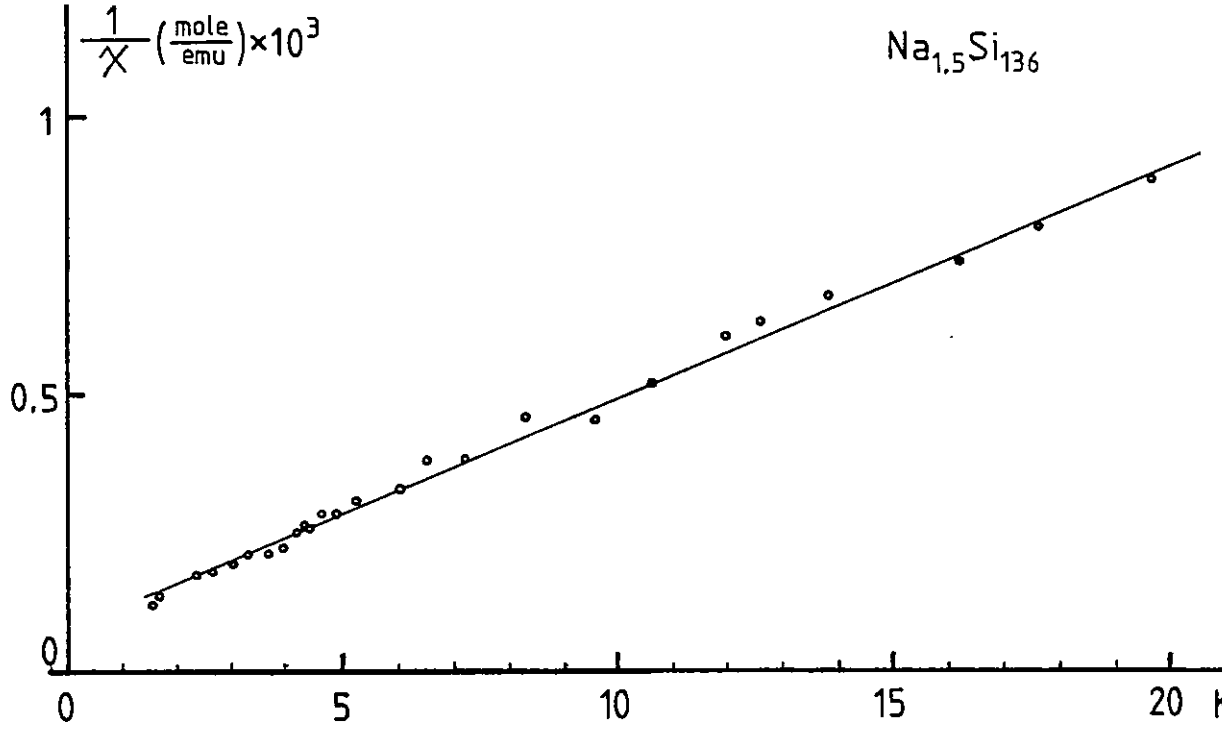

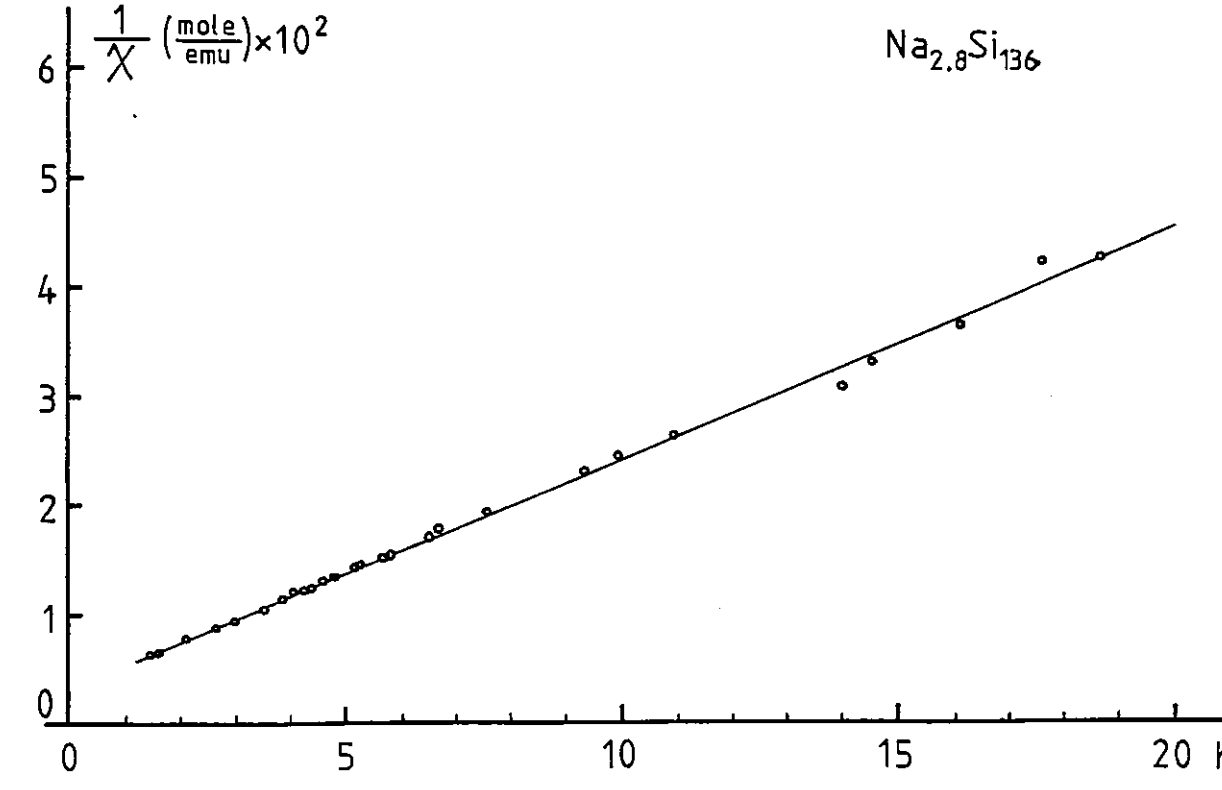

FIG. 5-2 (*continue*)

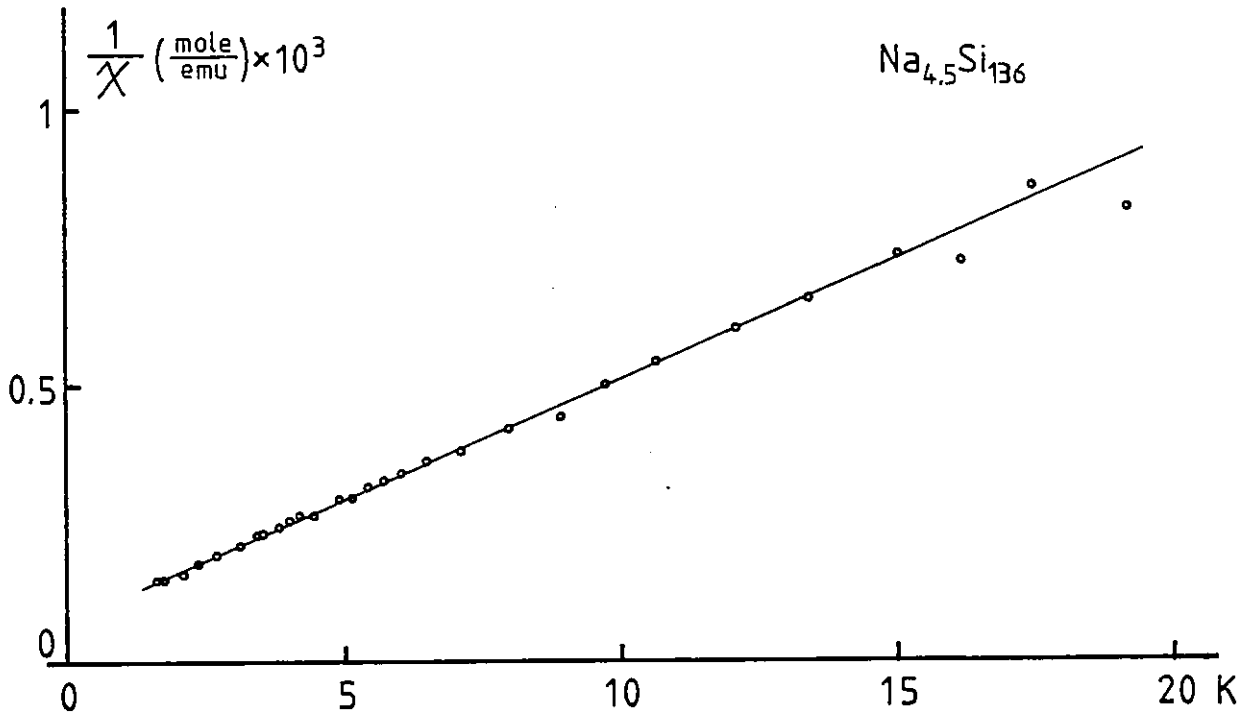

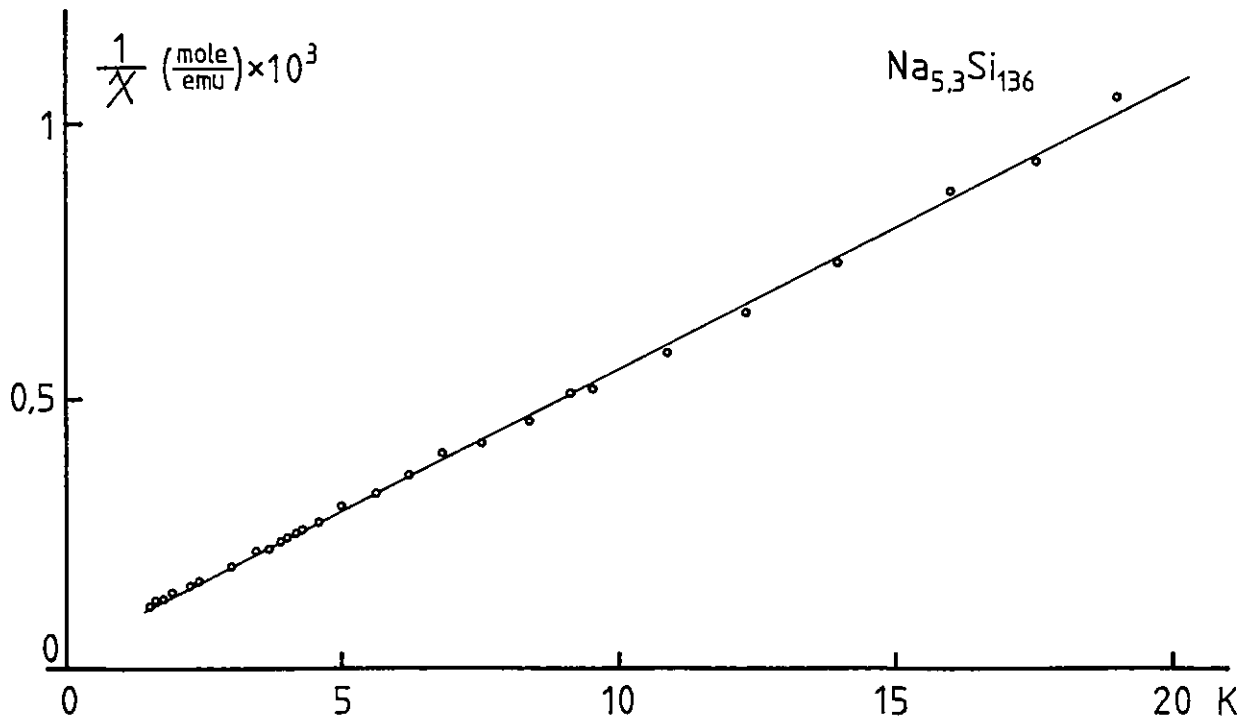

FIG. 5-2 (*continue*)

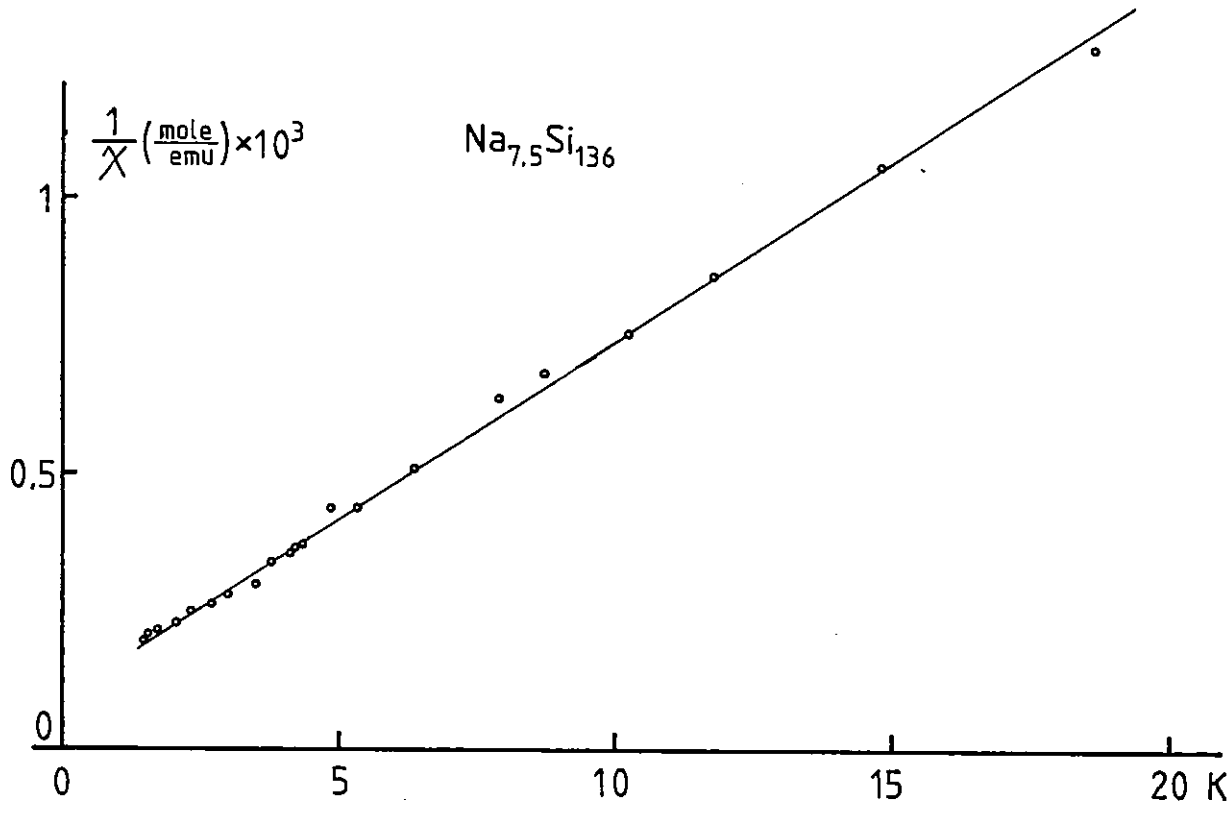

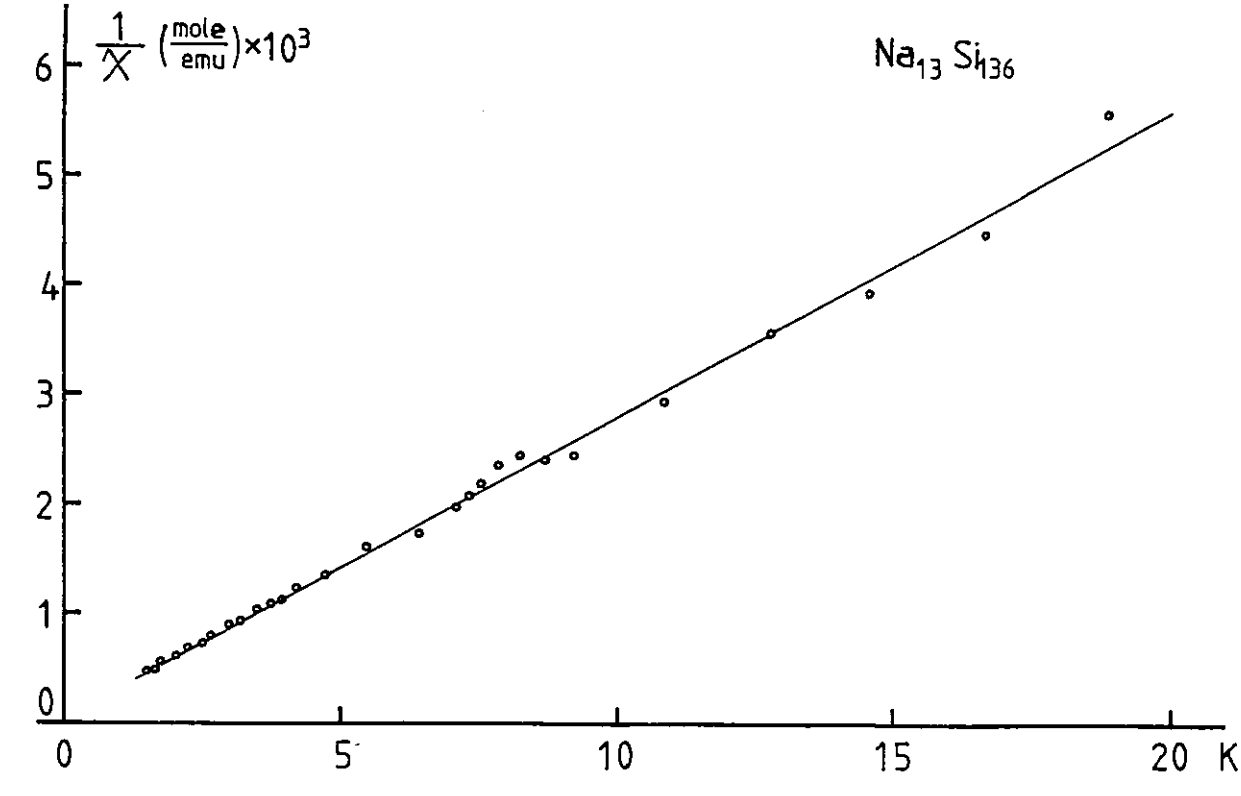

FIG. 5-2 (*continue*)

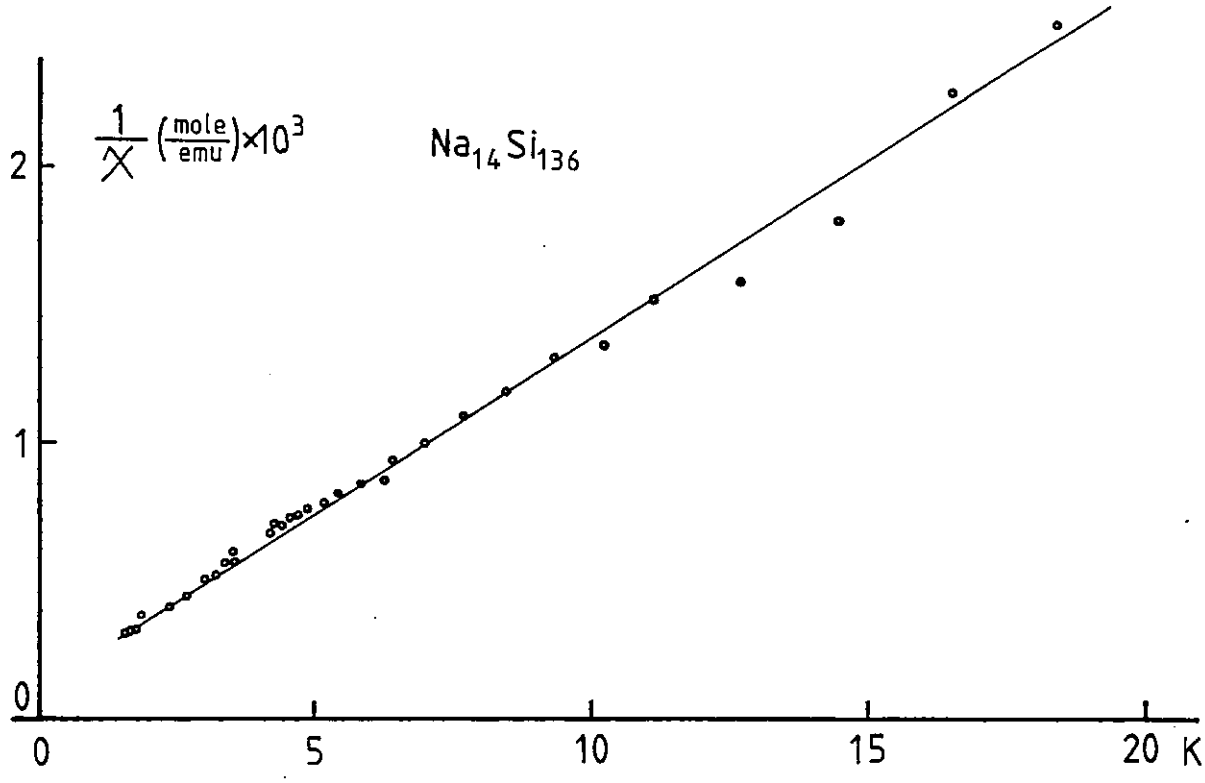

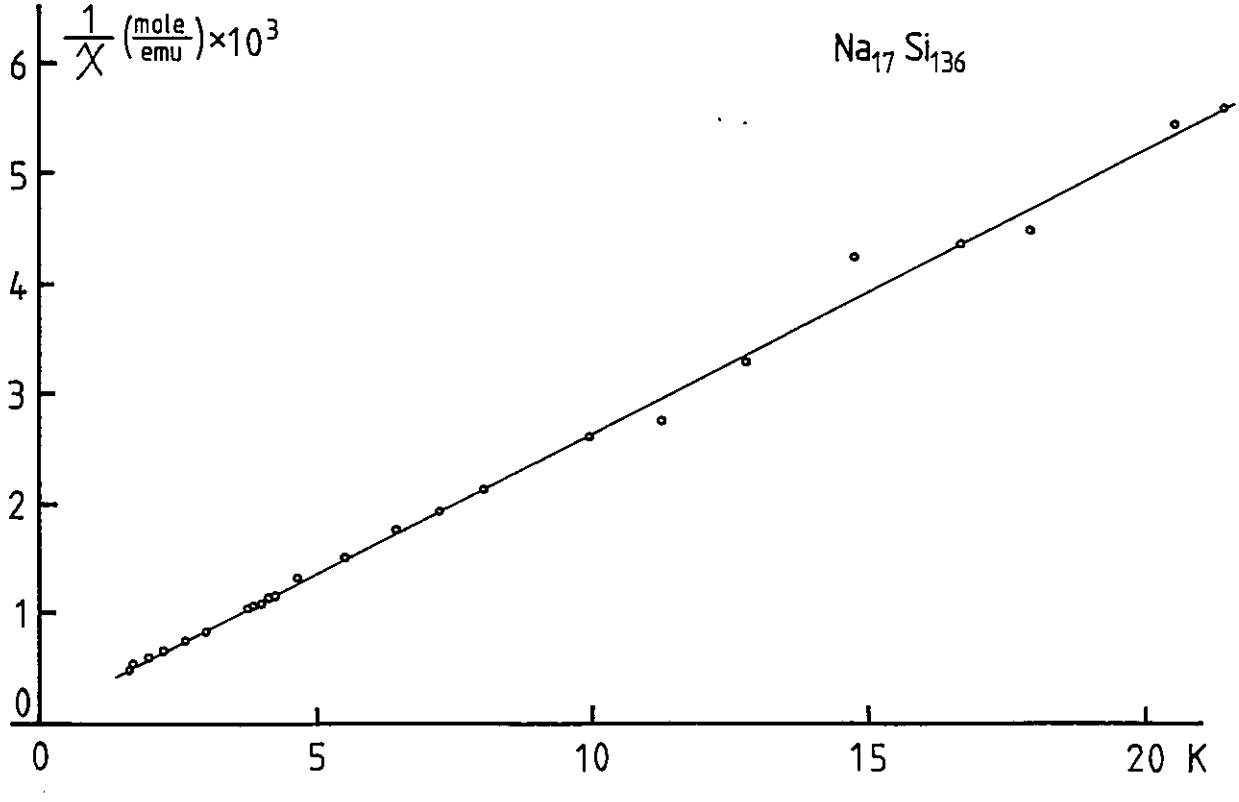

FIG. 5-2 (*continue*)

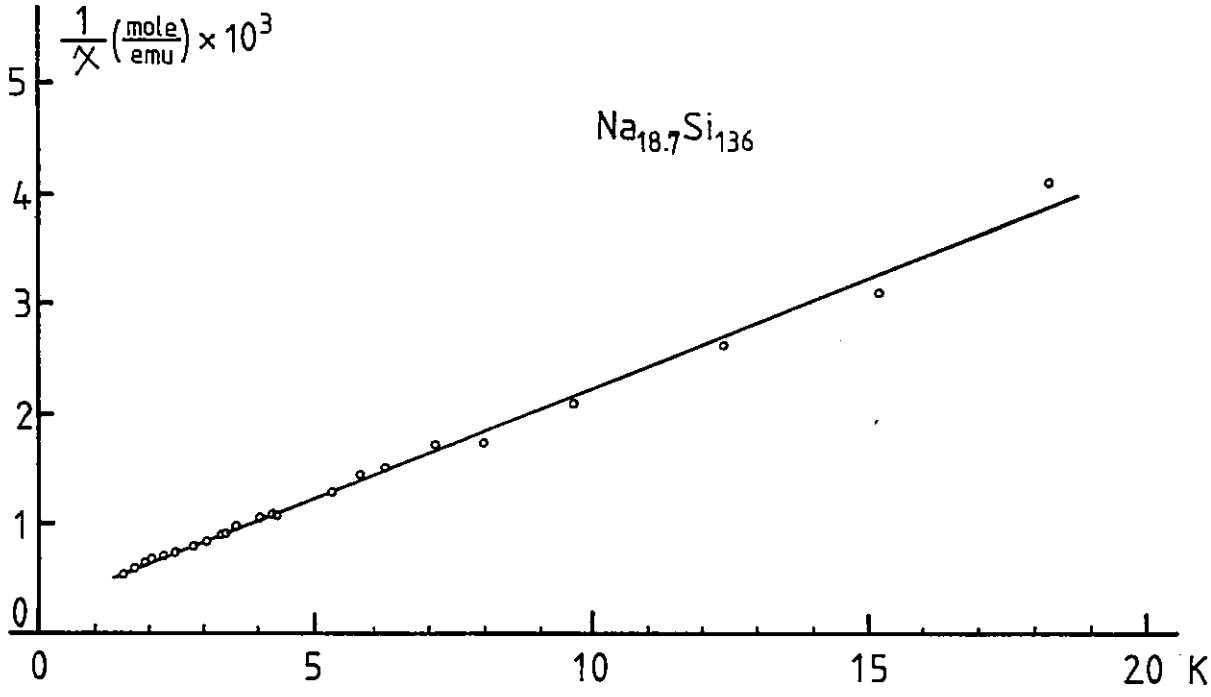

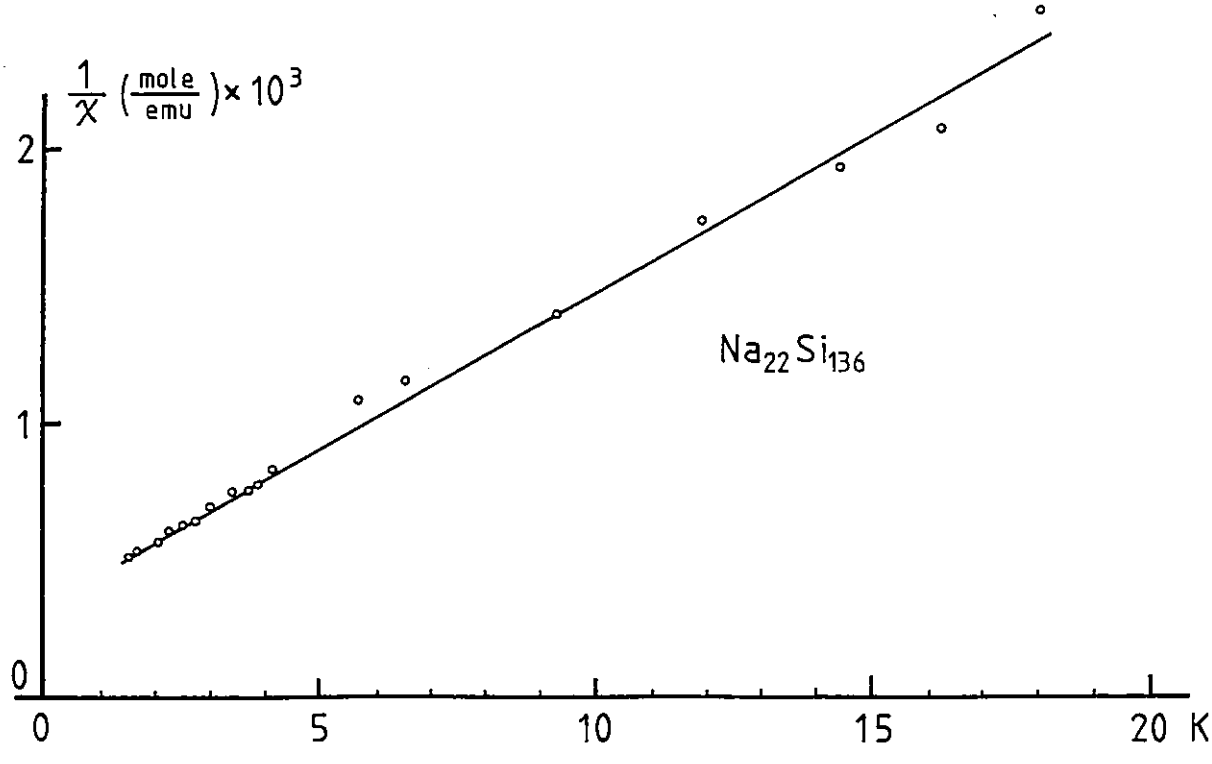

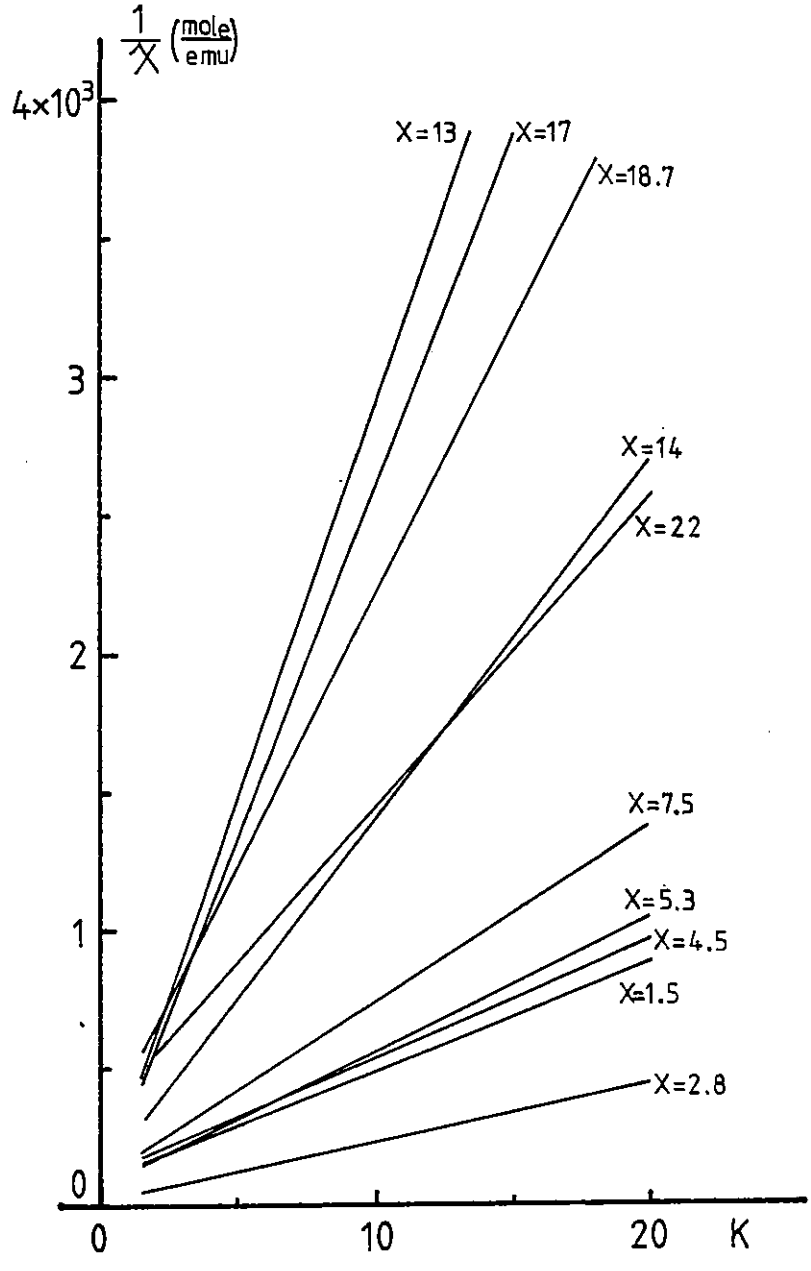

FIG. 5-3 RECIPROCAL SUSCEPTIBILITY FOR Na_XSi_{136}

(Data points are shown in FIG. 5-2)

TABLE 5-1 RESULTS OF MAGNETIC SUSCEPTIBILITY FOR Na_XSi_{136}

Sample No.	Composition (X) in Na_XSi_{136}	χ_o (10^{-8} emu/gram)	Curie const. C (10^{-3} emu K/mole)	Curie-Weiss temperature θ (K)	Magnetic moment, μ (erg/G)$\times 10^{-21}$	$\frac{\mu}{\mu_B}$ (%)
12	1.5	60.9	23.8	1.6	3.30	35.6
20	2.8	3.6	47.9	1.4	3.43	37.0
13	4.5	3.6	22.8	1.6	1.87	20.1
15	5.3	-5.9	19.4	0.6	1.59	17.1
20-D	7.5	5.3	15.4	1.4	1.19	12.8
26	13.0	-2.3	3.62	0.0	0.44	4.7
9	14.0	1.3	7.82	0.8	0.62	6.7
11	17.0	-0.7	3.90	0.3	0.40	4.3
25	18.7	9.6	5.04	1.2	0.43	4.6
25-D	22.0	4.8	8.76	2.9	0.52	5.6

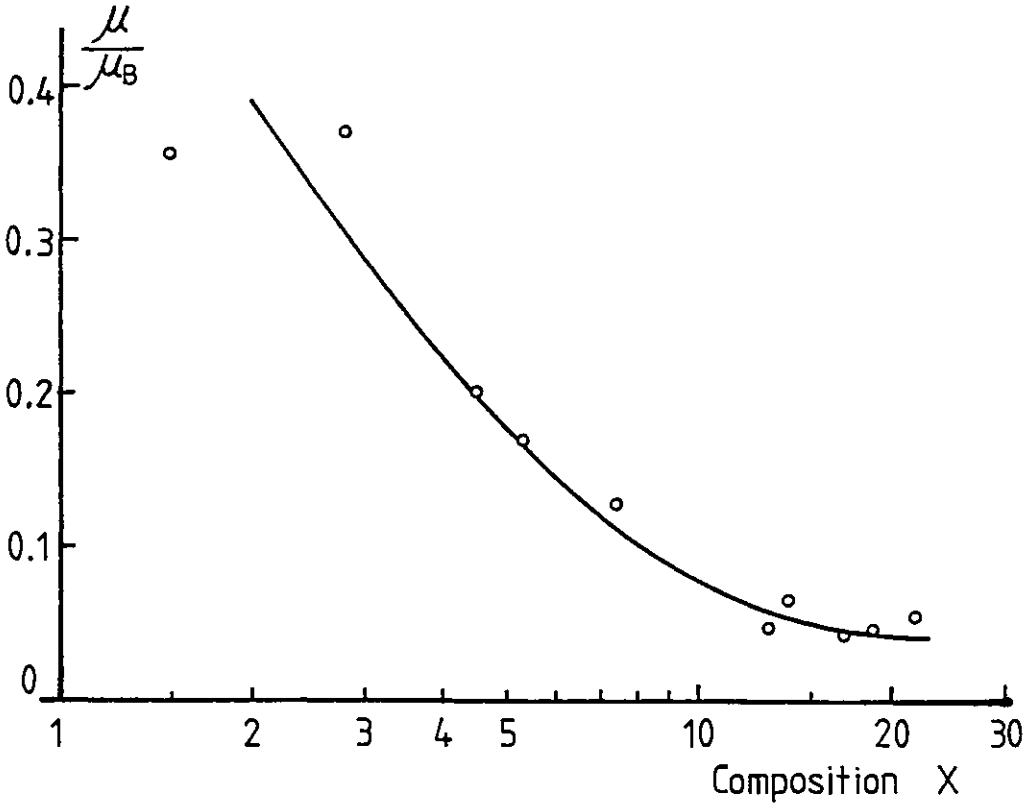

FIG. 5-4 APPARENT MAGNETIC MOMENT μ PER Na ATOM AS A FUNCTION OF COMPOSITION X FOR Na_XSi_{136}

(The curve is solely to guide the eye)

Na_8Si_{46} at low temperatures is not known, therefore it was impossible to estimate its contribution to the total susceptibility of the sample. Since this Na_8Si_{46} phase compound is thought to be metallic, it is probable that its susceptibility has Pauli (temperature-independent) character so that it would not change the Curie constant of the Na_xSi_{136}. The magnetic moments for these two samples were $0.07\mu_B$ and $0.04\mu_B$ per sodium atom respectively. All these high sodium concentration samples showed no sign of an ordered antiferromagnetic character at temperatures down to 1.5 K.

5.4 DISCUSSION AND CONCLUSIONS

It is readily observable that the plots of $1/\chi$ versus temperature for all samples are straight lines, as one would expect from Eq.5-7. However, right down to the lowest experimental temperature, none of the plots (Fig.5-2) show an upturn which would be characteristic of an ordered antiferromagnetic transition. The reciprocal susceptibilities versus temperature for all ten samples are re-plotted in Fig.5-3. For low sodium concentration samples, the magnetic moment per atom drops (Fig.5-4). For $x > 13$, the susceptibility increases again. In fact, there is a tendency towards Pauli paramagnetism, which can be understood as electrons being created by the increasingly important interaction between filled sodium sites. The reason for the apparent decrease of atomic magnetic moment with increasing sodium concentration is as follows. The wavefunction of the sodium 3s-electrons extends much further in the clathrate compound than in an isolated atom. Therefore even at low concentrations some

3s states will overlap such that the spins are paired in opposite directions causing them to be magnetically inactive (ie. the average magnetic moment is small). As the concentration of sodium increases , the extended wavefunction will cause more and more of the 3s-electrons to be paired until a small temperature-independent Pauli paramagnetism sets in and the sample becomes a metallic phase.

It is possible to make a crude estimate of the number of isolated sodium atoms in the clathrate compound which contribute to the free-spin paramagnetic susceptibility. We assume that an isolated sodium atom has a local moment μ_B and a spin $S=\frac{1}{2}$ with g-factor $g = 2$. For example, the Curie constant data of the $Na_{2.8}Si_{136}$ sample (Table 5-1), we have from Eq.5-7

$$C = \frac{N_s \mu^2}{3 k_B} = \frac{N_s g^2 \mu_B^2 s(s+1)}{3 k_B}$$

Therefore, $N_s = 7.7 \times 10^{22}$ spins $mole^{-1}$ and hence the number of 'isolated' sodium atoms is about 5% of the total in the sample. There are still fewer isolated spins at higher concentrations. It is remarkable that the wavefunction of a 3s-electron extends to such a great radius that most of the spins are paired even when the sodium atoms are located two or three sites away from one another. The spin interaction would involved two or more electrons forming some kind of cluster as happens in Si:P system. Within the cluster, the interaction is of antiferromagnetic type. Although the experimental data extends only down to approximately 1.5 K, it may argued that the Na_xSi_{136} system does not exhibit the susceptibility peak characteristic of an ordered antiferromagnet. Because the sodium atoms randomly occupy

the available sites in Na_xSi_{136}, a very wide range of nearest-neighbour interactions are expected to exist in this system. Si:P has a wide range of nearest-neighbour interactions between donors which is created by the rapid decrease of exchange interactions with interdonor distance[14]. In this respect the reciprocal susceptibility of Si:P approaches zero as the temperature falls to zero, this is thought to be the effect of inter-cluster interaction. In an analogous way, it is reasonable to anticipate that Na_xSi_{136} would exhibit similar behaviour and the reciprocal susceptibility will drop to zero at lower temperatures.

CHAPTER 6

ELECTRON PARAMAGNETIC RESONANCE STUDIES ON Na_xSi_{136}

6.1 BACKGROUND THEORY

The magnetic susceptibility of Na_xSi_{136} compounds shows Curie-Weiss behaviour, indicative of some overlap of the 3s electron wavefunctions of adjacent sodium atoms. These atoms may, of course, be several sodium sites apart depending on the distribution between the two types of cage and the overall concentration of sodium. The average local magnetic moment of sodium in the compound is small, and it decreases as the sodium concentration increases. At higher concentrations the susceptibility shows a tendency to Pauli paramagnetism which is a characteristic of conduction electrons. It is of interest to have a closer look at the 3s wavefunctions of sodium in the silicon clathrate cage by means of electron paramagnetic resonance. This technique has proved to be powerful in investigating the motion of donor electrons in semiconductors and can provide, for example, information about the electron wavefunctions and the exchange interaction between the electrons of the donors. In phosphorus doped silicon (Si:P), four of the valence electrons of the impurity form covalent bonds with their nearest silicon neighbours and therefore exhibit the usual diamagnetic behaviour. The fifth electron of phosphorus, however, can exhibit a paramagnetic resonance. This electron moves in the Coulomb-like potential of the donor nucleus and, at low temperatures, is loosely bound in the ground state of the donor atom. There are several perturbations on the resonance in Si:P, namely the electron - nucleus interaction (hyperfine interaction),

cluster resonance [19,20], and exchange interaction. Resonance studies have given precise information on these interactions [19-21].

In Na_xSi_{136}, the sodium atom, unlike the impurity in Si:P, does not substitute for a silicon atom but occupies a special site in a clathrate cage. Because the cage is big (radius > 3 Å), it may be thought that the sodium is isolated from other like atoms. However, the presence of silicon atoms surrounding the sodium atom tends to reduce its potential well. Accordingly, the sodium 3s electron wavefunction expands and penetrates nearby cages.

Consider first an atom with a nuclear spin $\vec{I}$ in a magnetic field. The electronic spin Hamiltonian may be written as

$$H = g_S \mu_B \vec{B}\cdot\vec{S} - g_I \mu_N \vec{B}\cdot\vec{I} + A\,\vec{I}\cdot\vec{S} \qquad \text{Eq.6-1}$$

where the first term of the right hand side is the Zeeman interaction, the second term the nucleus - magnetic field interaction, and the third term the magnetic hyperfine interaction. The hyperfine interaction is a magnetic interaction between the magnetic moments of the unpaired electron and the nucleus. There are two types of contribution. One is the so-called dipole-dipole interaction which is contributed by non s-state electrons :

$$H_{IS} = \frac{\vec{\mu}_e\cdot\vec{\mu}_n}{r^3} - \frac{3(\vec{\mu}_e\cdot\vec{r})(\vec{\mu}_n\cdot\vec{r})}{r^5} \qquad \text{Eq.6-2}$$

where $\vec{\mu}_n$ and $\vec{\mu}_e$ are the nuclear and electron moments respectively. For s-states, the effective current about the nucleus is zero but there is only an effect due to the electron wavefunction being nonzero at

the nucleus; this is the Fermi contact interaction. The magnitude of this can be interpreted in terms of the unpaired spin of the s-electron. When the orbiting electron penetrates the nucleus it experiences an interaction due to its magnetization. The magnetic polarization of the nucleus is

$$\vec{P}_N = \frac{\vec{\mu}_n}{V} = \mu_N g_I \frac{\vec{I}}{V_n} \qquad \text{Eq.6-3}$$

where V_n is the nuclear volume. The magnetic field within a spherical nucleus is

$$\vec{B}_{IN} = \frac{8\pi}{3} \vec{P}_N \qquad \text{Eq.6-4}$$

Therefore the interaction of this field with the spin magnetic moment of the electron within the nuclear volume becomes

$$H_{IS} = -(\mu_B g_S)\, \vec{S} \cdot \vec{B}_{IN}$$

$$= -\frac{8\pi}{3} (\mu_B g_S)(\mu_N g_I) \delta(\vec{r})\, \vec{S} \cdot \vec{I} \qquad \text{Eq.6-5}$$

where $\delta(\vec{r})$ is the Dirac function.

The expectation value of A (Eq.6-1) is

$$\langle A \rangle = -\frac{8\pi}{3} (\mu_B g_S)(\mu_N g_I) \left| \Psi_S(0) \right|^2 \qquad \text{Eq.6-6}$$

where $\left|\Psi_S(0)\right|^2$ is the s-electron density at the nuclear centre.

The selection rules for this transition are

$$\Delta F = \pm 1 \quad , \quad \Delta m_F = \pm 1 \qquad \text{Eq.6-7}$$

where $\vec{F} = \vec{I} + \vec{S}$ is the total momentum of the electron - nucleus system.

In a strong field approximation, the electron spin Zeeman energy is much bigger than the hyperfine coupling energy. Therefore, the Hamiltonian H commutes with S_z and its eigenvalue is m_s. The z-component of nuclear spin I_z also commutes with the Hamiltonian, its eigenvalue being m_I. The first-order energy levels are

$$E = g_S \mu_B B m_s - g_I \mu_N B m_I + \langle A \rangle m_s m_I \qquad \text{Eq.6-8}$$

In an ordinary microwave resonance experiment, the transitions are allowed only if the frequency ν satisfies the conservation of energy. The selection rules for transitions are

$$\Delta m_s = \pm 1 \quad , \quad \Delta m_I = 0 \qquad \text{Eq.6-9}$$

This results in a set of hyperfine lines which are resolved and occur at

$$\Delta E = h\nu = g_s \mu_B B + \langle A \rangle m_I \qquad \text{Eq.6-10}$$

where $m_I = -I, -I+1, \cdots\cdots, I-1, I$ Eq.6-11

Thus the electron resonance is split into 2I+1 equally spaced lines (59).

In an intermediate field case, it is necessary to solve the secular equation corresponding to the complete perturbation of Eq.6-1. An approximate solution of this secular equation leads to the well-known Breit-Rabi formula for the energy levels (60) :

$$E = -\frac{\Delta\mathcal{E}}{2(2I+1)} - g_I \mu_N B m_F \pm \frac{\Delta\mathcal{E}}{2}\sqrt{1 + \frac{4m_F}{2I+1}X + X^2} \qquad \text{Eq.6-12}$$

where $$\Delta\mathcal{E} = \langle A \rangle (I + \frac{1}{2}) \qquad \text{Eq.6-13}$$

is the doublet F energy separation,

$$X = (g_S \mu_B - g_I \mu_N)\frac{B}{\Delta\mathcal{E}} = \frac{g_I \mu_B}{\Delta\mathcal{E}} B \qquad \text{Eq.6-14}$$

$$m_F = m_I + m_s \qquad \text{Eq.6-15}$$

We rewrite the Breit-Rabi formula for the resonance transition :

$$\alpha\langle A \rangle^2 + \beta\langle A \rangle + \gamma = 0 \qquad \text{Eq.6-16}$$

where $$\alpha = \frac{1}{4}\left[\left(\frac{g_T \mu_B B}{h\nu + g_I \mu_N B}\right)^2 - (2I+1)^2\right]$$

$$\beta = -2 g_T \mu_B B m_I$$

and $$\gamma = (h\nu + g_I \mu_N B)^2 - (g_T \mu_B B)^2$$

The hyperfine coupling constant $\langle A \rangle$ thus can be determined from the resonance spectrum using the Breit-Rabi formula.

The nuclear spin of a sodium atom is I = 3/2, and therefore its resonance spectrum is expected to consist of four hyperfine split lines of unequal spacing. On the other hand, in sodium metal, the 3s electrons are in the conduction band and give no hyperfine splitting. In this case, the resonance spectrum consists of only one broadened line which is due to a spin-lattice relaxation mechanism. This type of relaxation mechanism in sodium metal has been extensively studied, and is considered as an electron-phonon scattering accompanied by a spin flip [61-63].

6.2 EXPERIMENTAL

Five Na_xSi_{136} samples of differing sodium concentration have been studied by electron paramagnetic resonance. The experiments were carried out and performed with the collaboration of Dr.J.E.Cousins and his team at the University of Exeter.

The equipment was a standard X-band microwave working at about 9 GHz (resonance field at about 3 kG. for g = 2). A small amount of irradiated LiF was used as a g-marker (g_{LiF} = 2.0026).

Low temperatures were obtained by allowing liquid helium gas to flow through a small flow cryostat within the microwave cavity. In this way, temperatures down to 9 K could be reached. About 20 mg of each powder sample were packed in a small cylindrical teflon container which was then sealed with bees' wax and inserted in the flow cryostat.

6.3 PRESENTATION OF RESULTS

Five samples (Nos. 12, 20, 15, 26 and 25) have been studied by electron paramagnetic resonance in a temperature range from 9 to 80 K.

6.3.1 Resonance spectrum

Sample 12 ($Na_{1.5}Si_{136}$) was the most dilute sample studied and gave four hyperfine split resonance lines (P_1 - P_4), a broad line (C_1) and two narrow resonance line (C_2 and C_3) which were superimposed on the broad line. The third hyperfine line (P_3) was also superimposed on the narrow line (C_3) on the high field side (Fig. 6-1(a)). The hyperfine coupling constant <A> was obtained by using the Breit-Rabi formula (Eq.6-16) and for sample 12, it is 373 MHz. The g-factor is 2.023±0.004 (TABLE 6-1). The other three resonance lines (C_1, C_2 and C_3) probably result from the formation of spin clusters

in the clathrate compound. The cluster is formed when the separation between the atoms is less than a critical distance, an interaction between the atoms takes place. Thus, the 3s electrons delocalize and experience the hyperfine interaction of several sodium nuclei. The effect of this is the appearance of cluster lines in the resonance spectrum as is the case in Si:P where cluster resonance lines appear in between the two hyperfine lines of the phosphorus[19,20]. The peak-to-peak line widths of the three lines are respectively 70, 10 and 6 gauss. The corresponding g_s-factor are 2.021, 1.994 and 1.993.

Sample 20 ($Na_{2.8}Si_{136}$) gives a similar resonance pattern to $Na_{1.5}Si_{136}$, that is, it consists four hyperfine split lines, one broad and two narrow lines (Figs. 6-1(b)&(c)). The hyperfine constant $\langle A \rangle$ is 373 MHz and the g_s-factor is 2.023 ± 0.002 (TABLE 6-1). The peak-to-peak line width of broad line (C_1) is 79 gauss; for the narrow lines, they are 9 gauss (C_2) and 2 gauss (C_3). The g_s-factor are 2.027, 1.997 and 1.996 respectively.

Whereas the resonance centres of the broad line (C_1) and the narrow line (C_2) in $Na_{1.5}Si_{136}$ (sample 12) are 44 gauss apart; in $Na_{2.8}Si_{136}$ (sample 20) they are separated by 48 gauss. However, centres C_2 and C_3 are 2 gauss apart in both samples.

For $Na_{5.3}Si_{136}$ (sample 15) the hyperfine split lines have disappeared, leaving only the resonance lines C_1, C_2 and C_3. This suggests that all the 3s-electrons of the sodium atoms are involved in clusters although only 20% of the metallic sites are occpuied. However, it should be noted that the spin resonance investigation of this sample has not been as detailed as that on other samples.

$Na_{13}Si_{136}$ (sample 26) also gave a broad line and two narrow

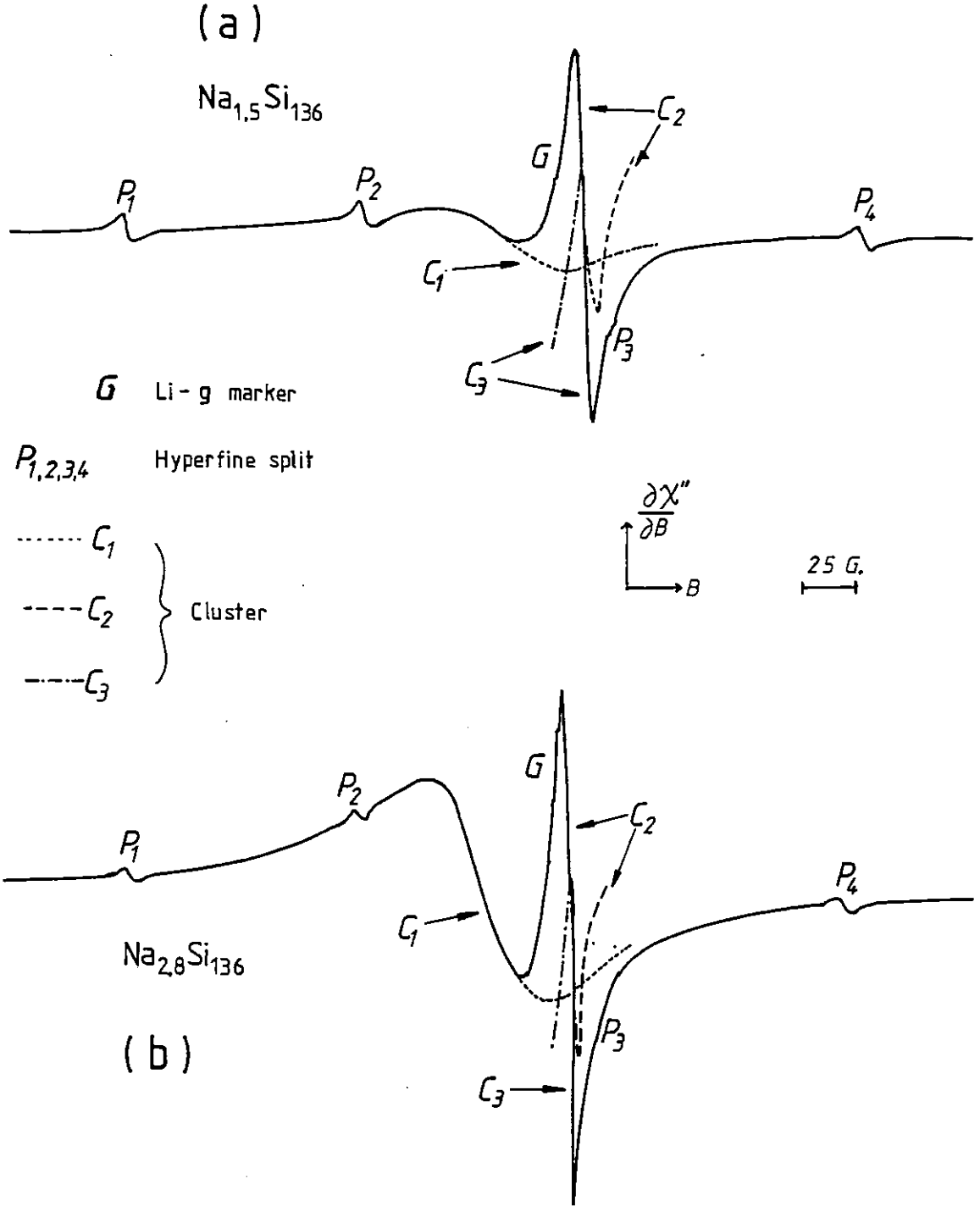

FIG. 6-1 ELECTRON PARAMAGNETIC RESONANCE SPECTRA FOR Na_xSi_{136}

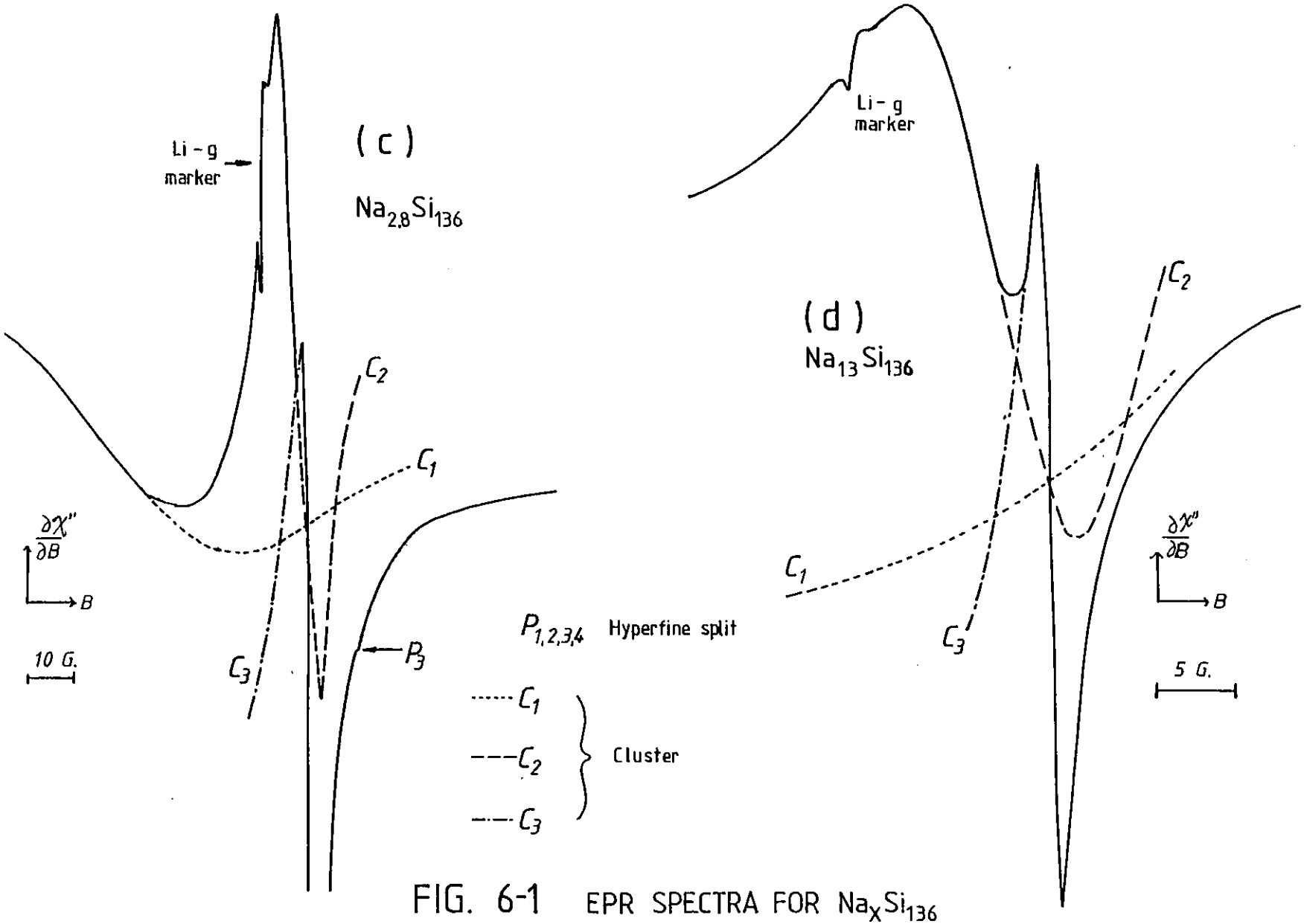

FIG. 6-1 EPR SPECTRA FOR Na_xSi_{136}

TABLE 6-1 ELECTRON PARAMAGNETIC RESONANCE EXPERIMENTAL RESULTS

Sample No.	Na_xSi_{136} X	Hyperfine constant <A> MHz	$\|\Psi_s(0)\|^2$ 10^{24} (cm^{-3})	g_s - factor	Cluster	$\Delta B_{cluster-cluster}$ (gauss)	g_s - factor	$\Delta B_{peck-peck}$ (gauss)
12	1.5	373	2.11	2.023	C_1 C_2 C_3	44 2	2.021 1.994 1.993	70 10 6
20	2.8	373	2.11	2.023	C_1 C_2 C_3	48 2	2.027 1.997 1.996	79 9 2
15	5.3	0	—	—	C_1 C_2 C_3	— —	– 1.997 –	– 9 –
26	13	0	—	—	C_1 C_2 C_3	— 2	– 1.997 1.996	– 10 2
25	18.7	No resonance visible						

ones but no hyperfine splitting has been observed here either, as always, narrow lines are superimposed on the broad line (Fig. 6-1(d)). Line C_1 is now very broad, so its resonance centre cannot be determined precisely. However, the centre to centre distance of the two narror lines (C_2 and C_3) is 2 gauss apart. The g_s-factors of these two lines are 1.997 and 1.996 respectively.

The highest sodium concentration sample in this investigation, $Na_{18.7}Si_{136}$ (sample 25) has not given any observable resonance. About 78% of metallic sites in this compound are occupied by sodium and thus most of the 3s-electrons are antiparallel coupled.

We also investigated the temperature dependence of the resonance spectrum and found that, for all five samples, the position of the peaks did not shift, but the amplitude of the resonance lines decreased as the temperature increased.

6.3.2 Paramagnetic susceptibility

It is essential to estimate the number of spins which contribute to the clusters and the hyperfine splitting. The paramagnetic susceptibility χ_s is expressed by the following equation [59] :

$$\chi_s = \chi'\Big|_{\omega=0} = \frac{2}{\pi}\frac{1}{B_0}\int_0^\infty \chi''(B)\,dB \qquad \text{Eq.6-17}$$

where $\omega_0 = \gamma B_0$ is the angular frequency of the microwave source, γ the magnetogyric ratio constant, $\chi''(B)$ the imaginary part of the complex magnetic susceptibility $\chi = \chi' + i\chi''$ and B the variable

static magnetic field. The integral in equation 6-17 is the area under the paramagnetic resonance absorption curve, $\chi''(B)$. In order to obtain a reliable value of the susceptibility χ_S, the integrated area should be compared with that of a measured amount of reference sample of known spin susceptibility. Compound $CuSO_4 \cdot 5H_2O$ is used as the standard in the work. The line shape of the absorption curve $\chi''(B)$ is known to have a Lorentzian profile [59]:

$$\chi''(B) = \frac{1}{2} \chi_S \, B_o \frac{\Delta B_{\frac{1}{2}}}{(\Delta B_{\frac{1}{2}})^2 + (B_o - B)^2} \qquad \text{Eq.6-18}$$

where $\Delta B_{\frac{1}{2}}$ is the half-line width. The first-order derivative of equation 6-18 has a maximum value at $B_o - B = \Delta B_{\frac{1}{2}}/\sqrt{3}$. Therefore the spin susceptibility χ_S can be written in the form

$$\chi_S = C \frac{(\Delta B)^2}{B_o} \left(\frac{d\chi''}{dB}\right)_{max} \qquad \text{Eq.6-19}$$

In practice and experimentally, the derivative of resonance absorption is measured and plotted directly on a chart recorder. Hence the spin susceptibility measured by electron paramagnetic resonance is in fact determined by

$$\chi_S = C' \frac{(\Delta B_{p\text{-}p})^2}{B_o} \left(\frac{d\chi''}{dB}\right)_{max} \qquad \text{Eq.6-20}$$

where $\frac{1}{2}\Delta B_{p-p} = \Delta B_{\frac{1}{2}}/\sqrt{2}$ is the peak to-peak field strength of $\frac{d\chi''}{dB}$. C' is a constant dependent upon the spectrometer sensitivity, so it is therefore essential to make a comparison measurement, relating the resonance absorption to that of a standard.

The spin susceptibility (Curie law) is given by

$$\chi_S = \frac{N g_s^2 s(s+1) \mu_B^2}{3 k_B T} \qquad \text{Eq.6-21}$$

where N is the number of spins per mole. For both sodium and copper, $S = \frac{1}{2}$. The ratio of susceptibilities for Na_xSi_{136} and the standard sample $CuSO_4 \cdot 5H_2O$ is thus given by

$$\frac{\chi_s(Na)}{\chi_s(Cu)} = \frac{N(Na)}{N(Cu)} \times \frac{T(Cu)}{T(Na)} \qquad \text{Eq.6-22}$$

$T(Cu) = 300$ K is the temperature at which the resonance measurement of the standard sample was made. The number of spins per mole for $CuSO_4 \cdot 5H_2O$ is 6.022×10^{23}. Plots of $\chi_s(Cu)/\chi_s(Na)$ versus temperature $T(Na)$ for four types of resonance in Na_xSi_{136} (sample 20) are shown in Fig.6-2. The hyperfine contributed susceptibility, as expected, obeys the Curie law whereas the three clusters also obey the Curie law at $T > 9$ K. The susceptibility behaviour of the cluster below this temperature is not known because the lowest experimental temperature was 9 K. The number of spins per mole in Na_xSi_{136} is then calculated

FIG. 6-2 RECIPROCAL SUSCEPTIBILITIES PLOTTED AGAINST TEMPERATURE FOR $Na_{2.8}Si_{136}$

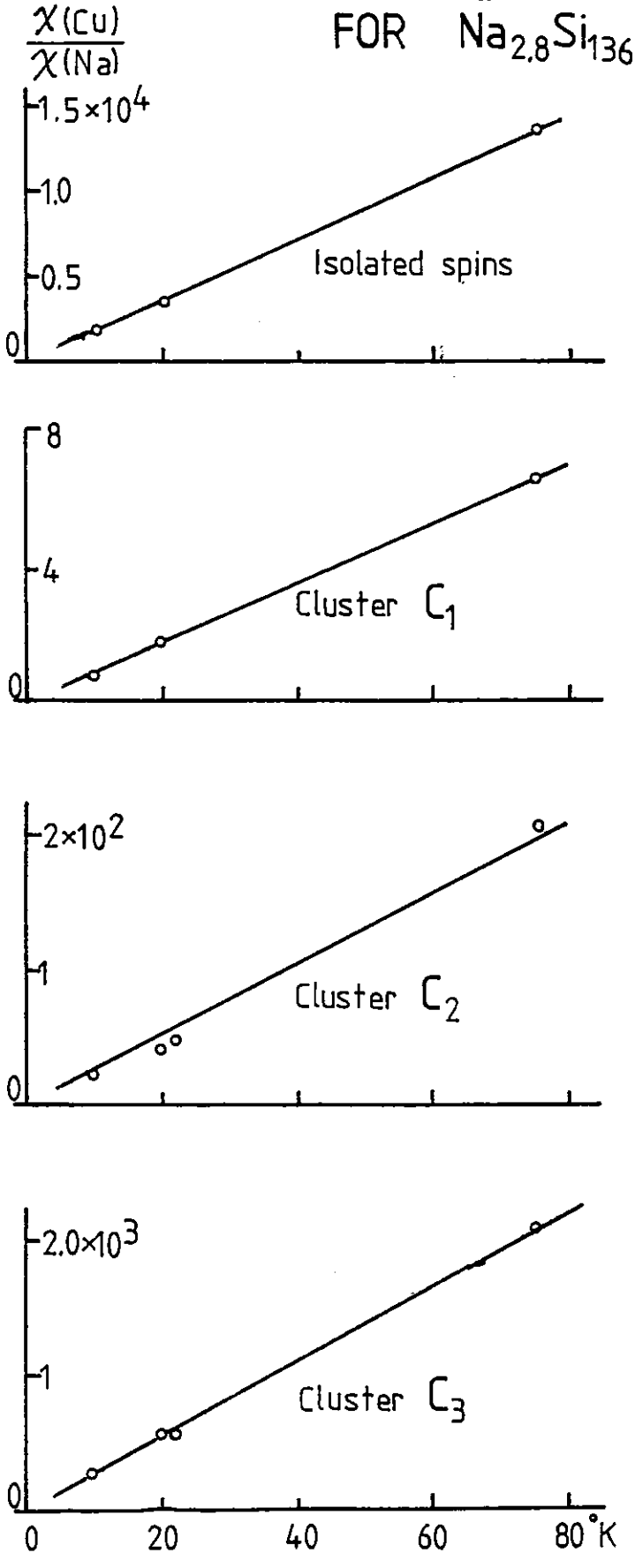

FIG. 6-3 NUMBER OF SPINS AS A FUNCTION OF COMPOSITION FOR Na_xSi_{136}

(The curves are solely to guide the eye)

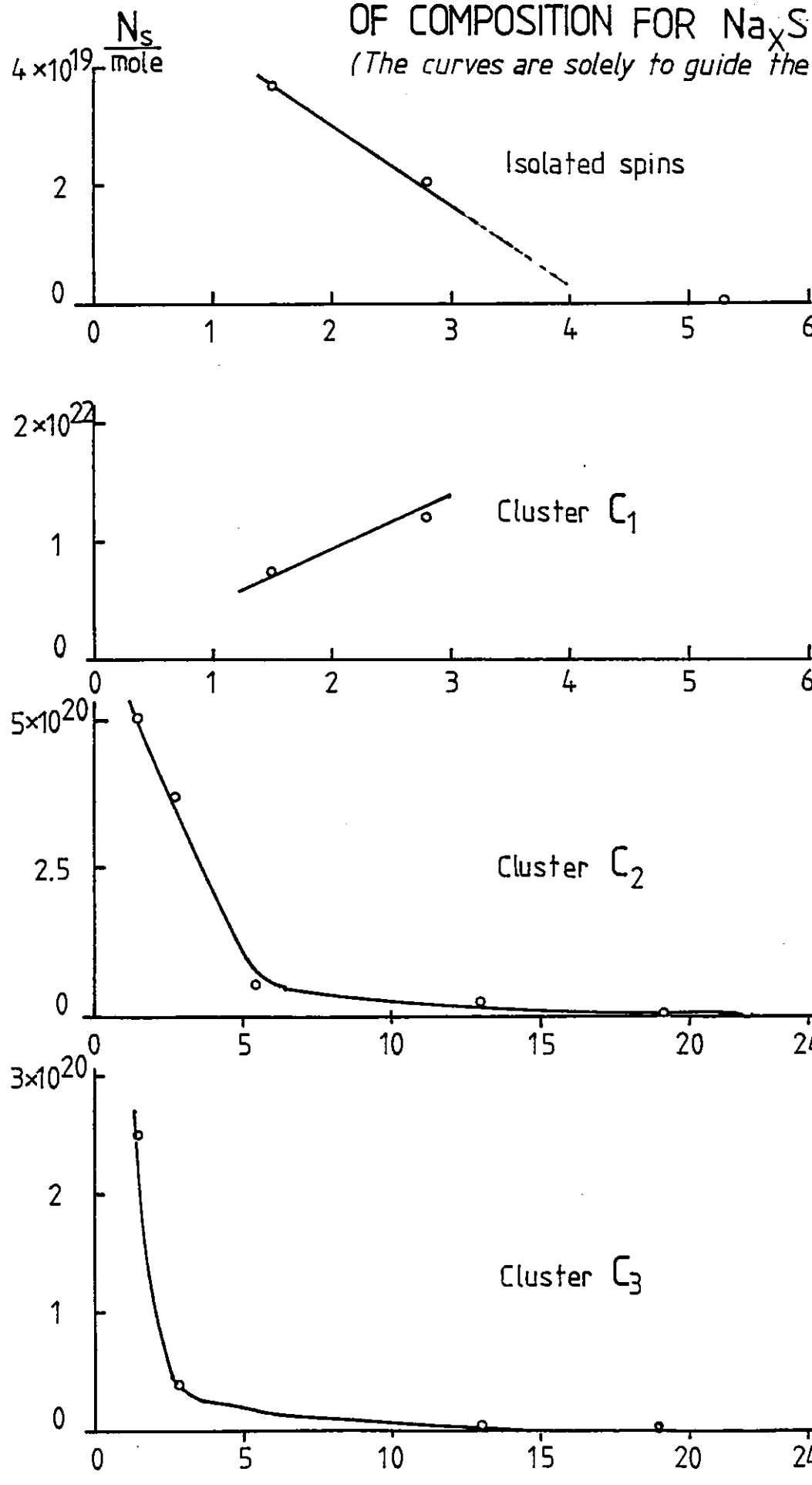

TABLE 6-2 NUMBER OF SPINS FOR Na_xSi_{136}, ESTIMATED FROM ELECTRON PARAMAGNETIC RESONANCE

Sample No.	Na_xSi_{136} X	Isolated spins 10^{-19}/mole	Cluster C C_1 10^{22}/mole	Cluster C C_2 10^{20}/mole	Cluster C C_3 10^{20}/mole	Total spins 10^{22}/mole	Number of spins * 10^{22}/mole
12	1.5	3.7	0.74	5.0	2.5	0.82	3.8
20	2.8	2.2	1.2	3.8	0.37	1.2	7.7
15	5.3	0	—	0.48	—	—	3.1
26	13	0	—	0.22	0.012	—	0.58
25	18.7	0	0	0	0	0	0.81

* *Estimated from the static susceptibility.*

by using Eq.6-22 (TABLE 6-2). The number of isolated electrons which contribute to the hyperfine splitting decreases as the concentration of sodium increases (Fig.6-3). As the occupancy of the metallic sites increases to 20% the hyperfine split line disappears indicating that all the sodium 3s-electrons have completely delocalized. It is interesting to note that the number of spins in cluster C_1 tends to increase as the concentration of sodium increases whilst the spins in both clusters C_2 and C_3 drop to approximately 10^{19} per mole when about 20% of the available sites are occupied. Eventually, the narrow clusters (C_2 and C_3) disappear altogether leaving only the broad clusters C_1 . However, at very high concentrations, $x > 18$, even the resonance due to the cluster becomes unobservable.

6.4 SIMPLE MODEL CALCULATION OF THE ELECTRON DENSITY AT THE SODIUM NUCLEUS

The hyperfine coupling constants, $\langle A \rangle$, of $Na_{1.5}Si_{136}$ (sample 12), and $Na_{2.8}Si_{136}$ (sample 20) deduced from the resonance spectra are 373 MHz. This value is about 42% of that of an isolated sodium atom (886 MHz)[64]. The reduced hyperfine constant is evidence of an expansion of the sodium 3s wavefunction due to screening of the sodium ion's potential well by the silicon atoms forming the clathrate cage (B-type cage for these two dilute samples). In this section, a simple model calculation, which accounts for the reduced hyperfine constant, is discussed.

6.4.1 Muffin-tin potential model

We consider an isolated sodium atom sitting at the centre of a silicon cage which we assume is spherical. The screening effect shifts the potential energy of the guest atom to a new value. To take account of this, a muffin-tin potential is constructed such that the potential is zero beyond a critical distance r_c from the nuclear centre. Another assumption must be made that the critical point r_c is closer to the silicon atoms than the central sodium atom. The sodium and silicon atoms in a B-type clathrate cage are at least 3.2 Å apart. Therefore, it is justifiable to assume that the potential is changed very little in the region close to the sodium core. For the sake of simplicity, we assume that, everywhere within the region $0 \leq r \leq r_c$, the potential is shifted by a constant amount from the original value (ie. from that of an isolated atom). Thus, the new potential is defined as :

$$V'(r) = 0 , \qquad r \geq r_c \qquad \text{Eq.6-23(a)}$$

$$V'(r) = V(r) - V(r_c) , \quad 0 \leq r \leq r_c \qquad \text{Eq.6-23(b)}$$

where $V(r)$ is the original potential of the isolated sodium atom (Fig.6-4). The Schrodinger equation for the motion of a 3s-electron in the spherically symmetric potential $V(r)$ of an isolated sodium atom can be separated into two equations :

$$[\hat{L}^2 - \ell(\ell+1)]Y(\theta,\varphi) = 0 \qquad \text{Eq.6-24(a)}$$

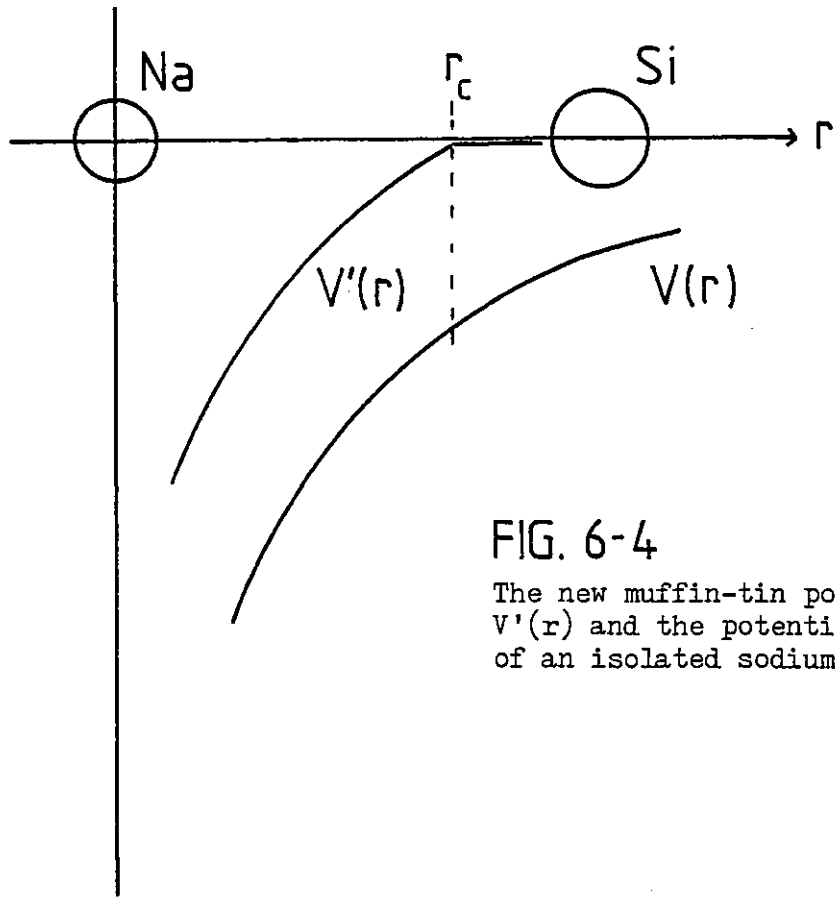

FIG. 6-4
The new muffin-tin potential V'(r) and the potential V(r) of an isolated sodium atom

and $$\left[\frac{d^2}{dr^2} + E - V(r) - \frac{\ell(\ell+1)}{r^2}\right] P(r) \qquad \text{Eq.6-24(b)}$$

where the equations are written in atomic units (E and $V(r)$ in Rydbergs, r in Bohr radii) and $\hat{L}$ is the angular momentum operator inspherical coordinates. The eigenfunctions have the form

$$\Psi = Y_{\ell m}(\theta,\varphi)\frac{P(r)}{r} \qquad \text{Eq.6-25}$$

where $Y_{\ell m}(\theta, \varphi)$ is a constant $(= (4\pi)^{-\frac{1}{2}})$ for the 3s wavefunction and $P(r)/r$ is the radial function. For an s-orbital ($\ell = 0$), Eq.6-24(b) takes the form

$$\left[\frac{d^2}{dr^2} + E + V(r)\right]P(r) = 0 \qquad \text{Eq.6-26}$$

Similarly, the Schrodinger equation for a 3s-electron in the new potential can be written as :

$$\left[\frac{d^2}{dr^2} + E' + V'(r)\right]Q(r) = 0 \qquad \text{Eq.6-27}$$

where $Q(r)/r$ is a new 3s radial wavefunction. This equation can only be solved numerically if the new energy E' and potential $V'(r)$ are known. The potential $V(r)$ is known from the Herman-Skillman tables[68] and $V'(r)$ can be calculated from Eq.6-23. The energy E' may be estimated by the Hartree self-consistent method[65].

We assume that the new wavefunction $Q(r)$ is shifted from the self-consistent wavefunction $P(r)$ (again, the normalized function tabulated in the Herman-Skillman tables) by a small alteration of $T(r)$:

$$Q(r) = P(r) + T(r) \qquad \text{Eq.6-28}$$

To avoid divergence at the origin, $Q(0) = P(0) = 0$. Substituting $Q(r)$ in Eq.6-27 and substituting Eq.6-26, we obtain,

$$\left[\frac{d^2}{dr^2} + E' - V'(r)\right]T(r) + \left[E' - E + V(r) - V'(r)\right]P(r) = 0 \qquad \text{Eq.6-29}$$

Letting $$\delta = E' - E + V(r_c) \qquad \text{Eq.6-30}$$

and combining Eqs.6-23(b), 6-29 and 6-30,

$$P(r)\frac{d}{dr}T(r) - T(r)\frac{d}{dr}P(r) =$$

$$-\delta\int_0^{r_c} P^2(r)dr - \delta\int_0^{r_c} P(r)\,T(r)dr \qquad \text{Eq.6-31}$$

Eq.6-30 represents an alteration of the kinetic energy by δ . Since this is small, the second term on the right hand side of Eq.6-31 can be neglected and the equation rewritten as

$$\frac{d}{dr}\left(\frac{T(r)}{P(r)}\right) \simeq -\frac{\delta}{P^2(r)}\int_0^{r_c} P^2(r)dr \qquad \text{Eq.6-32}$$

The condition of continuity of the logarithmic derivative at r_c must be satisfied :

$$\frac{\dot{Q}(r)}{Q(r)} \simeq \frac{\dot{P}(r)}{P(r)} + \frac{d}{dr}\left(\frac{T(r)}{P(r)}\right) \qquad \text{Eq.6-33}$$

The wavefunction $Q(r)$ has a form of e^{-kr} in the region $r_c \le r < \infty$, hence

$$Q(r) = C e^{-kr} \qquad \text{at} \qquad r \ge r_c$$

where $$k^2 = -E'$$

Rearranging Eq.6-33 and combining with Eq.6-32 :

$$-\sqrt{-E'} = \frac{\dot{P}}{P}\Big|_{r_c} - \frac{\delta}{P^2(r_c)}\int_0^{r_c} P^2(r)\,dr$$

That is,

$$[E' - E + V(r_c)]\,\frac{1}{P^2(r_c)}\int_0^{r_c} P^2(r)\,dr$$

$$-\sqrt{-E'} - \frac{\dot{P}}{P}\Big|_{r_c} = 0 \qquad \text{Eq.6-34}$$

The energy $-E$ is the first ionization energy of sodium and is equal to 0.3777 Ryd. (=5.14 eV). With $P(r)$ and $V(r_c)$ also known, an initial estimate of E' can be obtained by quadratic solution of Eq.6-34.

6.4.2 Determination of the new wavefunction $Q(r)$ by numerical integration

A practical method for solving Eq.6-27 for the new wavefunction $Q(r)$ is by numerical integration. For the Schrodinger equation, the integration is made easy by using Slater power series expansion method[66] in which the wavefunction is expanded in a Taylor series about the point r_n . Let

$$g_n = -[E - V(r)] \qquad \text{Eq.6-35}$$

Substituting in Eq.6-26 :

$$\frac{d^2}{dr^2} P(r) = g_n P(r) \qquad \text{Eq.6-36}$$

Suppose the function $P(r)$ has a set of values, namely $(\ldots P_{n-2}, P_{n-1}, P_n, P_{n+1}, \ldots)$ at positions $(\ldots r_{n-2}, r_{n-1}, r_n, r_{n+1}, \ldots)$, each of which are a distance h apart. Then $P(r)$ may be expanded in a Taylor series,

$$P_{n\pm1} = P_n \pm h P'_n + \frac{h^2}{2} P''_n \pm \cdots\cdots$$

where P'_n, P''_n and so on are the successive derivatives of $P(r)$ with respect to r, computed at r_n. Then

$$P_{n+1} + P_{n-1} \simeq 2P_n + h P''_n$$

Because h is small, the higher order terms can be neglected. From Eq.6-36

$$P_{n\pm1} \simeq (2 + g_n h^2) P_n - P_{n-1} \qquad \text{Eq.6-37}$$

Similarly, for the new wavefunction $Q(r)$,

$$g' = -[E' - V'(r)]$$

$$= -[E' - V(r) + V(r_c)] \qquad \text{Eq.6-38}$$

and from Eq.6-27 :

$$\frac{d^2}{dr^2} Q(r) = g'_n Q(r) \qquad \text{Eq.6-39}$$

Hence, the expression corresponding to Eq.6-37 is

$$Q_{n+1} \simeq (2 + g'_n h^2) Q_n - Q_{n-1} \qquad \text{Eq.6-40}$$

This allow us to compute Q_{n+1} if Q_n and Q_{n-1} are known and, by repetition, to get the whole series. The initial values of Q_n and Q_{n-1} in the expression can be determined by the following approach.

The potential $V(r)$ itself consists of two parts : a nuclear potential $-2Z/r$ (in Rydberg units) and an electronic potential $-V_e$. The nuclear potential goes as $1/r$ which would lead to a singularity in the Schrodinger equation at $r = 0$ if the wavefunction were not zero at this point. The electronic potential $-V_e$ can be expressed as a power series $\sum_{m=0} V_m r^m$ (66). Therefore, from Eq.6-38,

$$g'_n = -\frac{2Z}{r} - E' - V(r_c) + \sum_{m=0} V_m r^m \qquad \text{Eq.6-41}$$

The wavefunction $Q(r)$ also can be expressed as a power series :

$$Q(r) \equiv Q_n = \sum_{k=0} q_k r^k \qquad \text{Eq.6-42}$$

$$\frac{d^2}{dr^2} Q_n = k(k-1) \sum q_k r^{k-2} \qquad \text{Eq.6-43}$$

The product $g'_n Q_n$ has the form :

$$g'_n Q_n = -2Z \sum q_k r^{k-1} - [E' + V(r_c)] \sum q_k r^k$$

$$+ \sum V_m q_k r^{m+k} \qquad \text{Eq.6-44}$$

From Eqs.6-30, 6-39, 6-43 and 6-44, a recurrence relation is obtained :

$$k(k-1)q_k = -2Z q_{k-1} + [V_o - E - \delta] q_{k-2}$$

$$+ \sum_{m=1} V_m q_{k-m-2} \qquad \text{Eq.6-45}$$

Similarly,

$$g_n = -\frac{2Z}{r} - E + \sum_{m=0} V_m r^m \qquad \text{Eq.6-46}$$

and $$P(r) \equiv P_n = \sum_{k=0} p_k r^k \qquad \text{Eq.6-47}$$

Hence, from Eq.6-36

$$k(k-1)p_k = -2Zp_{k-1} + [V_o - E]p_{k-2} + \sum_{m=1} V_m p_{k-m-2} \qquad \text{Eq.6-48}$$

Recalling Eq.6-28

$$Q_n = P_n + T_n$$

and also writing T_n in a power series $T_n = \sum_{k=0} t_k r^k$, we have

$$q_k = p_k + t_k \qquad \text{Eq.6-49}$$

Hence,

$$k(k-1)t_k = -2Z\,t_{k-1} + [V_o - E - \delta]\,t_{k-2} + \sum_{m=1} V_m\, t_{k-m-2} + \delta p_{k-2} \qquad \text{Eq.6-50}$$

As a starting point, we define ,

$$q_1 = p_1 = 1$$

Hence,

$$q_2 = p_2 = -Z \qquad \text{Eq.6-51}$$

and $$t_1 = t_2 = 0$$

These values are chosen for simplicity, the normalization process being carried in the final step in the calculation.

The values of $\Sigma V_m r^m$ as a function of r are determined from Herman and Skillman's values of U (= rV/2Z) by the equation

$$\Sigma V_m r^m = \frac{2Z}{r}(1 - U) \qquad \text{Eq.6-52}$$

This gradually decreases to zero as r becomes infinite. A tenth order polynomial in r has been set up by Slater[67] for describing such a function $\Sigma V_m r^m$ (Appendix D). A polynomial is obtained for sodium, using the method described in the Appendix D, by fitting exactly to the following Herman-Skillman entries for U. This method requires eleven entries spaced at intervals of $h' = h/\mu$ ($\mu = (9\pi^2/128Z)^{1/3}$, Z is the atomic number) about a central entry at $r/\mu = 0.42$ (TABLE 6-3).

TABLE 6-3 ENTRIES OF TENTH ORDER POLYNOMIAL FITTING

$\frac{r}{\mu}$	U	$\frac{r}{\mu}$	U	$\frac{r}{\mu}$	U
0.02	0.98349	0.34	0.73447	0.66	0.56589
0.10	0.91388	0.42	0.68580	0.74	0.53366 *
0.18	0.84770	0.50	0.64160	0.82	0.50436 *
0.26	0.78811	0.58	0.60170		

* interpolated

The corresponding coefficients of the polynomial $\Sigma V_m r^m$ are given in TABLE 6-4

TABLE 6-4 COEFFICIENTS OF $\Sigma V_m r^m$

m	V_m	m	V_m	m	V_m
0	44.24692824	4	-252854.7714	8	-22702076.90
1	204.1794880	5	1186836.537	9	26539310.57
2	-4278.603139	6	-4316434.868	10	-14106431.70
3	40113.64204	7	11853126.37		

With the tabulated values of V_m and using Eqs.6-48, 6-50 and 6-49, the first two initial values of $T(r)$ (ie. T_{n-1} and T_n) can be calculated. The power series $T(r)=\Sigma t_k r^k$ was expanded up to twelfth order.

Combining Eqs.6-28, 6-37 and 6-40, we have

$$T_{n+1} = Q_{n+1} - P_{n+1}$$

$$= [2 + (g_n - \delta)h^2]T_n - T_{n-1} - \delta h^2 P_n \qquad \text{Eq.6-53}$$

where $g_n - \delta = g'_n = -E + V(r) - \delta$

and $$h = r_n - r_{n-1}$$

It should be noted that P_n in Eq.6-53 is an un-normalized radial function of a free sodium atom. It may be obtained by de-normalizing Herman and Skillman's tabulated values for (the normalized) $P_{HS}(r)$. Using Eqs.6-48 and 6-47 we have the un-normalized P_1 at $r/\mu = 0.01$, and from the Herman-Skillman tables the de-normalized factor is

$$D = \frac{P(0.01)}{P_{HS}(0.01)} = 0.322843$$

hence $$P_n = D\, P_{HS}(r) \qquad \text{Eq.6-54}$$

The values of the new wavefunction $Q(r)$ thus can be calculated by repetition of Eq.6-53 to get the whole series of T_n . Using these values of T_n and the known values of P_n (Eq.6-54), Q_n can be obtained by simple addition (Eq.6-28).

6.4.3 Calculation of the new energy E' by a self-consistent method

It is necessary to check the mismatch between the logarithmic derivative $\dot{Q}/Q$ at r_c and $-\sqrt{-E'}$ (previously estimated, §6.4.1). If the two values agree to within a criterion (say 0.01%), it is then satisfactory, and one can proceed to normalize the new wavefunction

$Q(r)$ to calculate the electron density $|\Psi_s(0)|^2$. On the other hand, if it is not self-consistent, the energy E' should be adjusted in order to find another new set of self-consistent wavefunction values. This procedure may be repeated several times until a self-consistent wavefunction $Q(r)$ and energy E' are found.

Suppose it is necessary to adjust the energy E' by $\Delta E'$. Again, the Schrodinger equation is written as

$$\frac{d^2}{dr^2} Q_o = [-E'_o + V'(r)] Q_o$$

Q_o is the old wavefunction and $-\sqrt{-E'_o} = \dot{Q}_o/Q_o$ at r_c. For the new wavefunction (caused by the adjustment to the energy E'), the Schrodinger equation is

$$\frac{d^2}{dr^2} Q = [-E' - \Delta E' + V'(r)] Q$$

where $Q = Q_o + \Delta Q_o$

Following the procedure described in §6.4.1 (Eqs.6-29 to 6-34) :

$$\frac{\Delta E'}{Q_o^2(r_c)} \int_0^{r_c} Q_o^2(r) dr + \sqrt{-E'_o} - \sqrt{-E'} = 0 \qquad \text{Eq.6-55}$$

where $-E' = -E'_o - \Delta E'$ is the new energy, and

$$\frac{\dot{Q}}{Q} = -\sqrt{-E'} \quad \text{at} \quad r \geq r_c \qquad \text{Eq.6-56}$$

A new energy E' is obtained by solving Eq.6-55. Using this new energy, the wavefunction is obtained by repeating the procedure of §6.4.2. The self-consistency criterion is then applied.

6.4.4 Computer program and calculated results

A BASIC computer program was written to calculate the wavefunction $Q(r)$ (program is listed in Appendix E). The computer program flow chart is shown in Fig.6-5. Series of $Q(r)$ values for different muffin-tin radii r_c were tabulated in order to estimate a critical radius r_c . It was found that a critical radius of 2.56 Å accounted for the experimentally observed reduction in the hyperfine coupling constant (to 42% of its original value). A set of $Q(r)$ values for this radius is compiled in TABLE 6-5. The new wavefunction $Q(r)$ is plotted against the distance r_c (in Å unit) in Fig.6-6. The calculated results of the electron density of sodium 3s-electrons, the energy E' and the shift of the kinetic energy δ are listed in TABLE 6-6. The ratio of the electron density to that of a free sodium atom as a function of r_c is plotted in Fig.6-7. The energy E' is also plotted in Fig.6-7.

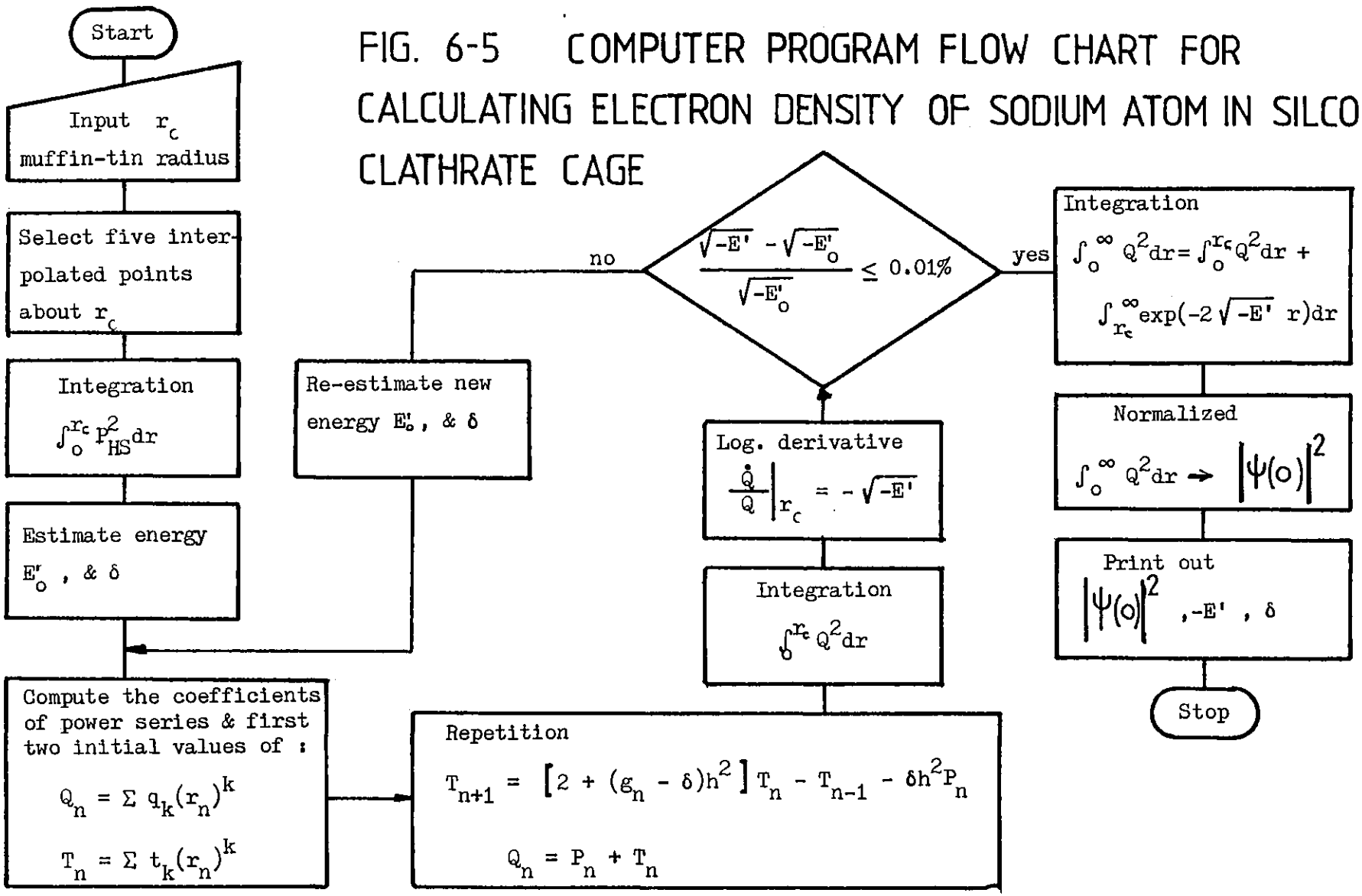

FIG. 6-5 COMPUTER PROGRAM FLOW CHART FOR CALCULATING ELECTRON DENSITY OF SODIUM ATOM IN SILCON CLATHRATE CAGE

TABLE 6-5 Values for the 3s orbital of sodium atom in silicon clathrate cage with a muffin-tin radius = 2.56 Å .
$x = r/\mu$, $\mu = 8.854 \times 10^{-1}$.

x	Q(r)	x	Q(r)	x	Q(r)
0.00	0.000	0.70	-2.795×10^{-2}	6.30	1.564×10^{-1}
0.01	3.810×10^{-3}	0.78	-3.631	6.94	1.658
0.02	7.264	0.86	-4.339	7.58	1.719
0.03	1.043×10^{-2}	0.94	-4.907	8.22	1.752
0.04	1.330	1.02	-5.341	8.86	1.764
0.05	1.588	1.10	-5.649	9.50	1.759
0.06	1.818	1.18	-5.840	10.14	1.741
0.07	2.024	1.26	-5.992	10.78	1.716
0.08	2.208	1.34	-5.908	11.42	1.684
0.09	2.366	1.42	-5.809	12.06	1.650
0.10	2.505	1.50	-5.631	12.16	1.645
0.12	2.725	1.66	-5.089	12.43	1.631
0.14	2.870	1.82	-4.348	12.70	1.717
0.16	2.954	1.98	-3.468	13.98	1.552
0.18	2.983	2.14	-2.494	15.26	1.490
0.20	2.961	2.30	-1.462	17.82	1.372
0.22	2.899	2.46	-4.009×10^{-3}	20.38	1.264
0.24	2.796	2.64	6.643	22.94	1.165
0.26	2.661	2.78	1.724×10^{-2}	25.50	1.073
0.28	2.499	2.94	2.761	28.06	9.884×10^{-2}
0.30	2.312	3.10	3.768	35.74	7.729
0.34	1.880	3.42	5.661	43.42	6.041
0.38	1.389	3.74	7.385	51.10	4.723
0.42	8.629×10^{-3}	4.06	8.928	56.22	4.008
0.46	3.174	4.38	1.029×10^{-1}	71.58	2.540
0.50	-2.346	4.70	1.150	86.94	1.497
0.54	-7.833	5.02	1.257	102.30	9.151×10^{-3}
0.58	-1.319×10^{-2}	5.34	1.350	112.54	6.591
0.62	-1.836	5.66	1.432	133.02	3.419
0.66	-2.330	5.98	1.503	163.74	1.277

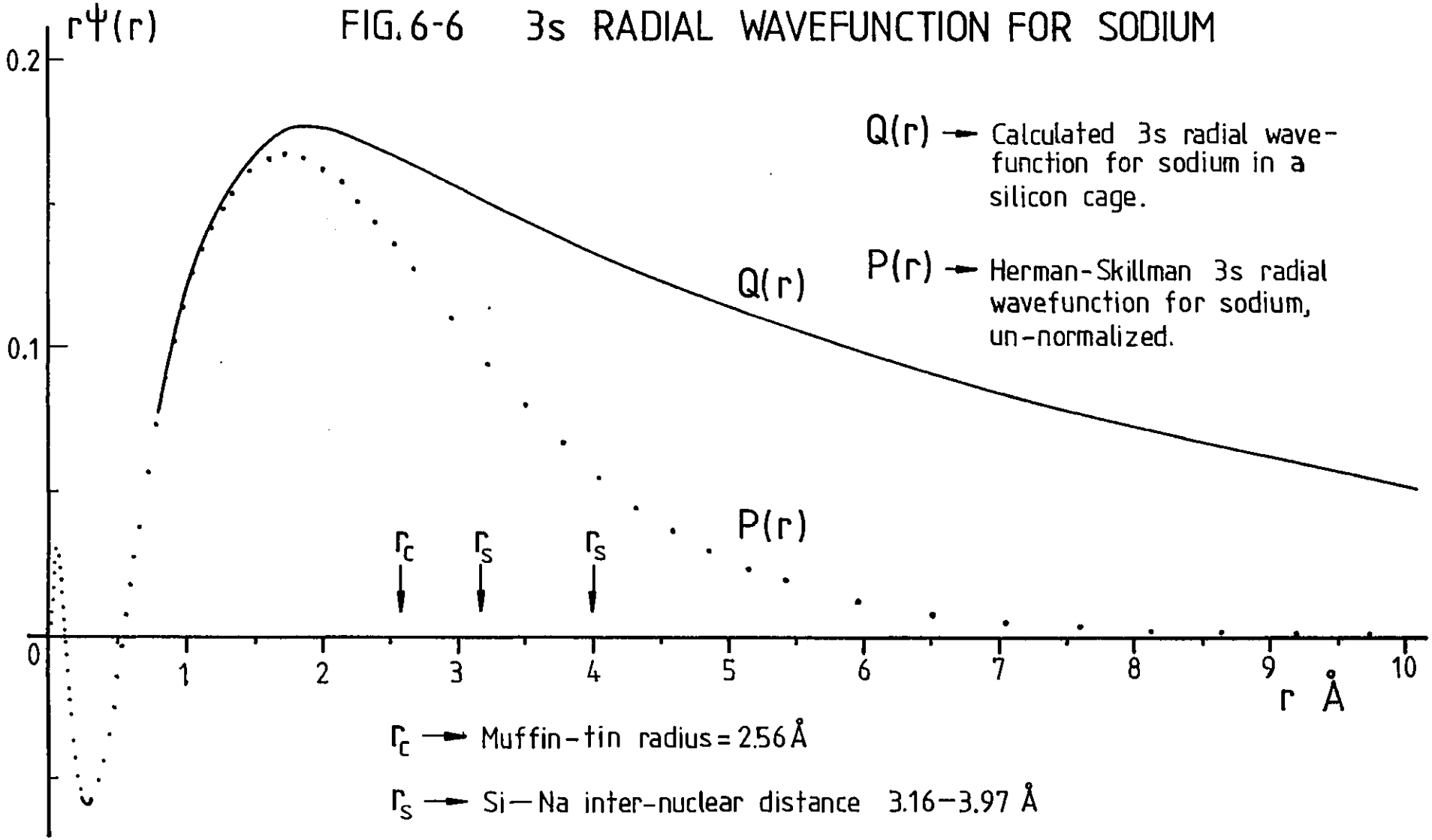
rΨ(r)
FIG. 6-6 3s RADIAL WAVEFUNCTION FOR SODIUM
0.2
0.1
0
Q(r) → Calculated 3s radial wave-function for sodium in a silicon cage.
P(r) → Herman-Skillman 3s radial wavefunction for sodium, un-normalized.
Q(r)
P(r)
r_c
r_s
r_s
1
2
3
4
5
6
7
8
9
10
r Å
r_c → Muffin-tin radius = 2.56 Å
r_s → Si—Na inter-nuclear distance 3.16–3.97 Å

TABLE 6-6 3s electron density and energy of an sodium atom with a muffin-tin potential in a silicon clathrate cage

Muffin-tin radius Γ_c (Å)	Energy -E' (Ryd)	Shift of K.E. δ (Ryd)	Electron density $\lvert\Psi_s(0)\rvert^2$ (cm^{-3})	$\frac{\lvert\Psi_s(0)\rvert^2}{\lvert\Psi_s(0)\rvert^2_f}$ (%)
4.00	1.15×10^{-1}	1.47×10^{-3}	5.02×10^{24}	99.1
3.50	7.98×10^{-2}	4.48×10^{-3}	4.78×10^{24}	94.5
3.00	3.93×10^{-2}	1.44×10^{-2}	4.06×10^{24}	80.1
2.70	1.57×10^{-2}	3.00×10^{-2}	2.98×10^{24}	58.9
2.60	8.66×10^{-3}	3.80×10^{-2}	2.38×10^{24}	46.9
2.57	6.92×10^{-3}	4.10×10^{-2}	2.17×10^{24}	42.8
2.56	6.50×10^{-3}	4.19×10^{-2}	2.11×10^{24}	41.7
2.55	5.84×10^{-3}	4.32×10^{-2}	2.02×10^{24}	39.8
2.50	3.45×10^{-3}	4.91×10^{-2}	1.61×10^{24}	31.7
2.45	1.59×10^{-3}	5.59×10^{-2}	1.13×10^{24}	22.3

Note : $\lvert\Psi_s(0)\rvert^2_f = 5.07 \times 10^{24}$ (cm^{-3}) = electron density at the nuclear centre of an isolated sodium atom

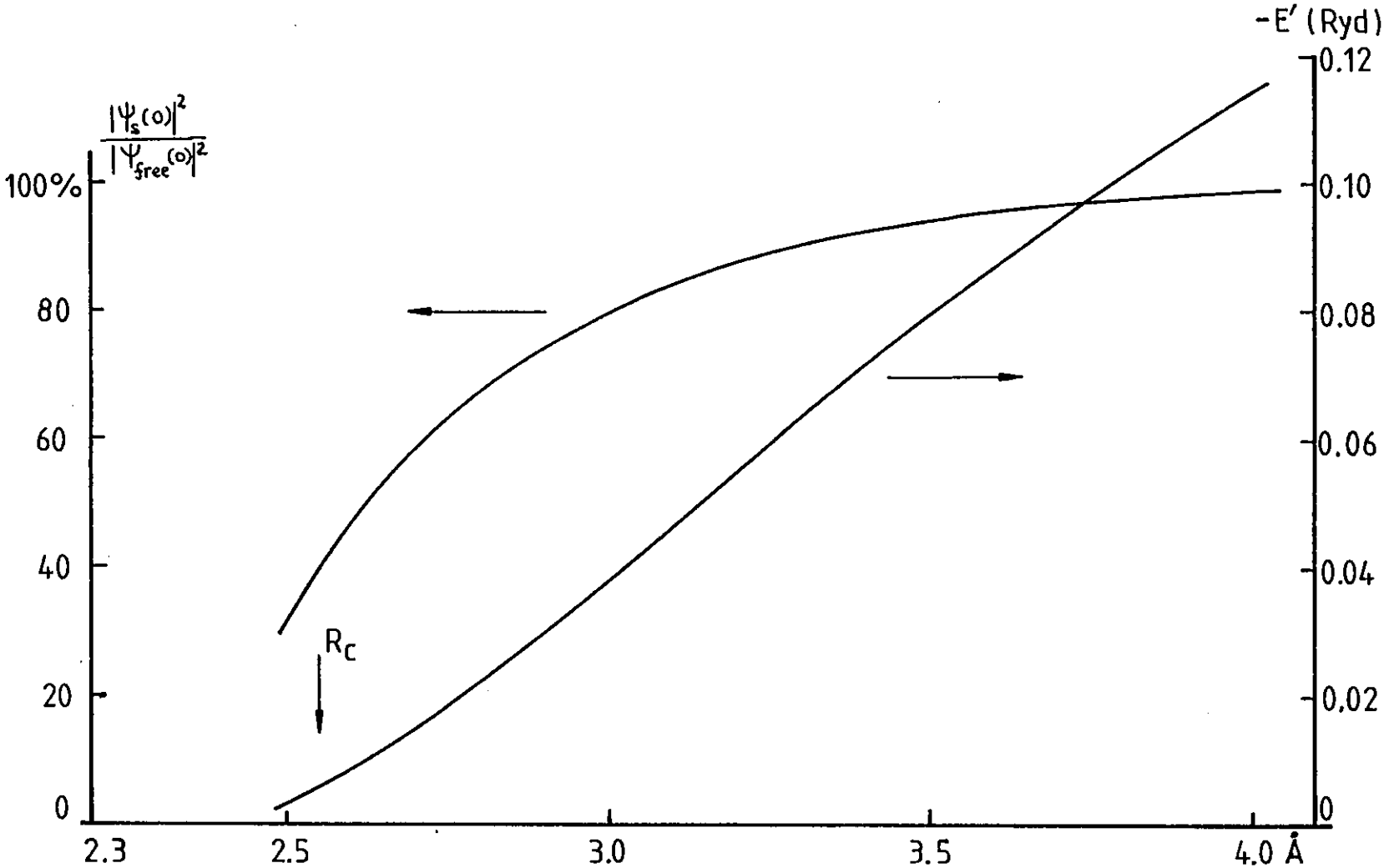

FIG. 6-7 REDUCED HYPERFINE CONSTANT AND ENERGY FOR SODIUM IN A METALLIC CAGE. R_c IS THE MUFFIN-TIN RADIUS.

6.5 CONCLUSIONS

The structure of the electron paramagnetic resonance spectrum shows that the number of localized 3s spins which contribute to the line with hyperfine splitting is small ($\sim 10^{19}$ spins per mole) for low sodium concentration samples. In the intermediate concentration region ($x > 5$), the hyperfine splitting fades, but the three cluster resonances remain. The clusters eventually fade into one unresolved broad line in the high concentration region ($x > 18$). The nature of these clusters is not fully understood. We believe these resonances are the result of the delocalized sodium 3s-electrons experiencing the hyperfine interaction of several sodium nuclei that within the cluster the electrons are antiparallel coupled. The exchange energy of the cluster electrons is expected to be higher than the hyperfine interaction energy (373 MHz). It is interesting to note that in phosphorus doped silicon system there are several extra resonance lines between the two hyperfine split lines of the phosphorus. These cluster resonances are formed because an electron can experience a hyperfine interaction with two or more impurity nuclei. The positions of these cluster lines are located symmetrically at the centre between the two hyperfine lines. In the Na_xSi_{136} system, the position of the broad line C_1 is slightly shifted from the centre between the two hyperfine lines (P_2 and P_3) to high field side. The other two narrow lines (C_2 and C_3) locate at the high field side towards the third hyperfine line (P_3). It is not clear at the present time what causes the shift of position of these cluster lines. It is hoped that more detailed experimental studies would clarify the situation.

The experimental results for the hyperfine coupling constant for both samples $Na_{1.5}Si_{136}$ and $Na_{2.8}Si_{136}$ are 42% of that of a free sodium atom. At $r_c = 2.56$ Å, the simple model calculation of the electron density at the nuclear centre of sodium is reduced to 41.7%. At this critical radius, the energy of the 3s-electrons is 88 meV. The wavefunction penetrates into the adjacent cage and perhaps even more distant cages.

CHAPTER 7

CONCLUSIONS

7.1 INTRODUCTION

This is the most thorough investigation to date of the interesting magnetic properties of Na_xSi_{136} compounds. In this work the magnetic susceptibilities and the electron paramagnetic resonance spectra of sodium-silicon clathrate compounds have been measured at low temperatures. The concentration of sodium in these compounds ranges from 1.1 to 14 at.% ($1.5 \leq x \leq 22$).

7.2 CONCLUSIONS

The static magnetic susceptibility shows an increase as the temperature is reduced down to 1.5 K and, in fact, follows the Curie-Weiss law. The Curie-Weiss temperature parameter θ for low sodium concentration Na_xSi_{136} sample is about 1.6 K. However, down to 1.5 K, the Curie-Weiss plots ($1/\chi$ versus T) do not show any upturns which would indicate the onset of ordered antiferromagnetic character (Fig.5-2). For compositions $x > 12$, the Pauli susceptibility due to conduction electrons starts to set in significantly, adding substantially to the contribution from Curie-Weiss paramagnetism. This indicates that Na_xSi_{136} compounds undergo a metal non-metal transition as the concentration of sodium is varied. The experimental results for the susceptibility combined with electron paramagnetic resonance of Na_xSi_{136} show that the percentage of isolated sodium atoms contributing

the Curie-Weiss paramagnetism ranges from 5% (in low concentration samples) to less than 0.1% (in high concentration samples). The majority of 3s-electrons from the sodium atoms form clusters in low concentration samples. Within the cluster the electrons are anti-parallel coupled . As the density of sodium increases, the 3s-electrons become conduction electron because of strong exchange interaction between the electrons of the nearest sodium atoms, and hence contribute to the Pauli paramagnetism. Because of the nature of the crystal structure of the clathrate compounds, the magnetic centres (sodium atoms) are randomly distributed. This leads to a very wide range of nearest-neighbour exchange interactions causing the susceptibility to exhibit amorphous antiferromagnetic behaviour. As the sodium concentration increases, the 3s-electrons start to delocalize and couple in an antiparallel fashion. The mean distance between sodium atoms decreases and the exchange interactions become stronger so that the sample eventually exhibits a metallic character leading to the Pauli paramagnetism.

The electron paramagnetic resonance spectra of very low sodium concentration Na_xSi_{136} compounds show hyperfine splitting plus three cluster resonance lines. For $x > 5$, the hyperfine split line disappears but the three cluster lines remain and gradually lose the line intensity until, when $x > 18$, the sample exhibits one unresolved broad resonance line. These indicate that, for low concentration samples, there exist some isolated sodium atoms of which the 3s-electrons experience a hyperfine interaction with the nucleus and thus cause four hyperfine lines to appear. On the other hand, the cluster resonances are due to those sodium atoms which are located sufficiently

close to each other for the 3s-wavefunctions to overlap. The sodium concentration is increased, the mean distance between sodium atoms becomes shorter and the exchange effect dominates the hyperfine interaction causing the hyperfine resonance to disappear and the population of the clusters to increase. Hence, the electrical conductivity is expected to increase as the overlap interaction becomes stronger. The results of the electrical conductivity of Na_xSi_{136} compacted samples measured by the Bordeaux group (see §2.2) show this metallic non-metallic character which is consistent with our conclusion drawn from the magnetic susceptibility. At much higher concentrations, all clusters merge into one unresolved broad resonance, the 3s-electrons become conduction electrons.

Professor P. Wachter of Eidgenossische Technische Hochschule (Zurich) has measured the optical absorption of $Na_{1.5}Si_{136}$ (sample 12) at room temperature. He concludes that this sample has a significant free carrier absorption and an absorption edge at 1.37 eV which is not very pronounced. His qualitative conclusion that there are a large number of conduction electrons in the compound is in agreement with the conclusion drawn from our susceptibility measurements and electron paramagnetic resonance experiments.

The reduced hyperfine constant of the isolated sodium atoms in the low sodium concentration samples is 373 MHz which is about 42% of that of a free sodium atom. A model calculation of sodium 3s-wavefunction, which accounts for the reduced hyperfine constant, shows that the wavefunction penetrates into the adjacent cages, hence, the exchange interaction of the 3s-electrons is stronger as the concentration of sodium increases.

Finally, several attempts were made to measure the specific heat of Na_xSi_{136} but unresolved technical problems prevented any useful measurements. Further measurements of the magnetic susceptibility and resonance of these clathrate compounds down to very low temperature would be useful.

APPENDIX A-1

Computer program : X-ray diffraction line intensity calculation for Na_xSi_{136}

```
READY.

 100 REM X-RAY INTENSITY OF NA-SI CLATHRATE COMPOUND
 200 DATA 5,1,1,15.89,9.76,8.48,24,0.1776
 210 DATA 3,3,3,15.89,9.76,8.48,8,0.1776
 215 DATA 1,1,1,5.223,12.37,10.21,8,0.0591
 220 DATA 2,2,0,8.575,11.43,9.7,12,0.0967
 225 DATA 3,1,1,10.07,11.02,9.45,24,0.1134
 230 DATA 2,2,2,10.55,10.93,9.37,8,0.1188
 240 DATA 4,0,0,12.17,10.53,9.08,6,0.1368
 250 DATA 4,2,2,14.97,9.95,8.63,24,0.1676
 280 DATA 4,4,0,17.36,9.51,8.26,12,0.1935
 290 DATA 5,3,1,18.16,9.37,8.15,48,0.2022
 300 DATA 7,3,3,25.57,8.4,7.03,24,0.280
 311 DATA 8,2,2,26.58,8.28,6.85,24,0.2902
 312 DATA 6,6,0,26.58,8.28,6.85,12,0.2902
 315 DATA 7,5,1,27.16,8.24,6.77,48,0.296
 320 DATA 5,5,5,27.16,8.24,6.77,8,0.296
 330 DIM G(15)
 335 PRINT"% OF NA=?":INPUT F(5)
 336 PRINT"FACTOR:2B=?":INPUT F(9)
 337 PRINT"BETA=?":INPUT N(2)
 340 OPEN 7,4
 345 PRINT#7
 352 IF F(5)>25 GOTO 1160
 420 N(1)=(F(5)-8*N(2))/16
 435 IF N(2)>1 GOTO 1160
 440 IF N(2)< 0 GOTO 1160
 445 IF N(1)>1 GOTO 1160
 450 IF N(1)< 0 GOTO 1160
 460 PRINT#7, "% OF SODIUM = ";F(5),"ALPHA = ";N(1),"BETA = ";N(2):CHR$(13)
 470 PRINT"% OF SODIUM = ";F(5);"ALPHA = ";N(1);"BETA = ";N(2)
 500 X=-0.188
 510 Y=-0.116
 520 Z=-0.492
 530 FOR M=0 TO 14
 540 READ H,K,L,E,F(1),F(2),F(3),F(4)
 570 Q=(H+K+L)*π
 580 P=(H+K)*π
 590 Q=(K+L)*π
 600 R=(H+L)*π
 610 H=H*π
 620 K=K*π
 630 L=L*π
 640 A(0)=1+COS(P)+COS(Q)+COS(R)
 650 B(0)=A(0)
 660 A(1)=A(0)*(1+COS(Q/2))
 670 B(1)=B(0)*SIN(Q/2)
 680 C(1)=(H-K-L)*X
 690 C(2)=(-H+K-L)*Y
 700 C(3)=(-H-K+L)*Z
 710 A(2)=COS(Q*X)+COS(C(1))+COS(C(2))+COS(C(3))+COS(Q/2-Q*X)+COS(Q/2-C(1))
```

```
 720 A(2)=(A(2)+COS(O/2-C(2))+COS(O/2-C(3)))*A(0)
 730 B(2)=SIN(O*X)+SIN(C(1))+SIN(C(2))+SIN(C(3))+SIN(O/2-O*X)+SIN(O/2-C(1))
 740 B(2)=(B(2)+SIN(O/2-C(2))+SIN(O/2-C(3)))*B(0)
 750 FOR J=1 TO 3
 760 IF J=1 THEN U=Y:V=Y:W=Z
 770 IF J=2 THEN U=Z:V=Y:W=Y
 780 IF J=3 THEN U=Y:V=Z:W=Y
 790 S(0)=H*U+K*V+L*W
 800 S(1)=H*U-K*V-L*W
 810 S(2)=-H*U+K*V-L*W
 820 S(3)=-H*U-K*V+L*W
 830 FOR I=0 TO 3
 840 D(I)=COS(S(I))+COS(O/2-S(I))
 850 D(I+4)=SIN(S(I))+SIN(O/2-S(I))
 860 NEXT I
 870 E(J)=D(0)+D(1)+D(2)+D(3)
 880 E(J+3)=D(4)+D(5)+D(6)+D(7)
 890 NEXT J
 900 A(3)=(E(1)+E(2)+E(3))*A(0)
 910 B(3)=(E(4)+E(5)+E(6))*B(0)
 915 C(4)=(O+2*P)/4
 920 C(5)=(O+2*Q)/4
 930 C(6)=(O+2*R)/4
 940 A(4)=(COS(O/4)+COS(C(4))+COS(C(5))+COS(C(6)))*A(0)
 950 B(4)=(SIN(O/4)+SIN(C(4))+SIN(C(5))+SIN(C(6)))*B(0)
 960 A(5)=(COS(O)+COS(3*O/2))*A(0)
 970 B(5)=(SIN(O)+SIN(3*O/2))*B(0)
 980 A(6)=((A(1)+A(2)+A(3))*F(1)+(A(4)*N(1)+A(5)*N(2))*F(2))↑2
 990 B(6)=((B(1)+B(2)+B(3))*F(1)+(B(4)*N(1)+B(5)*N(2))*F(2))↑2
1000 F(6)=A(6)+B(6)
1010 C(7)=π*E/180
1020 C(8)=F(6)*F(3)*(1+(COS(2*C(7)))↑2)/(SIN(C(7)))↑2/COS(C(7))
1030 G(M)= C(8)*EXP(-F(9)*F(4)↑2)
1040 IF M=1 THEN F(7)=100:GOTO 1100
1050 F(7)=G(M)/(G(0)+G(1))*1000
1060 IF F(7)-INT(F(7))=0.5 THEN F(7)=INT(F(7))+1:GOTO 1090
1080 F(7)=INT(F(7))
1090 F(7)=F(7)*0.1
1100 PRINT#7,"HKL = ";H/π;K/π;L/π,"F(HKL) = ";C(8),"% = ";F(7)
1110 NEXT M
1120 PRINT#7
1160 CLOSE7
1170 IF F(5)<24 THEN RESTORE: GOTO 335
1200 END
READY.
```

APPENDIX A-2

Computer program : X-ray diffraction line intensity calculation for Na_8Si_{46} .

```
READY.
 200 DATA 2,1,0,9.750,11.12,9.50,24,0.1098
 210 DATA 2,1,1,10.70,10.78,9.33,24,0.1204
 220 DATA 3,2,0,15.25,9.88,8.58,24,0.1706
 230 DATA 3,2,1,16.48,9.65,8.40,48,0.1840
 240 DATA 4,1,0,17.63,9.45,8.23,24,0.1964
 250 DATA 4,1,1,18.68,9.28,8.07,24,0.2077
 260 DATA 3,3,0,18.68,9.28,8.07,12,0.2077
 270 DATA 5,3,0,26.18,8.83,6.92,24,0.2862
 280 DATA 4,3,3,26.18,8.83,6.92,24,0.2862
 290 DATA 6,1,1,27.78,8.18,6.68,24,0.3023
 300 DATA 5,3,2,27.78,8.18,6.68,48,0.3023
 310 DIM G(12)
 400 PRINT "TEMPERATURE FACTOR":INPUT F(7)
 500 X=2*0.183
 510 Y=2*0.310
 520 Z=2*0.116
 530 FOR M=1 TO 11
 540 READ H,K,L,E,F(1),F(2),F(3),F(4)
 550 O(1)=(H+K+L)*π
 560 O(2)=(H-K-L)*π
 570 O(3)=(H-K+L)*π
 580 O(4)=(H+K-L)*π
 590 H=H*π
 600 K=K*π
 610 L=L*π
 620 C(1)=(H+2*L)/2
 630 C(2)=(K+2*H)/2
 640 C(3)=(L+2*K)/2
 650 C(4)=(3*H+2*L)/2
 660 C(5)=(3*K+2*H)/2
 670 C(6)=(3*L+2*K)/2
 680 A(0)=0
 690 B(0)=0
 700 FOR I=1 TO 6
 710 A(I)=A(I-1)+COS(C(I))
 720 B(I)=B(I-1)+SIN(C(I))
 730 NEXT I
 740 A(1)=A(6)
 750 B(1)=B(6)
 760 C(0)=0
 770 FOR J=1 TO 4
 780 C(J)=C(J-1)+COS(O(J)*X)
 790 NEXT J
 800 A(2)=2*C(4)*(1+COS(O(1)))
 810 B(2)=2*C(4)*SIN(O(1))
 820 C(0)=COS(Z*K)*COS(Y*L)+COS(Y*H)*COS(Z*L)+COS(Z*H)*COS(Y*K)
 830 C(1)=COS(Y*K)*COS(Z*L)+COS(Z*H)*COS(Y*L)+COS(Y*H)*COS(Z*K)
 840 A(3)=4*(C(1)+C(0)*COS(O(1)))
 850 B(3)=4*C(0)*SIN(O(1))
 860 A(4)=1+COS(O(1))
 870 B(4)=SIN(O(1))
 880 C(1)=(H+2*K)/2
 890 C(2)=(K+2*L)/2
 900 C(3)=(L+2*H)/2
 910 C(4)=(3*H+2*K)/2
 920 C(5)=(3*K+2*L)/2
 930 C(6)=(3*L+2*H)/2
 940 P(0)=0
 950 Q(0)=0
 960 FOR I=1 TO 6
 970 P(I)=P(I-1)+COS(C(I))
 980 Q(I)=Q(I-1)+SIN(C(I))
 990 NEXT I
1000 A(5)=P(6)
1010 B(5)=Q(6)
1020 A(6)=(A(1)+A(2)+A(3))*F(1)+(A(4)+A(5))*F(2)
1030 B(6)=(B(1)+B(2)+B(3))*F(1)+(B(4)+B(5))*F(2)
1040 F(6)=A(6)↑2+B(6)↑2
1050 C(7)=π*E/180
1060 G(8)=F(6)*F(3)*(1+COS(2*C(7))↑2)/(SIN(C(7))↑2*COS(C(7)))
1070 G(M)=C(8)*EXP(-F(7)*F(4)^2)
1080 PRINT H/π;K/π;L/π;TAB(12);C(8);TAB(25);G(M)
1090 NEXT M
READY.
```

APPENDIX B

SPECIFIC HEAT OF SOME CRYOGENICS MATERIALS

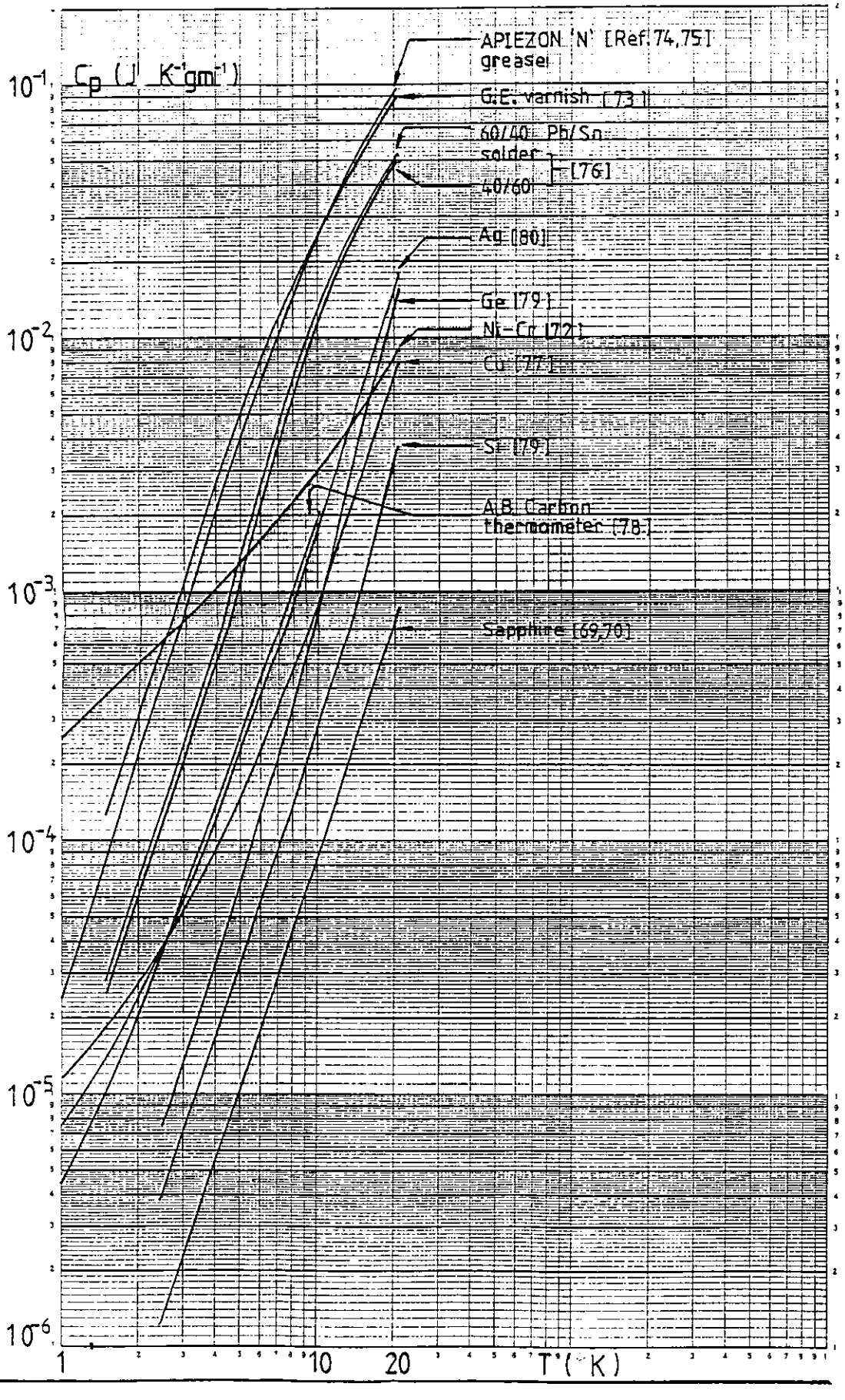

APPENDIX C

Magnetic susceptibility experimental data for Na_xSi_{136}

Sample 12

Concentration of sodium: 1.09 at.% — X-ray analysis

Composition of sodium in Na_xSi_{136}: 1.5

1 mole = 3854.18 gm

χ_0 = 6.09×10^{-7} (emu/gm)

θ = 1.6 K

C = 2.38×10^{-2} (emu K/mole)

μ = 3.30×10^{-21} (erg/G)

$\chi = \chi_S - \chi_0$

T(°K)	χ (10^{-3} emu/mole)	$\frac{1}{\chi}$ (10^{2} mole/emu)
1.65	9.28	1.08
1.67	8.06	1.24
2.39	6.00	1.67
2.68	5.87	1.70
3.03	5.19	1.93
3.36	4.93	2.03
3.72	4.89	2.05
3.96	4.57	2.19
4.22	4.08	2.45
4.31	3.80	2.63
4.45	3.99	2.51
4.63	3.56	2.81
4.87	3.52	2.84
5.26	3.27	3.06
6.03	3.06	3.27
6.56	2.63	3.81
7.27	2.58	3.88
8.33	2.18	4.59
9.59	2.23	4.49
10.7	1.97	5.08
11.9	1.65	6.05
13.6	1.58	6.33
14.9	1.47	6.80
16.2	1.37	7.33
17.7	1.26	7.96
19.7	1.13	8.83
21.5	1.33	7.53
23.2	1.07	9.35

Sample 20

Concentration of sodium: 2.02 at.% X - ray analysis

Composition of sodium in Na_xSi_{136}: 2.8

1 mole = 3884.07 gm

$\chi_o = 3.6 \times 10^{-8}$ (emu/gm)

$\theta = 1.4$ K

$C = 4.97 \times 10^{-2}$ (emu K/mole)

$\mu = 3.43 \times 10^{-21}$ (erg/G)

$\chi = \chi_s - \chi_o$

T(°K)	$\chi(10^{-3}$ emu/mole)	$\frac{1}{\chi}(10^2$ mole/emu)
1.46	17.0	0.590
1.55	16.5	0.605
1.61	16.2	0.616
2.11	13.7	0.728
2.65	12.0	0.831
3.03	11.4	0.875
3.55	10.1	0.995
3.82	9.16	1.09
3.88	9.30	1.08
4.03	8.69	1.15
4.12	8.53	1.17
4.21	8.66	1.16
4.22	8.44	1.19
4.39	8.21	1.22
4.56	7.90	1.27
4.63	7.76	1.29
4.81	7.58	1.32
5.18	7.18	1.39
5.26	7.04	1.42
5.67	6.73	1.49
5.80	6.59	1.52
6.52	5.95	1.68
6.69	5.75	1.74
7.59	5.28	1.90
9.37	4.42	2.26
9.96	4.13	2.42
11.0	3.90	2.57
14.0	3.32	3.01
14.6	3.10	3.23
16.2	2.81	3.56
17.6	2.39	4.18
18.7	2.38	4.20

Sample 13

Concentration of sodium: 3.20 at.% X - ray analysis

Composition of sodium in Na_xSi_{136}: 4.5

1 mole = 3923.15 gm

χ_o = 3.6×10^{-8} (emu/gm)

θ = 1.6 K

C = 2.28×10^{-2} (emu K/mole)

μ = 1.87×10^{-21} (erg/G)

$\chi = \chi_S - \chi_o$

T(°K)	χ(10^{-3} emu/mole)	$\frac{1}{\chi}$(10^2 mole/emu)
1.65	7.21	1.39
1.69	7.14	1.40
1.77	6.82	1.47
2.13	6.54	1.53
2.39	5.92	1.69
2.75	5.25	1.91
3.16	4.93	2.03
3.45	4.37	2.29
3.65	4.27	2.34
3.76	4.16	2.40
3.82	4.14	2.42
3.90	4.04	2.48
4.01	3.95	2.53
4.07	3.86	2.59
4.15	3.72	2.69
4.22	3.75	2.67
4.94	3.40	2.94
5.16	3.37	2.97
5.46	3.18	3.14
5.74	3.05	3.28
6.09	2.95	3.39
6.53	2.75	3.64
7.15	2.66	3.76
8.04	2.42	4.13
8.98	2.28	4.39
9.77	1.99	5.04
10.7	1.84	5.43
12.1	1.67	6.01
13.4	1.53	6.55
15.1	1.39	7.37
16.2	1.40	7.16
19.2	1.24	8.10
22.0	1.18	8.48
24.5	1.02	9.78

sample 15

Concentration of sodium: 3.75 at.% X - ray analysis

Composition of sodium in Na_xSi_{136}: 5.3

$\chi = \chi_S - \chi_o$

1 mole = 3941.54 gm

$\chi_o = -5.9 \times 10^{-8}$ (emu/gm)

$\theta = 0.6$ K

$C = 1.94 \times 10^{-2}$ (emu K/mole)

$\mu = 1.59 \times 10^{-21}$ (erg/G)

T(°K)	χ (10^{-3} emu/mole)	$\frac{1}{\chi}$ (10^{2} mole/emu)
1.67	7.96	1.26
1.79	7.83	1.28
1.92	7.21	1.39
2.25	6.64	1.51
2.40	6.18	1.62
3.02	5.37	1.86
3.43	4.62	2.16
3.77	4.64	2.16
3.93	4.29	2.33
4.08	4.16	2.40
4.18	4.04	2.47
4.22	4.02	2.49
4.31	3.96	2.53
4.60	3.72	2.69
5.01	3.42	2.93
5.66	3.14	3.19
6.25	2.86	3.49
7.55	2.48	4.03
8.43	2.24	4.47
9.54	1.97	5.08
10.9	1.76	5.68
12.4	1.55	6.45
14.0	1.36	7.38
16.0	1.14	8.76
17.6	1.08	9.23
19.0	0.958	10.4
20.4	0.777	12.9
23.3	0.637	15.7
25.4	0.572	17.5

Sample 20-D

Concentration of sodium: 5.23 at.% — X - ray analysis

Composition of sodium in Na_xSi_{136}: 7.5

1 mole = 3992.12 gm

$\chi_0 = 5.3 \times 10^{-8}$ (emu/gm)

$\theta = 1.4$ K

$C = 1.54 \times 10^{-2}$ (emu K/mole)

$\mu = 1.19 \times 10^{-21}$ (erg/G)

$\chi = \chi_S - \chi_0$

T(°K)	$\chi(10^{-3}$ emu/mole)	$\frac{1}{\chi}(10^2$ mole/emu)
1.57	4.74	2.11
1.77	4.56	2.19
2.35	3.98	2.51
2.76	3.86	2.59
3.06	3.70	2.71
3.55	3.38	2.96
3.86	3.00	3.34
4.20	2.90	3.45
4.23	2.82	3.55
4.40	2.74	3.65
4.92	2.25	4.45
5.37	2.30	4.35
6.42	1.97	5.07
7.90	1.56	6.40
8.71	1.46	6.87
10.3	1.33	7.52
11.8	1.16	8.60
14.8	0.941	10.6
18.6	0.788	12.7
30.4	0.520	19.2

Sample 26

Concentration of sodium: 8.7 at.% X - ray analysis

Composition of sodium in Na_xSi_{136}: 13

1 mole = 4118.56 gm

$\chi_o = -2.3 \times 10^{-8}$ (emu/gm)

$\theta = 0.04$ K

$C = 3.62 \times 10^{-3}$ (emu K/mole)

$\mu = 4.38 \times 10^{-22}$ (erg/G)

$\chi = \chi_s - \chi_o$

T(°K)	$\chi(10^{-4}$ emu/mole)	$\frac{1}{\chi}(10^3$ mole/emu)
1.56	22.4	0.446
1.65	21.5	0.466
1.80	19.4	0.515
1.95	18.2	0.551
2.33	15.3	0.655
2.52	14.7	0.680
2.68	13.2	0.758
2.99	11.4	0.878
3.19	10.8	0.924
3.49	9.76	1.02
3.76	9.38	1.07
3.97	9.07	1.10
4.23	8.26	1.21
5.48	6.20	1.61
6.46	6.01	1.67
7.12	5.07	1.97
7.37	4.94	2.02
7.54	4.63	2.16
7.89	4.26	2.35
8.27	4.13	2.42
8.74	4.22	2.37
9.26	4.19	2.39
10.9	3.44	2.91
12.8	2.81	3.56
14.6	2.57	3.90
16.7	2.25	4.45
18.8	1.79	5.59
25.5	1.44	6.96
77.6	0.62	16.1

Sample 9

Concentration of sodium: 9.3 at.% X - ray analysis

Composition of sodium in Na_xSi_{136}: 14

1 mole = 4141.55 gm

$\chi_o = 1.3 \times 10^{-8}$ (emu/gm)

$\theta = 0.8$ K

$C = 7.82 \times 10^{-3}$ (emu K/mole)

$\mu = 6.20 \times 10^{-22}$ (erg/G)

$\chi = \chi_S - \chi_o$

T(°K)	$\chi(10^{-3}$ emu/mole)	$\frac{1}{\chi}(10^2$ mole/emu)
1.57	3.30	3.03
1.78	3.30	3.03
1.84	2.72	3.68
2.38	2.57	3.90
2.72	2.31	4.34
3.01	1.98	5.06
3.24	1.97	5.09
3.39	1.76	5.70
3.54	1.65	6.06
4.22	1.51	6.62
4.25	1.42	7.06
4.40	1.44	6.94
4.55	1.38	7.25
4.68	1.37	7.33
4.88	1.30	7.71
5.15	1.27	7.86
5.41	1.22	8.18
5.80	1.19	8.44
6.29	1.17	8.53
6.36	1.08	9.28
6.94	0.995	10.1
7.65	0.909	11.0
8.46	0.851	11.8
9.30	0.762	13.1
10.2	0.745	13.4
11.1	0.663	15.1
12.7	0.638	15.7
14.5	0.557	18.0
16.5	0.438	22.8
18.4	0.395	25.3
21.7	0.340	29.5
25.3	0.309	32.4

Sample 11

Concentration of sodium: 11.1 at.% X - ray analysis

Composition of sodium in 17

$\chi = \chi_s - \chi_o$

1 mole = 4210.52 gm

$\chi_o = -0.7 \times 10^{-8}$ (emu/gm)

$\theta = 0.3$ K

$C = 3.90 \times 10^{-3}$ (emu K/mole)

$\mu = 3.97 \times 10^{-22}$ (erg/G)

T(^{o}K)	χ(10^{-4} emu/mole)	$\frac{1}{\chi}$(10^{3} mole/emu)
1.59	16.9	0.594
1.65	17.5	0.571
1.95	16.4	0.611
2.22	14.9	0.672
2.64	13.6	0.723
3.04	12.4	0.810
3.74	9.70	1.03
3.85	9.69	1.03
3.93	9.59	1.04
4.01	9.38	1.07
4.17	8.82	1.13
4.23	8.75	1.14
4.66	7.44	1.34
5.50	6.58	1.52
6.43	5.68	1.76
7.23	5.28	1.90
8.03	4.71	2.12
9.95	3.85	2.60
11.3	3.67	2.73
12.8	3.07	3.26
14.8	2.35	4.25
16.7	2.30	4.34
17.9	2.14	4.67
20.5	1.83	5.46
21.4	1.78	5.60
22.6	1.64	6.10
24.5	0.98	10.2

Sample 25

Concentration of sodium 12.1 at.% X - ray analysis

Composition of sodium in $Na_x Si_{136}$ 18.7

1 mole = 4249.61 gm

$\chi_0 = 9.6 \times 10^{-8}$ (emu/gm)

$\theta = 1.2$ K

$C = 5.04 \times 10^{-3}$ (emu K/mole)

$\mu = 4.31 \times 10^{-22}$ (erg/G)

$\chi = \chi_S - \chi_0$

T(°K)	$\chi(10^{-3}$ emu/mole)	$1/\chi$ (10^2 mole/emu)
1.57	1.82	5.51
1.73	1.72	5.83
1.84	1.56	6.40
2.07	1.45	6.91
2.31	1.40	7.13
2.53	1.35	7.42
2.90	1.26	7.93
3.12	1.20	8.36
3.33	1.13	8.87
3.43	1.10	9.09
3.62	1.00	10.0
4.00	0.927	10.8
4.21	0.905	11.1
4.22	0.887	11.3
4.23	0.886	11.3
4.33	0.907	11.0
5.35	0.773	12.9
5.84	0.687	14.6
6.31	0.666	15.0
7.20	0.585	17.1
8.12	0.585	17.1
9.71	0.485	20.6
12.4	0.385	26.0
15.2	0.325	30.8
18.3	0.244	41.0

Sample 25-D

Concentration of sodium: 13.9 at.% X - ray analysis

Composition of sodium in Na_xSi_{136}: 22

1 mole = 4325.47 gm

$\chi_0 = 4.8 \times 10^{-8}$ (emu/gm)

$\theta = 2.9$ K

$C = 8.76 \times 10^{-3}$ (emu K/mole)

$\mu = 5.24 \times 10^{-22}$ (erg/G)

$\chi = \chi_S - \chi_0$

T(°K)	$\chi(10^{-3}$ emu/mole)	$1/\chi$ (10^2 mole/emu)
1.60	2.01	4.97
1.69	1.89	5.28
2.09	1.78	5.63
2.33	1.63	6.13
2.57	1.59	6.30
2.85	1.59	6.29
3.08	1.43	7.02
3.48	1.33	7.51
3.76	1.34	7.48
3.96	1.31	7.64
4.21	1.20	8.34
6.76	0.921	10.9
7.63	0.863	11.6
9.35	0.717	14.0
12.0	0.577	17.3
14.5	0.519	19.3
16.3	0.484	20.6
18.1	0.400	25.0

APPENDIX D

Slater's tenth order polynomial for calculating the coefficients of the electronic potential of an isolated atom, $\Sigma\, v_m r^m$.

Definitions :

$$f(u) = \Sigma\, a_n u^n = \Sigma\, v_m r^m \quad ,$$

$$d^1(u) = f(u) - f(-u) \quad , \quad d^2(u) = f(u) - 2f(0) + f(-u) \quad ,$$

$$u = \frac{x - x_o}{h'} = 1, 2, 3, 4, \text{ and } 5 \quad ,$$

$h' = x_k - x_{k-1}$ (x is the Herman-Skillman variable quantity)

x_o is the central entry for computation

$r = \mu x$ (Bohr units) , $\mu = (9\pi^2/128\, Z)^{\frac{1}{3}}$,

where Z is the atomic number.

The coefficients are given as follows :

$$a_o = f(0) = \Sigma\, v_m (r_o)^m$$

$$a_1 = (10!)^{-1} [3024000\, d^1(1) - 864000\, d^1(2) + 216000\, d^1(3) - 36000\, d^1(4) + 2880\, d^1(5)]$$

$$a_2 = (10!)^{-1} [3024000\, d^2(1) - 432000\, d^2(2) + 72000\, d^2(3) - 9000\, d^2(4) + 576\, d^2(5)]$$

$$a_3 = (10!)^{-1}\,[-1401960\,d^1(1) + 1048560\,d^1(2) - 292140\,d^1(3) + 50440\,d^1(4) - 4100\,d^1(5)]$$

$$a_4 = (10!)^{-1}\,[-1401960\,d^2(1) + 524280\,d^2(2) - 97380\,d^2(3) + 12610\,d^2(4) - 820\,d^2(5)]$$

$$a_5 = (10!)^{-1}\,[203490\,d^1(1) - 196560\,d^1(2) + 82215\,d^1(3) - 15960\,d^1(4) + 1365\,d^1(5)]$$

$$a_6 = (10!)^{-1}\,[203490\,d^2(1) - 98280\,d^2(2) + 27405\,d^2(3) - 3990\,d^2(4) + 273\,d^2(5)]$$

$$a_7 = (10!)^{-1}\,[-11340\,d^1(1) + 12240\,d^1(2) - 6210\,d^1(3) + 1560\,d^1(4) - 150\,d^1(5)]$$

$$a_8 = (10!)^{-1}\,[-11340\,d^2(1) + 6120\,d^2(2) - 2070\,d^2(3) + 390\,d^2(4) - 30\,d^2(5)]$$

$$a_9 = (10!)^{-1}[210\,d^1(1) - 240\,d^1(2) + 135\,d^1(3) - 40\,d^1(4) + 5\,d^1(5)]$$

$$a_{10} = (10!)^{-1}\,[210\,d^2(1) - 120\,d^2(2) + 45\,d^2(3) - 10\,d^2(4) + d^2(5)]$$

APPENDIX E

Computer program for calculating new wavefunction Q(r) of sodium atom in a clathrate cage.

```
READY.

 10 REM NUMERICAL TABULATION FOR SODIUM 3S NEW WAVEFUNCTION IN SILICON CAGE
 20 DATA 0.99186, 0.0118,0.98349, 0.0225,0.97496, 0.0323,0.96630, 0.0412
 21 DATA 0.95758, 0.0492,0.94881, 0.0563,0.94003, 0.0627,0.93127, 0.0684
 22 DATA 0.92255, 0.0733,0.91388, 0.0776,0.89677, 0.0844,0.88001, 0.0889
 23 DATA 0.86364, 0.0915,0.84770, 0.0924,0.83219, 0.0917,0.81709, 0.0898
 24 DATA 0.80241, 0.0866,0.78811, 0.0824,0.77419, 0.0774,0.76062, 0.0716
 25 DATA 0.73447, 0.0582,0.70956, 0.0430,0.68580, 0.0267,0.66316, 0.0098
 26 DATA-0.64160,-0.0073,0.62112,-0.0243,0.60170,-0.0409,0.58331,-0.0569
 27 DATA 0.56589,-0.0722,0.54937,-0.0866,0.53368,-0.1125,0.49063,-0.1344
 28 DATA 0.46473,-0.1520,0.44063,-0.1654,0.41815,-0.1749,0.39714,-0.1808
 29 DATA 0.37752,-0.1833,0.35922,-0.1828,0.34216,-0.1797,0.32627,-0.1741
 30 DATA 0.29777,-0.1572,0.27315,-0.1341,0.25186,-0.1067,0.23338,-0.0764
 31 DATA 0.21726,-0.0443,0.20310,-0.0113,0.19057, 0.0218,0.17939, 0.0547
 32 DATA 0.16933, 0.0869,0.16022, 0.1181,0.14431, 0.1767,0.13086, 0.2299
 33 DATA 0.11941, 0.2773,0.10971, 0.3190,0.10162, 0.3556,0.09505, 0.3875
 34 DATA 0.09091, 0.4151,0.09091, 0.4390,0.09091, 0.4592,0.09091, 0.4760
 35 DATA 0.09091, 0.5000,0.09091, 0.5128,0.09091, 0.5161,0.09091, 0.5115
 36 DATA 0.09091, 0.5007,0.09091, 0.4849,0.09091, 0.4655,0.09091, 0.4433
 37 DATA 0.09091, 0.4193,0.09091, 0.3943,0.09091, 0.3433,0.09091, 0.2939
 38 DATA 0.09091, 0.2480,0.09091, 0.2069,0.09091, 0.1709,0.09091, 0.1400
 39 DATA 0.09091, 0.1138,0.09091, 0.0919,0.09091, 0.0738,0.09091, 0.0589
 50 DATA  44.24692824, 204.1794880
 51 DATA -4278.603139, 40113.64204
 52 DATA -252854.7714, 1186836.537
 53 DATA -4316434.868, 11853126.37
 54 DATA -22702026.90, 26539310.57
 55 DATA -14106431.70
 90 OPEN 7,4
100 REM FIRST ESTIMATED NEW ENERGY
120 DIM V(14),Q(14),T(14),N(14),F(14)
122 E=0.3777
124 Z=11
126 R(3)=0.322843
128 U=0.09091
130 PRINT#7,"NUMERICAL INTEGRATION FOR NEW Q-WAVEFUNCTION";CHR$(13)
132 PRINT"METALLIC CAGE RADIUS-R(0)=",:INPUT R
134 W=0.88534138/Z↑(1/3)
136 R(0)=R/(5.29177E-1)
138 U(0)=-2*Z*U/R(0)
140 E(0)=U(0)+E
142 R(0)=R(0)*100/W
144 IF R(0)-INT(R(0))>=0.5 THEN R(0)=INT(R(0))+1:GOTO 148
```

```
146 R(0)=INT(R(0))
148 R(0)=R(0)/100
150 FOR I=0 TO 10
152 IF R(0)<=12.7 THEN X=0.64:Z(1)=6.30:GOTO 158
154 X=1.28
156 Z(1)=12.7
158 Y=Z(1)+X*I
160 IF R(0)-1.28<=Y THEN PRINT I+1,Y
162 NEXT I
180 PRINT#7,"INTERPOLATING POINT OF X";CHR$(13)
190 PRINT"METALLIC CAGE RADIUS—— R(0) =";R(0)
192 FOR K=1 TO 5
194 PRINT"INDEX OF X",:INPUT O(K)
195 PRINT#7
196 J=O(K)
198 IF R(0)>12.70 THEN R(6)=12.70+1.28*(J-1):GOTO 202
200 R(6)=6.30+0.64*(J-1)
202 PRINT#7,K,O(K),R(6)
204 NEXT K
206 PRINT"————————————————————————————————"
208 PRINT#7
210 B(1)=0
212 X=0
214 Y=0.01
216 I=0
218 Q(0)=0
219 IF R(0)>12.70 THEN H=9:GOTO 221
220 H=7
221 FOR J=0 TO H
222 I=I+1
224 READ U,Q(I)
226 IF J=0 GOTO236
228 IF I=1 THEN N(11)=Q(1)↑2:GOTO262
230 IF I=10 THEN I=0:GOTO 248
232 IF J=H GOTO 253
234 GOTO 222
236 IF I=9 THEN I=0:GOTO240
238 GOTO222
240 FOR K=1 TO 10
242 N(K)=Q(K-1)↑2
244 NEXT K
246 GOTO 254
248 FOR K=1 TO 10
250 N(K)=Q(K)↑2
252 NEXT K
254 X=X+Y
256 Y=Y*2
258 NEXT J
260 GOTO 282
262 C(1)=4*(N(2)+N(4)+N(6)+N(8)+N(10))
264 C(2)=2*(N(3)+N(5)+N(7)+N(9))
266 G(J)=(C(1)+C(2)+N(1)+N(11))*(Y/2)/3
268 B(1)=B(1)+G(J)*W
272 GOTO 232
282 GOSUB 1000
294 PRINT#7,"THE DERIVATIVE AT R(0)       =";D
296 PRINT#7,"LOG.DERIVATIVE AT R(0)       =";L
298 A(1)=B(1)/Q(1)↑2
300 R(1)=1-4*A(1)*(L-A(1)*E(0))
302 R(1)=(SQR(R(1))-1)/(2*A(1))
304 E(1)=R(1)
306 R(1)=-(R(1)↑2)
308 M=R(1)+E(0)
312 PRINT#7,"ESTIMATED ENERGY -E(1)       =";R(1)
314 PRINT#7,"ETA———————————————— M       =";M
316 PRINT#7,"REDUCED POT.————— V          =";U(0)
```

```
319 PRINT#7,"ENERGY————————— -E         =";E
320 PRINT#7,"METALLIC CAGE RADIUS—— R(0) =";R(0)
325 PRINT#7
328 IF R(0)>12.70 GOTO 400
330 FOR K=0 TO 9
332 READ U,Q
334 NEXT K
400 PRINT"PRINT OUT Q-EIGENVALUE -- YES OR NO ?":INPUT W$
420 PRINT"COEFFS. OF THE POLYNOMIAL & INITIAL EIGENVALUES"
450 READ V
452 FOR I=1 TO 10
454 Q(I+3)=0
456 N(I+3)=0
458 F(I+3)=0
460 READ V(I)
462 NEXT I
464 V(0)=V+E-M
466 Y=-2*Z
468 Q(1)=1
470 Q(2)=-Z
472 Q(3)=(Y*Q(2)+V(0)*Q(1))/6
474 F(1)=Q(1)
476 F(2)=Q(2)
478 F(3)=Q(3)
480 PRINT1,Q(1)
482 PRINT2,Q(2)
484 PRINT3,Q(3)
486 I=4
488 GOSUB 580
490 Q(I)=F(I)
492 PRINTI,Q(I)
496 IF I<=11 THEN I=I+1:GOTO488
498 FOR J=1 TO 14
500 T(J)=0
502 N(J)=0
504 F(J)=0
506 NEXT J
518 V(0)=V+E
512 T(1)=0
512 T(2)=0
514 T(3)=-M/6
516 F(3)=T(3)
518 PRINT"————————————————————"
520 PRINT1,T(1)
522 PRINT2,T(2)
524 PRINT3,T(3)
526 I=4
528 GOSUB 580
530 T(I)=F(I)-M*Q(N(2))/(I*N(1))
531 F(I)=T(I)
532 PRINTI,T(I)
534 IF I<=13 THEN I=I+1:GOTO528
536 PRINT"————————————————————————————"
538 X=0
542 FOR I=1 TO 5
544 X=X+0.01
546 S(I)=T(13)*X*W
548 FOR J=0 TO 12
550 S(I)=(S(I)+T(13-J))*X*W
552 NEXT J
554 PRINTX,S(I)
555 NEXT I
558 GOTO 650
580 N(1)=I-1
582 N(2)=I-2
584 N(3)=I-3
```

```
586 IF I>=4 THEN N(4)=I-4:GOTO588
588 IF I>=5 THEN N(5)=I-5:GOTO590
590 IF I>=6 THEN N(6)=I-6:GOTO592
592 IF I>=7 THEN N(7)=I-7:GOTO594
594 IF I>=8 THEN N(8)=I-8:GOTO596
596 IF I>=9 THEN N(9)=I-9:GOTO598
598 IF I>=10THEN N(10)=I-10:GOTO600
600 IF I>=11THEN N(11)=I-11:GOTO602
602 IF I>=12THEN N(12)=I-12:GOTO604
604 IF I>=13THEN N(13)=I-13:GOTO606
606 F(0)=0
620 C(1)=Y*F(N(1))+V(0)*F(N(2))+V(1)*F(N(3))+V(2)*F(N(4))+V(3)*F(N(5))
622 C(2)=V(4)*F(N(6))+V(5)*F(N(7))+V(6)*F(N(8))+V(7)*F(N(9))+V(8)*F(N(10))
624 F(I)=(C(1)+C(2)+V(9)*F(N(11))+V(10)*F(N(12)))/(I*N(1))
626 RETURN
650 REM NUMERICAL INTEGRATION OF Q-WAVE
652 RESTORE
654 T(0)=S(1)
656 T(1)=S(2)
658 PRINT"————————————————————————"
660 X=0
664 READ U,P
666 Q(0)=T(0)+R(3)*P
668 X=0.01
669 Y=0.01
670 PRINT0;TAB(7);0;TAB(23);0
671 PRINTX;TAB(7);T(0);TAB(23);Q(0)
672 IF W$="NO" GOTO 676
673 PRINT#7,"  X   ","    T(X)   ","          Q(X)";CHR$(13)
674 PRINT#7,0,0,0
675 PRINT#7,X,T(0),Q(0)
676 I=0
678 FOR J=0 TO H
680 I=I+1
682 X=X+Y
684 READ U,P
686 G=(-U*2*Z/(X*W)+E-M)*(Y*W)↑2+2
688 T(2)=T(1)*G-T(0)-M*R(3)*P*(Y*W)↑2
690 Q(I)=T(1)+R(3)*P
692 X=X*100
694 IF X-INT(X)>=0.5 THEN X=INT(X)+1:GOTO 698
696 X=INT(X)
698 X=X*0.01
750 PRINTX;TAB(7);T(1);TAB(23);Q(I)
751 IF W$="NO" GOTO 754
752 IF X<=R(0) THEN PRINT#7,X,T(1),Q(I)
754 IF J=0 GOTO 768
756 IF I=1 THEN N(11)=Q(1)↑2:GOTO 800
758 IF I=10 THEN I=0:GOTO 792
760 T(0)=T(1)
762 T(1)=T(2)
764 IF J=H GOTO 796
766 GOTO 680
768 IF I=8 THEN I=0:GOTO 772
770 GOTO 760
772 N(1)=0
774 FOR K=2 TO 10
776 N(K)=Q(K-2)↑2
778 NEXT K
780 GOTO 788
782 FOR K=1 TO 10
784 N(K)=Q(K)↑2
786 NEXT K
788 T(0)=T(0)
790 T(1)=T(2)
792 X=X-Y
```

```
794 Y=Y*2
796 NEXT J
798 GOTO 820
800 C(1)=4*(N(2)+N(4)+N(6)+N(8)+N(10))
802 C(2)=2*(N(3)+N(5)+N(7)+N(9))
804 G(J)=(C(1)+C(2)+N(1)+N(11))*(Y/2)/3
806 GOTO 760
820 PRINT"-----------------------------------"
824 B(1)=0
826 FOR K=1 TO H
828 B(1)=B(1)+G(K)*W
832 NEXT K
850 GOSUB 1000
860 E(2)=ABS(L)
862 E(3)=(E(2)-E(1))*100/E(1)
868 A(2)=B(1)/Q(1)↑2
870 R(2)=1-4*A(2)*(L+A(2)*R(1))
872 R(2)=(SQR(R(2))-1)/(2*A(2))
874 E(2)=R(2)
876 R(1)=-R(2)↑2
878 M=R(1)+E(0)
880 E(1) = E(2)
882 A(3)=Q(1)/EXP(L*R(0)*W)
884 G(2)=EXP(2*L*R(0)*W)/(ABS(L)*2)
886 P=B(1)+G(2)*A(3)↑2
888 N=4*π*P*(5.29177E-9)↑3
890 N=1/N
892 K=-(L↑2)
894 M(0)=K+E(0)
896 IF ABS(E(3))>0.01 GOTO 932
897 IF W$="NO" GOTO 901
898 PRINT#7,"EXPONENTIAL PARTS OF Q-WAVEFUNTION,AT R>R(0)";CHR$(13)
899 PRINT#7,"  X  ","    Q(X)";CHR$(13)
900 PRINT"EXPONENTIAL PARTS OF Q-WAVEFUNCTION, AT R>R(0)"
901 R(6)=R(0)
902 H=11
904 FOR J=1 TO H
906 X=R(6)+X(6)*(J-1)
908 Q=A(3)*EXP(L*X*W)
909 PRINT X,Q
910 IF W$="NO" GOTO 912
911 IF Q>=0.01 THEN PRINT#7,X,Q
912 NEXT J
914 IF X=12.7 THEN X(6)=0.64:GOTO 920
916 IF X=25.5 THEN X(6)=1.28:GOTO 920
918 IF X>=204.7 GOTO 928
920 X(6)=2*X(6)
922 R(6)=X+X(6)
924 H=10
926 GOTO 904
928 PRINT#7
930 PRINT#7,"FINAL RESULTS",CHR$(13)
932 PRINT#7,"THE DERIVATIVE AT R(0)       =";D
934 PRINT#7,"LOG.DERIVATIVE AT R(0)       =";L
936 PRINT#7,"DIFF.FROM SQR(-E'),%,        =";E(3)
938 PRINT#7,"NEW ENERGY--------- -E'      =";K
940 PRINT#7,"THE PROB.--------- Q↑2       =";P
942 PRINT#7,"NORMALIZED---------- N       =";N
944 PRINT#7,"ETA----------------- M       =";M(0)
946 PRINT#7,"METALLIC CAGE RADIUS-- R(0) =";R(0)
948 PRINT#7
950 PRINT"-----------------------------------------"
952 GET A$:IFA$=""THEN 952
954 PRINT#7
956 IF ABS(E(3))<=0.01 GOTO 988
958 PRINT#7,"RE-ESTIMATE A NEW ENERGY";CHR$(13)
```

```
960 GOTO 312
988 CLOSE 7
990 END
992 REM INTERPOLATING
1000 FOR I=1 TO 5
1002 K=0(I)
1003 IF R(0)<=12.70 THEN X(I)=6.30+0.64*(K-1):GOTO 1006
1004 X(I)=12.70+1.28*(K-1)
1006 F(I)=SQR(N(K))
1008 NEXT I
1020 F(6)=F(1)
1022 N(0)=X(1)-X(2)
1024 N(1)=X(1)-X(3)
1026 N(2)=X(1)-X(4)
1028 N(3)=X(1)-X(5)
1030 N(4)=X(2)-X(3)
1032 N(5)=X(2)-X(4)
1034 N(6)=X(2)-X(5)
1036 N(7)=X(3)-X(4)
1037 N(8)=X(3)-X(5)
1038 N(9)=X(4)-X(5)
1040 F(7)=(F(1)-F(2))/N(0)
1042 F(8)=F(1)/(N(0)*N(1))-F(2)/(N(0)*N(4))+F(3)/(N(1)*N(4))
1044 F(9)=F(1)/N(0)/N(1)/N(2)-F(2)/N(0)/N(4)/N(5)+F(3)/N(1)/N(4)/N(7)
1046 F(9)=F(9)-F(4)/N(2)/N(5)/N(7)
1048 F(10)=F(1)/(N(0)*N(1)*N(2)*N(3))-F(2)/(N(0)*N(4)*N(5)*N(6))
1050 F(10)=F(10)+F(3)/(N(1)*N(4)*N(7)*N(8))-F(4)/(N(2)*N(5)*N(7)*N(9))
1052 F(10)=F(10)+F(5)/(N(3)*N(6)*N(8)*N(9))
1054 IF R(0)<=12.70 THEN X(6)=(12.70-R(0))/10:GOTO 1058
1056 X(6)=(25.50-R(0))/10
1058 FOR K=1 TO 13
1060 X=R(0)+X(6)*(K-1)
1062 IF K=12 THEN X=R(0)-0.0001:GOTO1066
1064 IF K=13 THEN X=R(0)+0.0001:GOTO1066
1066 N(10)=X-X(1)
1068 N(11)=X-X(2)
1070 N(12)=X-X(3)
1072 N(13)=X-X(4)
1074 Q(K)=F(6)+N(10)*(F(7)+N(11)*(F.3)+N(12)*(F(9)+N(13)*F(10)))
1078 NEXT K
1080 D=(Q(13)-Q(12))/(0.0002*W)
1082 L=D/Q(1)
1083 PRINT#7
1088 C(1)=4*(Q(2)↑2+Q(4)↑2+Q(6)↑2+Q(8)↑2+Q(10)↑2)
1090 C(2)=2*(Q(3)↑2+Q(5)↑2+Q(7)↑2+Q(9)↑2)
1092 G(1)=(C(1)+C(2)+Q(1)↑2+Q(11)↑2)*X(6)/3
1094 B(1)=B(1)-G(1)*W
1096 RETURN
READY.
```

REFERENCES

1. N.F.Mott, "Metal - Insulator Transitions", (Taylor and Francis, London, 1974).
2. N.F.Mott and E.A.Davis, "Electronic Processes in Non-crystalline Materials", 2nd. edition (O.U.P., 1979).
3. D.F.Holcomb, "The Metal Non-metal Transition in Disordered System", edited by L.R.Friedman and D.P.Tunstall, 251 (SUSSP, 1978).
4. C.Cros, M.Pouchard and P.Hagenmuller, C.R.Acad.Sci. (Paris), 260, 4764 (1965).
5. J.S.Kasper, P.Hagenmuller, M.Pouchard and C.Cros, Science 150, 1713 (1965).
6. D.Weaire, Contemp. Phys. 17, 173 (1976).
7. N.F.Mott, J.Solid State Chem. 6, 348 (1973).
8. H.Fritzche, "The Metal Non-metal Transition in Disordered System", edited by L.R.Friedman and D.P.Tunstall, 193 (SUSSP, 1078).
9. N.F.Mott, "The Metal Non-metal Transition in Disordered System", editied by L.R.Friedman and D.P.Tunstall, 149 (SUSSP, 1978).
10. W.Sasaki, Phil. Mag. B42, 725 (1980).
11. J.R.Marko and J.P.Harrison, Phys. Rev. B10, 2448 (1974).
12. N.Kobayashi, S.Ikehata, S.Kobayashi and W.Sasaki, Solid State Comm. 24, 67 (1977).
13. P.H.Keesom and G.Seidel, Phys. Rev. 113, 33 (1959).
14. K.Andres, R.N.Bhatt, P.Goalwin, T.M.Rice and R.E.Walstedt, Phys. Rev. B24, 244 (1981).

15. N.I.Franzen and K.F.Berggren, Phil. Mag. B43, 29 (1981).

16. N.I.Franzen and K.F.Berggren, Phys. Rev. B25, 1993 (1982).

17. M.Rosso, Phys. Rev. Letts. 44, 1541 (1980).

18. S.Geschwind, R.E.Walstedt, R.Romestain, V.Narayanamurti, R.B.Kummer and G.Devlin, J.de Phys. C5, 105 (1980).

19. S.Maekawa and N.Kinoshita, J. Phys. Soc. Japan 28, 1447 (1965),

20. K.Morigaki and S.Maekawa, J. Phys. Soc. Japan 32, 462 (1972).

21. G.Feher, Phys. Rev. 114, 1219 (1959).

22. J.D.Quit and J.R.Marko, Phys. Rev. Letts. 26, 318 (1971).

23. J.D.Quit and J.R.Marko, Phys. Rev. B5, 1716 (1972).

24. J.D.Quit and J.R.Marko, Phys. Rev. B7, 3842 (1973).

25. H.Ue and S.Maekawa, Phys. Rev. B3, 4232 (1971).

26. D.Jerome and J.M.Winter, Phys. Rev. 134, A1001 (1964).

27. P.R.Cullis and J.R.Marko, Phys. Rev. B11, 4184 (1975).

28. K.Morigaki and M.Rosso, J. de Phys. 36, 1131 (1975).

29. P.E.Kaus, Phys. Rev. 109, 1944 (1958).

30. K.Weiser, J. Phys. Chem. Solids 17, 149 (1960).

31. E.M.Pell, J. Phys. Chem. Solids 3, 77 (1957).

32. H.Reiss and C.S.Fuller, J. Phys. Chem. Solids 4, 58 (1958).

33. G.J.Brucker, Phys. Rev. 183, 712 (1969).

34. J.O.McCaldin and A.E.Widmer, J. Phys. Chem. Solids 24, 1073 (1963).

35. J.O.McCaldin and A.E.Widmer, Proc. IEEE 52, 301 (1964).

36. J.O.McCaldin, M.J.Little and A.E.Widmer, J. Phys. Chem. Solids 26, 1119 (1965).

37. E.I.Zorin, P.V.Pavlov, D.I.Tetel'baum and A.F.Khokhlov, Soviet Phys. - Semiconductors 6, 21 (1972).

38. E.I.Zorin, P.V.Pavlov, D.I.Tetel'baum and A.F.Khokhlov, Soviet Phys. - Semiconductors 6, 344 (1972).

39. A.V.Zastavnyi, V.M.Korol', A.N.Mikhaleva and V.D.Prozorovskii, Soviet Phys. - Semiconductors 13, 580 (1979).

40. N.Sclar, Bull. Amer. Phys. Soc. 6, 28 (1961).

41. A.S.Ribuick,B.Post and E.Banks, "Non-stoichiometric Compounds", Adv. in Chem. Series, Amer. Chem. Soc. 39, 246 (1963).

42. W.McNeil and L.E. Conroy, J.Chem. Phys. 36, 87 (1962).

43. P.A.Lightsey, D.A.Lilienfeld and D.F.Holcomb, Phys. Rev. B14, 4730 (1976).

44. F.C.Zumsteg, Phys. Rev. B14, 1406 (1976).

45. C.Cros, M.Pouchard and P.Hagenmuller, J. Solid State Chem. 2, 570 (1970).

46. C.Cros, M.Pouchard and P.Hagenmuller, Bull. Soc. Chim. (Fr.) 379 (1971).

47. C.Cros and J.C.Benejat, Bull. Soc. Chim. (Fr.) 5, 1739 (1972).

48. C.Cros, these de doctorat d'etat, Bordeaux, 1970.

49. F.P.Bundy and J.S.Kasper, High Temp. - High Press. 2, 429 (1970).

50. D.Henderson, Phys. Stat. Sol. B57, 661 (1973).

51. F.C.Weinstein, Intl. 5th Conf. Proc. on Amorphous and Liquid Semiconductors, 95 (1973).

52. F.C.Weinstein and E.A.Davis, J. Non-crystalline Solids 13, 153 (1973/74).

53. B.D.Cullity, "Elements of X-ray Diffraction", 2nd. edition (Addison - Wesley Pub. 1978).

54. Internation Union of Crystallography, "International Tables for X-ray Crystallography", Vol. II (Kynoch Press, Birmingham).

55. P.F.Sullivan and S.Seidel, Phys. Rev. 173, 679 (1968).

56. L.K.Nicholson, Ph.D. thesis, London (1976).

57. D.G.Dawes, Ph.D. thesis, London (1980).

58. S.E.Male, Ph.D. thesis, London (1976).

59. C.P.Slichter, "Principles of Magnetic Resonance", 2nd. edition, (Springe - Verley, Belian, 1980).

60. H.Kopfermann, "Nuclear Moments", (Acad. Press. Inc., N.Y., 1958).

61. G.Feher and A.F.Kip, Phys. Rev. 98, 337 (1955).

62. Y.Yafet, Solid State Phys. 14, 1 (1963).

63. F.Vescial, N.S.VanderVen and R.T.Schumacher, Phys. Rev. 134, A1286 (1964).

64. P.Kusch and H.Taub, Phys. Rev. 75, 1477 (1949).

65. D.R.Hartree, "The Calculation of Atomic Structure", (John Willey & Son Inc. 1957).

66. J.C.Slater, "The Calculation of Molecular Orbitals", (John Willey & Son, 1979).

67. J.C.Slater, "Quantum Science", edited by J.L.Calais et al. (Plenum Press. N.Y., 1976), 215.

68. F.Herman and S.Skillman, "Atomic Structure Calculations", (Prentic - Hall, 1963).

69. R.Q.Fugate and C.A.Swenson, J. Appl. Phys. 40, 3034 (1969).

70. R.Viswanathan, J. Appl. Phys. 46, 4086 (1975).

71. A.C.Rose-Innes, "Low Temperature Laboratory Technique"

72. W.N.Lawless, Cryogenics 20, 527 (1980).

73. R.B.Stephens, Cryogenics 15, 420 (1975).

74. A.J.Bevold, Cryogenics 14, 661 (1974).

75. M.Wun and N.E.Phillips , Cryogenics 15, 36 (1975)

76. J. de Nobel and F.J. du Chatenier, Physica 29, 1231 (1963).

77. J.C.Holste, J.C.Cetas and C.A.Swenson, Rev. Sci. Instr. 43, 670 (1972).

78. S.Slterovitz and M.Gesshenson, Cryogenics 14, 618 (1974).

79. P.Flubacher, A.J.Leadbettet and J.A.Morrison, Phil. Mag. 4, 273 (1958).

80. D.L.Martin, Phys. Rev. B8, 155 (1970).